UNIVERSITÉ LOUIS PASTEUR STRASBOURG

NOVARTIS INSTITUTES FOR BIOMEDICAL RESEARCH

Dissertation

Submitted to obtain the degree of

Docteur de l'Université Louis Pasteur Strasbourg I

Speciality : Life sciences
Molecular and cellular aspects of biology

By **François-Xavier BLÉ**

Lung magnetic resonance imaging as a non-invasive alternative to assess experimental pulmonary diseases in small rodents

Public defense held on December 3rd, 2007

Defense committee

Thesis Director	Dr Nelly FROSSARD, Faculté de Phamarcie, Illkirch
Thesis Co-director	Dr Nicolau BECKMANN, Novartis Pharma AG, Basel
Internal Referee	Prof Daniel GRUCKER, IPB, Strabourg
External Referee	Prof Vincent LAGENTE, Faculté des sciences, Rennes
External Referee	Dr Yannick CRÉMILLIEUX, UCB, Lyon

UNIVERSITÉ LOUIS PASTEUR STRASBOURG

NOVARTIS INSTITUTES FOR BIOMEDICAL RESEARCH

Thèse

Présentée pour obtenir le grade de

Docteur de l'Université Louis Pasteur Strasbourg I

Discipline: Sciences du vivant
Aspects moléculaires et cellulaires de la biologie

par **François-Xavier BLÉ**

Imagerie par résonance magnétique des poumons: un outil non invasif de caractérisation de modèles expérimentaux des maladies respiratoires chez le petit rongeur

Soutenue publiquement le 3 décembre 2007

Membres du Jury

Directeur de thèse	Dr Nelly FROSSARD, Faculté de Phamarcie, Illkirch
Co-directeur de thèse	Dr Nicolau BECKMANN, Novartis Pharma AG, Basel
Rapporteur interne	Prof Daniel GRUCKER, IPB, Strabourg
Rapporteur externe	Prof Vincent LAGENTE, Faculté des sciences, Rennes
Rapporteur externe	Dr Yannick CRÉMILLIEUX, UCB, Lyon

TABLE OF CONTENT

TABLE OF ABBREVIATIONS

Abbreviation	*Description*
µM	Micro ($x10^{-6}$) molar
2DFT	Two-dimensional Fourier Transformation
AB/PAS	Alcian blue/ periodic acid Schiff's staining
ADC	Apparent diffusion coefficient
ASL	Airway surface liquid
ASM	Airway smooth muscle
B_0	Homogeneous magnetic field
BAL	Bronchoalveolar lavage
BLM	Bleomycin
BN	Brown Norway
b.w.	Body weight
CCD	Charged coupled device
CF	Cystic Fibrosis
CFTR	Chloride Cystic Fibrosis Transepithelial Receptor
Compound 48/80 or c48/80	Condensation product of p-methoxphenethyl methylamine with formaldehyde. Mixture of low molecular weight polymers having a degree of polymerization between 3 and 6.
COPD	Chronic obstructive pulmonary disease
DMSO	Dimethylsulphoxide
DSCG	Di-sodium-cromoglycate
EDTA	Ethylenedaminetetraacetic acid
EGFR	Epithelial growth factor receptor
EIPA	Ethylisopropyl amiloride
ENaC	Epithelial Natrium Channel
EPO	Eosinophil peroxidase
et al.	*et alia*; and others
FcεRI	High affinity receptors for IgE
fMRI	Functional magnetic resonance imaging
FOV	Field of view

g	Gram
Gd-DTPA	Gadolinium and diethylenetriaminepentaacetic acid complex
h	Hour
HBSS	Hank's balanced salt solution
HEPES	4-(2-hydroxyethyl)-1-piperazineethanesulphonic acid
HS	Hypertoninc saline
Hz	Hertz
i.p.	Intraperitoneally
i.t.	Intratracheally
i.v.	Intravenously
Ig	Immunoglobulin
IL-	Interleukin-
INF	Interferon
kg	Kilogram
l	Litre
LPS	Lipopolysaccharide
LT	Leukotriene
µg	Microgram
mg	Milligram
min	Minute
ml	Millilitre
mM	Milli ($x10^{-3}$) molar
MCC	Mucociliary clearance
MPO	Myeloperoxidase
MR	Magnetic resonance
MRI	Magnetic resonance imaging
mRNA	Messenger ribonucleic acid
n	Number of replicates
ºC	Degrees centigrade
OPD	O-phenylenediamine
OVA	Ovalbumin
p.o.	*Per os* (by gavage)

per se	By its very nature; intrinsically
PET	Positron-emission tomography
PG	Prostaglandin
pH	$-\log_{10}$ hydrogen ion concentration
RF	Radiofrequency
R_L	Airway resistance
ROI	Region of interest
rpm	Revolutions per minute
s	Second
S1P	Sphingosine-1-Phosphate
$S1P_X$	Sphingosine-1-Phosphate receptor subtype
SEM	Standard error of the mean
T	Tesla (1T = 10 000 gauss) defines intensity of a magnetic field
T1	Longitudinal relaxation time
T2	Transversal relaxation time
T2*	Transversal relaxation time, taking into account microscopic magnetic field inhomogeneities
TE	Echo time (The time between the RF pulse and the echo signal)
TNF	Tumour necrosis factor
TR	Repetition time (the time interval with which the RF pulse sequence is repeated)
TRIS	Tris(hydroxymethyl)-amnithan
U	Units
UTP	Uridine Tri-Phosphate
α	Alpha
β	Beta
μ	Magnetic moment
ω	Larmor frequency
γ	Gyromagnetic ratio
θ	RF flip angle

FRENCH SUMMARY

Les maladies respiratoires et pulmonaires incluant l'asthme, les bronchopathies chroniques obstructives (BPCO), la fibrose, la pneumonie, le cancer du poumon et bien d'autres, comptent parmi celles dont l'incidence et la morbidité ont le plus considérablement augmenté dans les pays industrialisés au cours des dernières décennies. L'observation et la compréhension des mécanismes physiologiques impliqués dans ces pathologies sont essentielles pour progresser dans la connaissance de ces maladies et la recherche de nouveaux traitements. L'utilisation de modèles expérimentaux chez les petits rongeurs est essentielle dans ce domaine de recherche mais, bien souvent, les méthodes d'évaluation sont limitées par le fait qu'elles soient terminales (mesure de résistance bronchique, analyse des paramètres inflammatoire du lavage broncho-alvéolaire (BAL), analyse histologique) et/ou qu'elles fournissent seulement des informations globales sur la fonction pulmonaire (pléthysmographie).

Lors de cette thèse, l'imagerie par résonnance magnétique (IRM) du proton a été utilisée afin de valider un outil non-invasif, alternatif à ces méthodes et capable de fournir des informations d'ordre spatial et temporel en corrélation avec l'évolution et le statut pathophysiologique des poumons, dans plusieurs modèles de maladies respiratoires chez le petit rongeur.

Les contrastes observés sur les clichés IRM proviennent d'une différence de propriétés des tissus, principalement influencées par la densité et la mobilité des protons (de l'eau et des graisses), ainsi que par leur environnement moléculaire. Le poumon est un des organes les plus difficiles à imager par l'IRM. En effet, en plus des artéfacts de mouvements liés à la respiration et au rythme cardiaque, sa structure aérifère lui confère une densité de proton significativement plus faible que tout autre tissu. S'ajoute à cela, la différence de susceptibilité à l'interface tissu/air qui est source d'hétérogénéités locales du champ magnétique, responsable d'une perte de signal très marquée au niveau du parenchyme pulmonaire. Cette absence de signal se traduit par une apparence très sombre, proche de celle du bruit de fond sur les images RMN mais constitue cependant un excellent contraste avec les sécrétions de fluides, les fuites plasmatiques ou la densification de tissu qui peuvent être caractéristiques

de phénomènes pathophysiologiques décrits dans plusieurs modèles de maladies pulmonaires chez les petits rongeurs. Afin d'estimer les apports possibles de l'IRM du poumon pour ces espèces, quatre modèles ont été étudiés durant la thèse:

1) l'évaluation du statut inflammatoire des poumons dans un modèle d'inflammation pulmonaire allergénique chez la souris, et la validation de ce modèle dans une étude pharmacologique,
2) la validation *in vivo* de l'utilisation d'un agent de contraste permettant l'étude de la dynamique du mucus dans un modèle d'hypersécrétion provoquée par instillation d'une endotoxine chez le rat,
3) l'évaluation de composés permettant l'hydratation des sécrétions des voies aériennes induite par solution hypertonique dans un modèle non-inflammatoire chez le rat,
4) et l'étude longitudinale d'un modèle de fibrose induite par bléomycine chez la souris.

Dans un premier temps, le projet a consisté à valider l'utilisation de l'IRM afin de caractériser un modèle d'inflammation allergénique pulmonaire chez la souris (publication 1). En s'appuyant sur les travaux précédemment menés chez le rat, la première partie du travail de thèse a été dédiée au transfert vers la souris, du modèle biologique mais également de la méthode d'imagerie et d'analyse. L'étude du modèle d'inflammation pulmonaire développé chez la souris a consisté à l'administration intranasale et de manière répétée d'un allergène, l'ovalbumine, ou de son contrôle, une solution saline physiologique, chez des souris femelles BALB/c préalablement sensibilisées à l'allergène. Les examens IRM des poumons de souris ont été effectués une fois (24h après la 4ème provocation) ou plusieurs fois, entre et après les provocations allergéniques afin de déterminer les volumes de fluides sécrétés dans les voies aériennes en réponse à l'allergène. Pour la première fois dans ce modèle, les images de souris en respiration spontannée mais sous anesthésie gazeuse ont été acquises sans synchronisation avec le rythme cardiaque ou respiratoire. Les signaux détectés en utilisant une séquence d'écho de gradient ont été ensuite comparés avec les paramètres du lavage broncho-alvéolaire (BAL) ainsi qu'avec la présence éventuelle d'oedème périvasculaire et péribronchique et/ou de

mucus observés par analyse histologique des poumons. Malgré l'absence de synchronisation, la netteté des images obtenues a permis l'évaluation quantitative des réponses. Lors de la phase précoce (de la 2ème provocation jusqu'à 24h après la 4ème), des signaux intenses et massifs (volume de 40 à 50 microlitres) ont été détectés dans la partie antérieure des poumons. Soixante-douze heures après la dernière provocation, les signaux toujours en présence (environ 20 microlitres) étaient de plus faible intensité et de texture moins régulière. Les analyses des données du BAL et de l'histologie ont permis d'identifier l'origine des signaux de la phase précoce comme étant majoritairement oedémateuse alors qu'en phase tardive la présence de mucus dans les voies aériennes était principalement responsable des signaux observés par IRM. Ces résultats valident l'utilisation de l'IRM comme une méthode non-invasive d'évaluation de ce modèle d'inflammation pulmonaire chez la souris et ont fourni les bases nécessaires à l'étude de traitements pharmacologiques potentiels.

Souhaitant profiter de l'utilisation de souris transgéniques dans le cadre d'une étude pharmacologique pour valider ce modèle, nous avons au préalable établi une comparaison des souches de souris BALB/c, les plus décrites dans des nombreux modèles de sensibilité antigéniques, et des souris C57BL/6, majoritairement utilisées dans la genèse de souris transgéniques. Des différences notables au niveau de la course des signaux entre et après les provocations allergéniques ont été observées mais l'analyse du BAL et des coupes histologiques ont permis de mettre en évidence les mêmes caractéristiques de l'inflammation pouvant être impliquées dans les signaux IRM : fuite plasmatique et sécrétion de mucus.

Une fois la caractéristaion de notre modèle établie, la pertinence de l'application de la méthode d'IRM à des fins pharmacologiques a été illustrée dans des études en utilisant des outils pharmacologiques sélectifs et des souris génétiquement modifiées. Dans ces études, les effets d'un composé anti-inflammatoire ont été détectés par IRM et confirmés par histologie et par analyse du BAL (publication 2). En s'intéressant à la pharmacologie du sphingosine-1-phosphate (S1P), l'influence de la fuite plasmatique sur la détection des signaux a été mise en évidence dans notre modèle d'inflammation des voies aériennes chez la souris. Le FTY720, un agoniste de 4 des 5 récepteurs au S1P ($S1P_1$ to $_5$, except $S1P_2$), et l'agoniste sélectif du $S1P_1$: AUY954

ont prévenu de manière significative la formation de signaux liés aux fluides induite par l'allergène, alors que la délétion des souris pour le récepteur $S1P_3$ n'a eu aucune influence sur ces signaux (publication 2). Ces résultats ont été confortés par histologie démontrant une légère réduction de l'infiltration cellulaire et aucune modification concernant la sécrétion de mucus que ce soit en présence ou non de prétraitement par les agonistes. La réduction des signaux IRM a donc été majoritairement attribuée à une influence sur la fuite plasmatique. La présence de récepteurs $S1P_1$ exprimés au niveau de l'endothélium vasculaire a été précédemment impliquée dans le maintien de la perméabilité vasculaire *in vivo*, et nos résulats confortent cette hypothèse. Dans une seconde étude, nous avons examiné dans notre modèle les effets de l'antagoniste sélectif du récepteur $S1P_2$: JTE013 dont les voies de signalisation intracellulaire sont mises en opposition de celles du $S1P_1$. L'application du JTE013 a également démontré une réduction du volume des signaux IRM induits par la provocation allergénique sans que d'autres changements ne soient détectables par histologie ou par l'analyse du BAL (publication 3). Ces résultats démontrent non seulement la pertinence de l'utilisation de l'IRM pour l'évaluation des effets de composés anti-inflammatoires, mais mettent également en évidence le fait que, dans certains cas, l'IRM peut s'avérer plus sensible que les méthodes classiques utilisées en routine pour l'évaluation de traitements dans les modèles d'asthme allergique chez la souris.

En parallèle des études pharmacologiques du modèle d'inflammation pulmonaire chez la souris, une seconde partie des travaux de thèse a été orientée vers la mise au point d'une méthode permettant la dissociation des deux composantes détectées par IRM dans ce modèle. Pour se faire, un modèle d'hypersécrétion de mucus induite par l'instillation de lipopolysaccharide (LPS) : une endotoxine, chez le rat, a été utilisé. Précédemment, Beckmann et al. (2002) avaient décrit ce modèle et démontré les capacités de l'IRM à détecter des signaux reflétant la présence de mucus dans les voies aériennes, avec toutefois, une faible sensibilité. Nous avons donc évalué une possible amélioration de la détection du mucus par l'IRM en utilisant un moyen de contraste (NVP-BCR249/250), un aminodextran doublement marqué au gadolinium et au Cy-5.5 mis au point pour se lier spécifiquement au mucus. Suite à

l'administration du moyen de contraste, une augmentation significative des signaux a été quantifiée sur les images acquises par résonance magnétique 24h après l'instillation du LPS. L'effet du moyen de contraste sur les signaux était réduit mais toujours présent 24h après son administration. L'analyse histologique a confirmé par la superposition de la fluorescence du Cy-5.5 et de la coloration au alcian blue /periodic acid Schiff que le NVP-BCR249/250 était lié spécifiquement au mucus. Afin de conforter la validation du modèle pour étudier la dynamique du mucus, une substance de référence, l'uridine triphosphate (UTP), favorisant la sécrétion mais aussi la clairance du mucus, a été testée et a révélé une augmentation du volume des signaux en réponse au traitement mais également une nette diminution des signaux liés au moyen de contraste en comparaison au groupe contrôle. Ces résultats suggèrent que l'IRM a la capacité de fournir des informations sur le statut globale des fluides en présence dans les poumons, résultat net de la balance sécrétion/clairance, et peut s'avérer, en outre, un outil d'évaluation spécifique au mucus et à sa dynamique par l'utilisation de notre moyen de contraste.

Dans une troisième partie, un modèle non-inflammatoire a été développé chez le rat afin d'estimer la valeur de l'IRM du poumon en tant que moyen non-invasif d'évaluation du niveau et de la durée de l'hydratation des sécrétions des voies aériennes en réponse à l'instillation topique d'une solution saline hypertonique. En effet, de récentes découvertes indiquent que l'inhalation d'une solution saline hypertonique améliore substantiellement la fonction respiratoire des patients atteints de mucoviscidose. L'hypothèse suggérée afin d'expliquer ce mécanisme serait l'augmentation du volume de liquide de surface des voies aériennes qui représente la première ligne de défense de l'épithélium respiratoire contre les bactéries et les autres agents agresseurs de l'environnement. Cependant, l'effet de la solution hypertonique est de courte durée, et donc d'intérêt thérapeutique limité. Le blocage des canaux sodiques épithéliaux (ENaC), qui participent à la régulation du transport d'ions et de fluide au niveau épithélial, au préalable de l'inhalation de la solution hypertonique est appliqué comme stratégie pour prolonger l'action de l'hypertonicité. Nous proposons dans cette section de la thèse, la description d'un modèle *in vivo* démontrant l'utilité de l'IRM comme une méthode non-invasive de suivi de la

dynamique des fluides induits par instillation d'une solution hypertonique dans les poumons de rat, ainsi que la mise en application de ce modèle pour tester plusieurs composés capables d'interagir, directement (bloqueurs) ou indirectement (inhibiteur d'activation), avec les canaux ioniques ENaC. Les résultats obtenus apportent la preuve que l'augmentation des signaux observés par l'IRM suite aux prétraitements et au stimulus hypertonique reflète un effet dépendant du ENaC. Bien que cette méthode fournisse des informations à l'échelle macroscopique, elle offre la possibilité d'évaluer rapidement, au niveau préclinique, le potentiel de nouveaux bloqueurs ENaC et propose des perspectives de transposition direct à la recherche clinique.

Enfin, dans une dernière section, l'IRM a été appliquée dans le suivi d'un modèle de fibrose induite par bléomycine (BLM) chez la souris. Dans ce modèle, l'unique administration topique de l'antibiotique entraîne une réaction inflammatoire aigüe ainsi que l'évolution des tissus vers un état fibrotique qui se rapprochent histologiquement et physiologiquement de celles observées dans la forme humaine. La course et la texture des signaux IRM à partir de 1 jour et chaque semaine jusqu'à 28 jours après l'instillation de BLM ont été corrélées avec l'analyse histologique. Cette étude longitudinale a permis la mise en évidence de deux phases dans l'évolution du modèle. Des signaux localisés, de forte intensité, ont été détéctés une semaine après l'instillation de bléomycine et corrélés à la phase inflammatoire, illustrée par une forte infiltration cellulaire au niveau péribronchique. À partir de 14 jours, les signaux plus éparses ont été reliés à la présence de tissus fibrotiques sur les coupes histologiques. Bien que cette étude pilote nécessite encore un approfondissement de la caractérisation des signaux, elle a mis en évidence le potentiel de l'IRM dans l'étude longitudinale d'un modèle de fibrose chez la souris.

En conclusion, ce travail de thèse confirme le potentiel de l'IRM dans l'évaluation de différents modèles de maladies pulmonaires chez le petit rongeur. Une fois bien caractérisés, ces modèles deviennent un support idéal pour l'évaluation de nouveaux traitements et permettent une meilleure compréhension des mécanismes sous-jacents par l'utilisation d'outils pharmacologiques ou d'animaux transgéniques

disponibles chez le petit rongeur. Le caractère non-invasif de cette méthode d'imagerie offre également la possibilité de mesures répétées sur un nombre restreint d'animaux, avec un intérêt particulier dans des études dynamiques ou longitudinales. Bien que macroscopiques, les observations par IRM fournissent des informations d'ordre spatial qui peuvent s'avérer utiles à l'amélioration de la compréhension et la classification de la maladie respiratoire étudiée. Enfin, ces études fournissent également quelques preuves de la valeur de cette technique d'imagerie théoriquement directement transposable à des études cliniques.

FOREWORD

MAGNETIC RESONANCE IMAGING (MRI) is able to detect water content in the biological tissue and thus to non-invasively assess on a regional basis infiltrated water and/or secreted fluids and/or tissue densification. In pulmonary diseases such as asthma, chronic obstructive pulmonary diseases or fibrosis, plasma exudation, mucus secretion and thickening of the lung tissue constitutes hallmarks of the pathological status that directly contribute to functional impairment. These features are well conserved in experimental pulmonary disease models in the small rodents. A particular interest is given to murine models that have provided, in parallel to the technological progress in genetic engineering and molecular biology, a reliable *in vivo* support for lung disease understanding and investigation. Nowadays, routine methods used to evaluate disease state of the lung in these models are either terminal or gives functional estimation of the global airways.

Therefore, our purpose was to apply MRI to non-invasively depict different hallmarks occurring in a murine model of asthma. Thus, we have demonstrated that proton MRI provides a relevant mean to assess and follow signals associated with the plasma leakage and mucus secretions in the lung, which are both important features of the inflammatory response following allergenic provocation. To further confirm these findings, we also studied in this model the effect of pharmacological tools. We chose to study sphingosine-1-phosphate (S1P) pharmacology on the basis of recent publications indicating a possible implication of this endogenous mediator in inflammation and lung barrier integrity in models of asthma.

Additionally, since the technique had been previously set up in the rat, we extended the knowledge in this species by focusing on (i) mucus secretion monitoring with the use of a specific probe in a model of endotoxin-induced mucus hypersecretion as well as on (ii) the hydration of airway secretions induced by hypertonic instillation and enhanced by epithelial sodium channel-mediated effects in a non-inflammatory model, with the perspective of future translation to the mouse models for transgenic application.

Finally, our aim was also to try applying this technique to a less acute model, the murine bleomycin-induced fibrosis where description of the course of edematous, mucous and/or fibrotic components was partially given. This model has been chosen

regarding its admitted relevance to mimic global characteristics of human pulmonary fibrosis in addition to its simplicity to be set up.

Thus, the present work is bringing evidence of possible contributions of MRI in pulmonary disease investigations in mouse and rat, and postulates for its use to complete and/or replace the methods used nowadays to evaluate experimental murine models.

GENERAL INTRODUCTION

1. Respiratory diseases and animal models

Respiratory diseases such as asthma, chronic obstructive pulmonary disease (COPD) and fibrosis involve a complex interaction of many different inflammatory and structural cell types all of which release a variety of mediators that are involved in the genesis of the clinical manifestations of the disorders. Indeed, in this case, the abnormal inflammatory response produce many effects in the airways, including bronchoconstriction, plasma exudation, mucus secretion, and attraction and activation of inflammatory cells that are in turn responsible for the function impairments experienced by the patients.

Regarding asthma, infiltrated activated eosinophils are considered to play a major role because they contribute to epithelial cell damage, bronchial hyperresponsiveness, plasma exudation and oedema of the airway mucosa, in addition to smooth muscle hypertrophy and mucus plugging through the release of enzymes and proteins (Barnes, 1996; Kroegel et al., 1994; Moqbel, 1996). COPD is associated with an abnormal inflammatory response of the lungs to noxious particles and gases; it encompasses chronic obstructive bronchitis and obstruction of small airways reflecting mucous hypersecretion. Emphysema, a critical component of COPD, is defined as enlargement of air spaces as a result of destruction of the lung parenchyma, leading to loss of lung elasticity and closure of small airways. Moreover, fibrosis is induced by a critical evolution of asthma and persistent inflammation in the lung, and is consisting to a subepithelial, and subsequently interstitial deposition of collagen that compromise proper gas exchange through alveolar wall and lung elasticity during respiration.

Investigation and characterization of the respiratory diseases are motivated by the fact that these illnesses are nowadays among the most prevalent and the most rapidly expanding in prevalence world wide. Obviously, there is a demand for new therapies in this area, involving a growing interest for research in this field that just clinical studies can not insure.

Since abnormal inflammation is one of the key feature resulting in the disease state, dysregulation of the inflammatory response is induced in the lung of living animals using the appropriate stimuli. In this way, models have been established in an attempt to mimic and study specific aspects of human respiratory disease, and to evaluate new drugs (for reviews see Canning, 2003; Shapiro, 2000). Physiological changes that fit as close as possible to symptoms and impairment observed in human pathologies are required to provide the most reliable support. Determining the safety and efficacy of new therapies also depend upon animal experimentation.

Animal modeling of lung diseases is made possible by the fact that the processes associated with the regulation of breathing, gas exchange, airway smooth-muscle contraction and relaxation, blood flow through the pulmonary and bronchial vasculature, inflammatory cell recruitment, mucus secretion, mucociliary clearance and airway surface liquid composition are globally conserved in mammals. Moreover, among the mammals, the small rodents (especially the mouse) are proven to be invaluable tools to depict human diseases because : (1) we have great understanding of rodents biology and many molecular probes to study mice and rats; (2) breeding is rapid; (3) genetic homology maps are available to allow translation of genetic findings in laboratory mice to the human genome; and (4) we can manipulate the murine genome eliminating ("knock-outs") or enhancing (transgenics) the expression of individual gene products or introducing specific variants within a gene of interest ("knock-ins"). Thus, controlled genetic experiments in mammals can be performed. Disadvantages of these animals include their small size. Especially regarding the mouse size which precludes some surgical interventions and makes physiologic assessment more difficult, which includes quantitative measurements of morphometry (as imaging) and physiology. Although technological improvements are attempting to reduce this drawback for the mouse studies, using rat model could be a good compromise regarding issues of animal size.

The biggest criticism to the use of rodents, of course, is that rodents are not humans. Nevertheless, basic biological processes are usually conserved in mammals lung physiology. Overall, information derived from studies in mice and rat is best used to guide studies in humans, many of which have been incredibly informative. In fact, animal experimentation has been indispensable to establishing the safety,

selectivity and clinical efficacy of every major class of therapeutic used in the treatment of asthma and chronic obstructive pulmonary diseases. Animal experimentation has also proven instrumental to the growing knowledge of the physiological and pathophysiological processes associated with these illnesses (Canning, 2003; Kumar and Foster, 2002).

2. *Evaluation of pulmonary diseases models*

Being able to mimic the features of a lung disease in small rodents could not be of utility without a way to evaluate and understand the processes that underlie the symptoms. The inflammatory status of the lungs in respiratory disease models is usually inferred from the analysis of bronchoalveolar lavage (BAL) fluid or is determined histologically. Depicting BAL fluid content, inflammatory cells can be differentiated and numbered, their activity assessed and inflammatory mediators involved in the physiopathology quantified. Observations of the staining-treated histological sections can provide structural information on the tissues, and at cellular level, but this method is time-consuming and the evaluation is limited to a few slices of the lung. Moreover, the invasive nature of these procedures precludes repeated assessments in the same animal.

Pulmonary function tests in rodents are important for experimental research for various respiratory disorders such as asthma and COPD (for a recent review see Hoymann, 2006). The techniques used so far vary from non invasive barometric plethysmography ("Penh system") in unrestrained animals or in restrained animals (head-out plethysmorgraphy) to terminal methods such as *in vitro* measurement of tracheal or parenchymal smooth muscle contractility, or *in vivo* measurement of lung resistance or compliance after intravenous injection of bronchoconstrictive agents. Each of these methods have their limitations. The *in vitro* technique correlates well with allergic airway sensitization (Larsen et al., 1992) but the influence of mucus production, mucosal edema, or other changes in the lower airways after allergic reaction are not reflected in monitoring airway responsiveness. The *in vivo* techniques performing measurements of airway hyperresponsiveness on

orotracheally intubated animals or tracheotomized and ventilated animals (Hoymann, 2006) require anaesthesia and intravenous challenge of the animals with bronchoconstrictive agents might not solely reflect physiologic stimulation of airway smooth muscles. Finally, these invasive methods are technically demanding and time-consuming or complications can arise following repeated intubation (Hoymann, 2006). In contrast, studies carried out using barometric plethysmography have the serious advantage to provide measurement of airway responsiveness in conscious, spontaneously breathing animals, allowing repeated and long-term evaluation for investigation of kinetics and treatment protocols of airway hyperresponsiveness. However, the main concerns with the non invasive "Penh" approaches are the uncertainty of the site of obstruction since no spatial information is provided and that due to the lack of pressure signal, no actual changes in lung resistance and compliance can be determined. Additionally in restrained animals an added complication is the fact that the animal is stressed during measurements.

2.1. Imaging Pulmonary diseases models

Imaging in small animals has the enormous potential to provide further knowledge and to contribute to the understanding of lung biology in intact animals. Systems can offer a possibility for translation from animal to human studies (Schuster et al., 2003). In the last few years, small animal imaging has become an increasingly important research tool for studying disease models (Schuster et al., 2004) and for pre-clinical testing (Beckmann et al., 2003). This increase in popularity of small animal imaging has been fostered partly by the ready availability of commercial imaging systems and the demonstration of the value of in vivo, non-destructive, and survival capability of these imaging systems.

An ample variety of imaging devices includes "micro" X-ray computed tomography and positron-emission tomography (PET) scanners, high magnetic filed MRI scanners, and advances in ultrasound system technology can be used to study various processes such as ventilation, perfusion, pulmonary hypertension, lung inflammation, and gene transfer (for a recent review see Schuster et al., 2003).

MRI has been applied to several disease areas in pharmaceutical research and is a technique that is available in all large pharmaceutical companies (Beckmann et al., 2001; Rudin et al., 1999; Rudin and Wiessleder, 2003). The main assets of MRI are its non-invasiveness, high spatial resolution (of the order of 100 μm for rodent studies) and the wealth of information it can provide. Thus, MRI is a valuable tool for: (i) the diagnosis of diseases, tissue staging (classification) and *in vivo* morphometry (anatomical information); (ii) obtaining physiological and functional information; and (iii) deriving metabolic and target-specific tissue characteristics.

2.2. Magnetic Resonance Imaging (MRI)

Magnetic resonance imaging (MRI) is an imaging technique used primarily in medical settings to produce high quality images of the inside of the human body. MRI is based on the principles of nuclear magnetic resonance (NMR), a spectroscopic technique used by scientists to obtain microscopic chemical and physical information about molecules. The technique was called magnetic resonance imaging rather than nuclear magnetic resonance imaging (NMRI) because of the negative connotations associated with the word nuclear in the late 1970's.

2.2.1. MRI historical

Felix Bloch and Edward Purcell, both of whom were awarded the Nobel Prize in 1952, discovered the magnetic resonance phenomenon independently in 1946. In the period between 1950 and 1970, NMR was developed and used for chemical and physical molecular analysis.

In 1971 Raymond Damadian showed that the nuclear magnetic relaxation times of tissues and tumors differed, thus motivating scientists to consider magnetic resonance for the detection of disease. In 1973 the x-ray-based computerized tomography (CT) was introduced by Hounsfield. This date is important to the MRI timeline because it showed hospitals were willing to spend large amounts of money for medical imaging hardware. Magnetic resonance imaging was first demonstrated

on small test tube samples that same year by Paul Lauterbur. He used a back projection technique similar to that used in CT. In 1975 Richard Ernst proposed magnetic resonance imaging using phase and frequency encoding, and the Fourier Transform. This technique is the basis of current MRI techniques. A few years later, in 1977, Raymond Damadian demonstrated MRI called field-focusing nuclear magnetic resonance. In this same year, Peter Mansfield developed the echo-planar imaging technique. This technique will be developed in later years to produce images at video rates (30 ms / image).

Edelstein and coworkers demonstrated imaging of the body using Ernst's technique in 1980. A single image could be acquired in approximately five minutes by this technique. By 1986, the imaging time was reduced to about five seconds, without sacrificing too much image quality. The same year researchers were developing the NMR microscope, which allowed approximately 10 mm resolution on approximately one cm samples. In 1987 echo-planar imaging was used to perform real-time movie imaging of a single cardiac cycle. In this same year Charles Dumoulin was perfecting magnetic resonance angiography, which allowed imaging of flowing blood without the use of contrast agents.

In 1991, Richard Ernst was rewarded for his achievements in pulsed Fourier Transform NMR and MRI with the Nobel Prize in Chemistry. In 1992 functional MRI (fMRI) was developed. This technique allows the mapping of the function of the various regions of the human brain. Five years earlier many clinicians thought echo-planar imaging's primary applications was to be in real-time cardiac imaging. The development of fMRI opened up a new application for echo planar imaging in mapping the regions of the brain responsible for thought and motor control. In 1994, researchers at the State University of New York at Stony Brook and Princeton University demonstrated the imaging of hyperpolarized 129Xe gas for respiration studies.

In 2003, Paul C. Lauterbur of the University of Illinois and Sir Peter Mansfield of the University of Nottingham were awarded the Nobel Prize in Medicine for their discoveries concerning magnetic resonance imaging.

2.2.2. MRI basics

MR images reflect a weighted distribution of protons (hydrogen nuclei) within water and/or in fat in tissues (Boesch 1999). The necessary components for MRI are (figure 1):

- A superconducting magnet that generates a constant and homogeneous magnetic field (B_0). The magnet typically operates at a high magnetic field of 1.5 tesla (T) for clinical or 4.7 T for small animal systems. (1 T = 10^4 gauss).
- A gradient coil system capable of producing position-dependent magnetic fields along the x, y, and z directions that are responsible for creating the spatial differentiation required for imaging studies.
- A radiofrequency (RF) coil that is used to transmit an RF pulse required to excite protons and receive RF waves (echo signals) resulting from the relaxation of the protons.

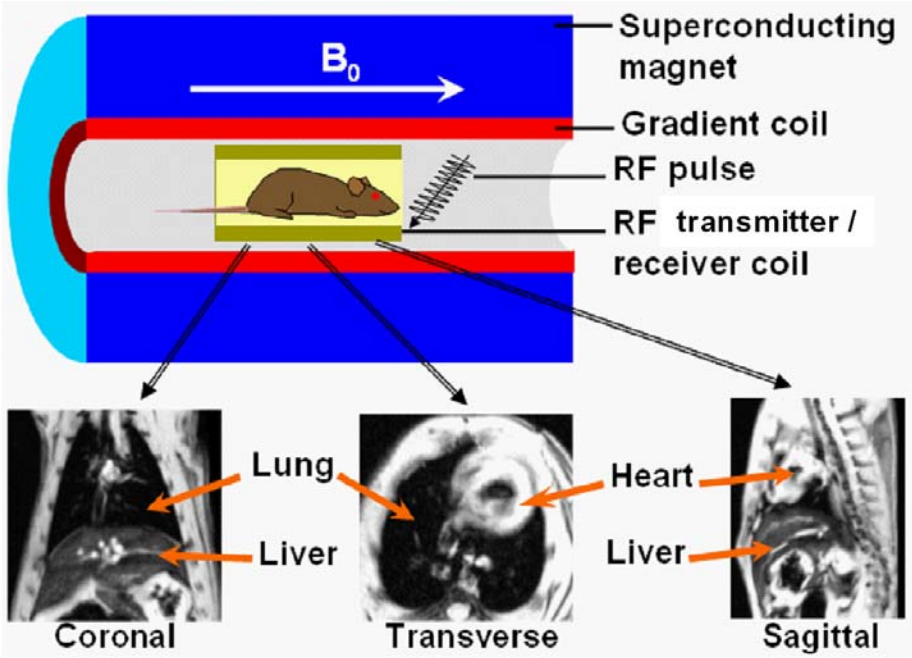

***Figure 1**- TOP - Diagrammatic representation of the components required for MRI. BOTTOM- Representative coronal, transverse and sagittal MR images of a rat showing the position of the lung, liver and heart in the different slices. B_0 represents the homogenous magnetic field at 4.7 T.*

An image is reconstructed from such signals and represents the weighted distribution of protons of water and/or fat in a region of the body. Images with an

arbitrary orientation (transversal, coronal, sagittal or oblique) can be easily obtained by MRI.

2.2.3. MRI Principle

Nuclei that possess an uneven atomic mass or atomic number possess an angular momentum, and have a characteristic spin quantum number. The spin characteristic of the nucleus, a positively charged particle, induces a magnetic field, known as the magnetic moment (μ) of the atom. Thus spinning nuclei can be thought of behaving like tiny magnets (figure 2). The ^{1}H nucleus (proton) is the type most commonly used for MRI, and the one used for this thesis. However imaging can be performed for ^{3}He, ^{129}Xe, ^{31}P, ^{13}C, ^{19}F and ^{23}Na, to cite a few examples.

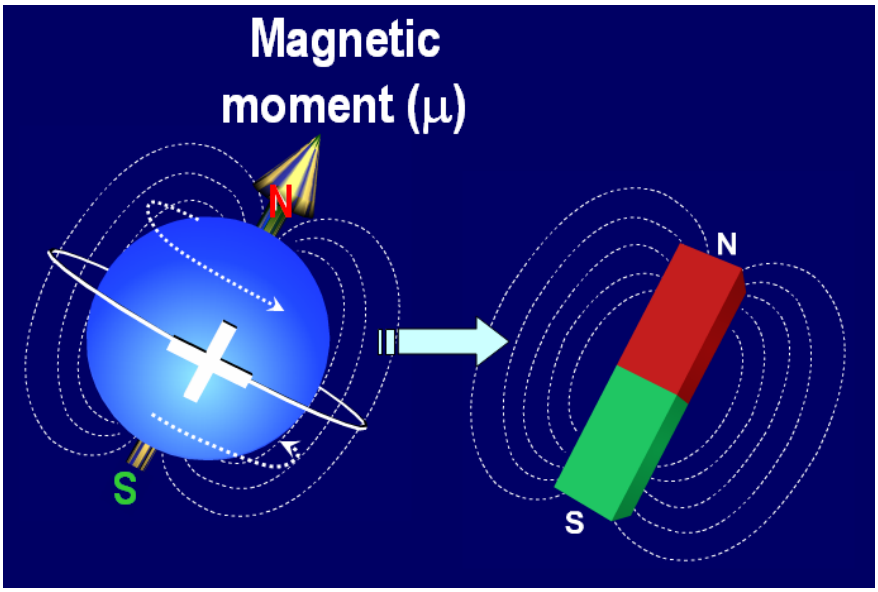

Figure 2 *- Diagramatic representation showing the spinning of a nucleus (left), the rotating charge (+) provides the nucleus with a magnetic moment (μ) and thus they can be thought of as magnets (right).*

Without an external magnetic field, the magnetic moments of a collection of protons in a tissue will be randomly oriented, as specified by the principles of Brownian motion. When a patient or animal is inserted in the magnet, the static magnetic field (B_0) causes the protons in the different tissues to assume discrete orientations, either with (parallel) or against (anti-parallel) B_0 (figure 3). Parallel alignment requires less energy and thus this type of orientation is preferred.

However, the difference in number of protons aligned in parallel compared to anti-parallel orientation is very small. Roughly for every 10 million protons aligned anti-parallel, 10 000 007 protons are parallel to B_0.

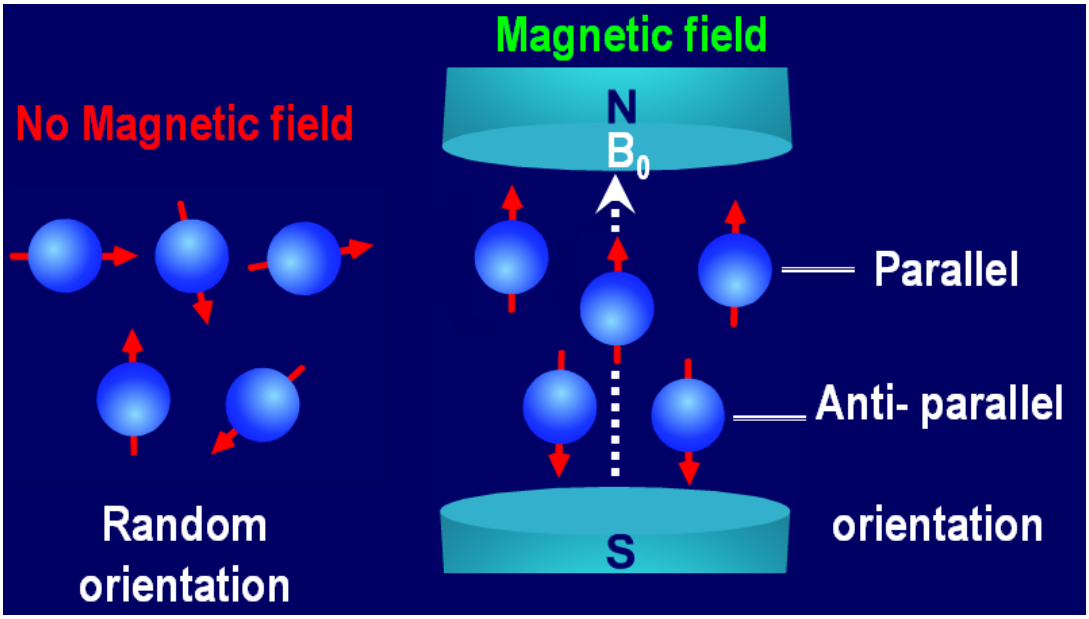

Figure 3- *Diagramatic representation showing the random orientation of protons in the absence of a static magnetic field (left). Under a static magnetic field (B_0) protons align themselves parallel or anti-parallel to B_0, (right); parallel orientation requires less energy and is thus preferred.*

However, the alignment in parallel to B_0 is not perfect. The spin vectors of the nuclei experience a torque, causing them to rotate around the axis of the magnetic field with a precise frequency. This cone shape rotation is known as Larmor precession (figure 4). The rate of precession (ω; in MHz [1 megahertz = 10^6 cycles per second]) is dependent on the gyromagnetic ratio of the given isotope (γ) and the strength of the magnetic field (B_0). This relationship is expressed as: $\boldsymbol{\omega = \gamma B_0}$.

Once a patient, animal, or tissue is inserted in the magnet it will become magnetized in the direction of B_0, defined as the Z axis. This net magnetization (sum of all magnetic moments) on the Z plane is known as the **longitudinal magnetization** (figure 4).

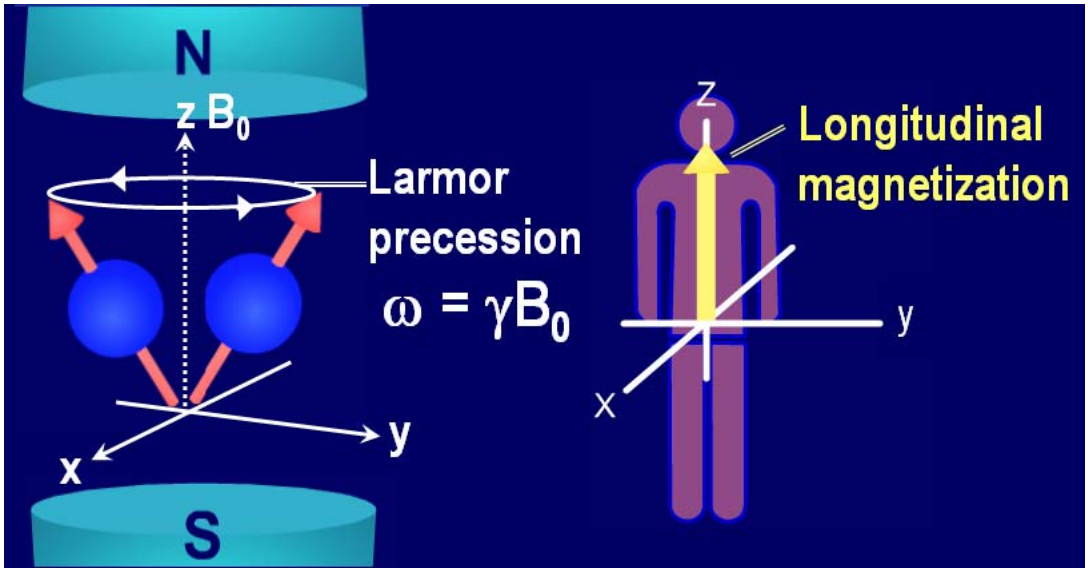

Figure 4 *- Diagramatic representation showing: Left - the torque experienced by protons in the magnetic field, the cone shape rotation is known as the Larmor precession (ω) it is dependent on the gyromagnetic ratio of the isotope (γ) and the strength of the magnetic field (B_0). Right - the sum of all magnetic moments present in the magnet field results in a net magnetization along the z-axis, known as the longitudinal magnetization. This system is at equilibrium and thus no information can be retrieved.*

This longitudinal magnetization in its state of equilibrium is constant and thus cannot induce a current in a receiver coil, as defined by Faraday's law of induction. Therefore, the protons must be perturbed or excited in order to obtain information about them. This can be achieved by irradiating the protons with a RF pulse matching the Larmor (precession) frequency (energy transfer is most efficiently transferred when the RF pulse frequency matches the Larmor frequency).

The irradiation with an RF pulse with a magnetic field B_1 perpendicular to B_0 (figure 5) causes the magnetization to precess additionally about B_1, rotating away from B_0 towards the transverse (x-y) plane (figure 5). The angle of rotation (θ) is known as the RF flip angle or the RF pulse angle.

- The RF flip angle is dependent on the gyromagnetic ratio (γ), the amplitude of B_1, and the duration of the pulse (t). It is expressed as:

$$\theta = \gamma B_1 t$$

Immediately after turning off the RF, the resulting new magnetization (M) can have an arbitrary initial angle with respect to the Z axis (along B_0), that can be modified depending on the aim of the experiment. This magnetization (M) has two vector components: M_{XY} on the transverse plane (**the transversal magnetization**) and M_Z along the longitudinal direction (**the longitudinal magnetization**). Only the component on the x-y-plane can be detected leading to the generation of a current in the RF coil (figure 5).

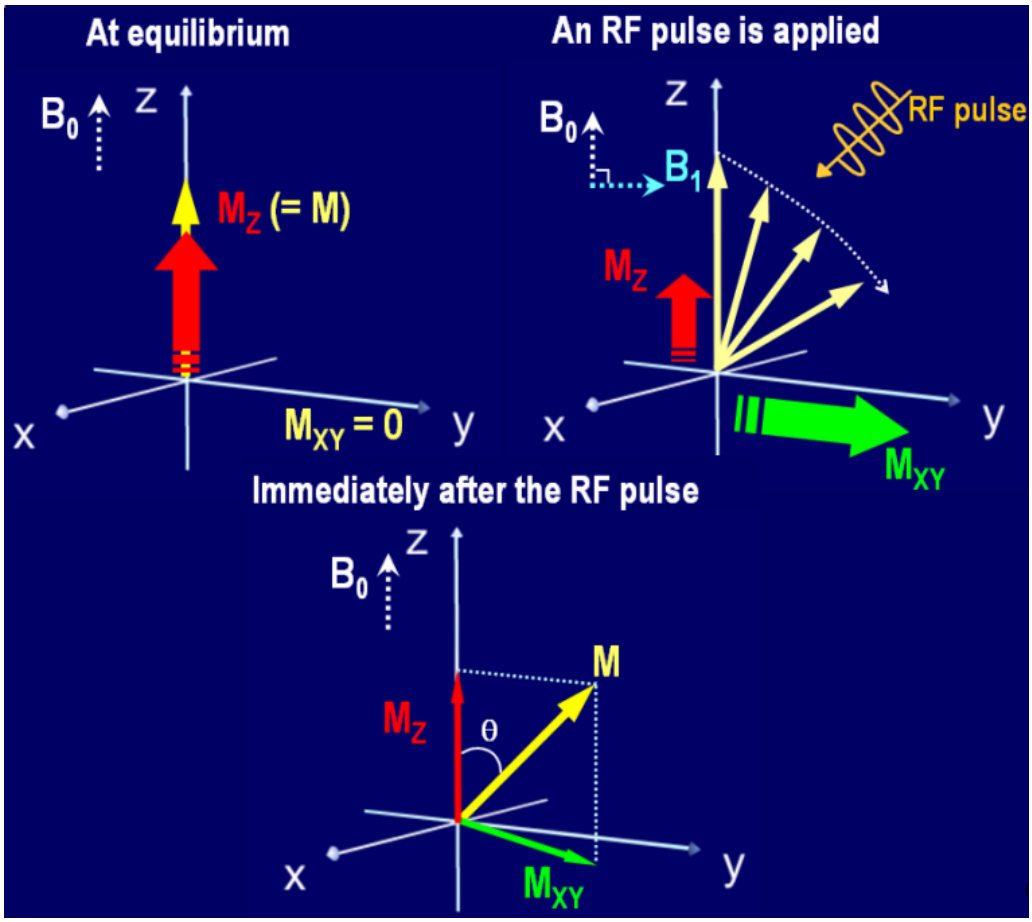

Figure 5 *- Diagramatic representation showing: Top left - the state of magnetization at equilibrium (before the RF pulse). At this stage there is no transversal magnetization (M_{XY}) and the net magnetization (M) matches the longitudinal magnetization (M_Z). Top Right – once the RF pulse is applied, its magnetic field (B_1) is perpendicular to B_0 and causes a movement of the net magnetization (M) towards the x-y-plane, resulting in a reduction in longitudinal magnetization (M_Z) and an increase in transversal magnetization (M_{XY}). Bottom – Immediately after the RF has been applied the net magnetization has both an M_Z and M_{XY} component. Only the M_{XY} component can lead to a signal in the receiver coil, known as an echo signal. The angle of rotation of M towards the x-y-plane is known as RF flip angle (θ).*

Once the RF pulse has stopped being applied, the magnetization will begin to move back to its original position (before the RF pulse) parallel to B_0. This movement results in an increase of the M_Z component (the longitudinal magnetization) and a reduction in the M_{XY} component (the transversal magnetization). The time required to return to 63% of the original M_Z component (before the RF pulse) is referred as **T1 or spin-lattice relaxation (as energy is lost to the surrounding tissue [the lattice])**. However, at the same time, because of dipolar interactions among the spins, the transversal magnetization relaxes with a characteristic time known as **T2 or spin-spin relaxation** (Figure 6). T1 relaxation time always takes longer than T2.

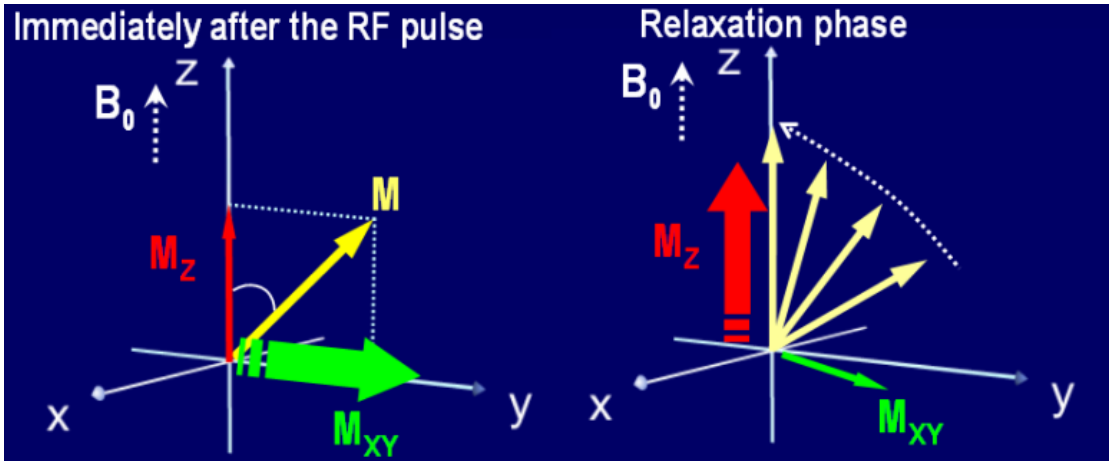

***Figure 6** - Diagramatic representation showing: Left - immediately after the RF has been applied the net magnetization has both M_Z and M_{XY} components. Right – upon cessation of the RF pulse the magnetization will begin to return to its original position, and thus the longitudinal magnetization (M_Z) will increase and the transversal magnetization will decrease. The time taken for M_Z to recover by 63% is known as T1; conversely, the time taken for the M_{XY} component to decline by 63% is referred to T2.*

Another relaxation constant, T2*, describes the loss of transversal magnetization (M_{XY}) taking into consideration local, microscopic magnetic inhomogeneities present within the sample positioned in an external field B_0. The relation $T2 \geq T2^*$ always holds. Samples such as a vial containing water are not subject to strong local magnetic susceptibilities, thus T2* constants are very close to those of T2. However, in tissues T2* values are much lower than T2 constants; this is particularly the case

for the lung where strong local inhomogeneities are present due to the interface between the lung parenchyma and the high content of air. Thus for *in vivo* imaging of the lung the decay in transversal magnetization (M_{XY}) is governed by T2*.

The excitation of protons by itself is not sufficient to generate an image. Spatial differentiation is necessary to distinguish the location of the different protons in the slice chosen. This is performed by activating magnetic field gradients along the x, y, and z-axis, during data acquisition as mentioned before and illustrated in figure 7.

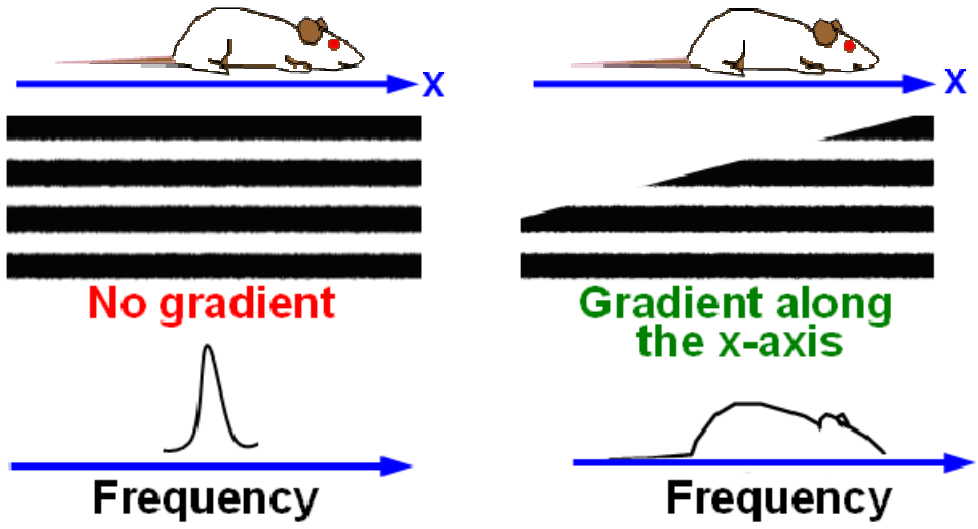

Figure 7 *- Diagramatic representation demonstrating that in the absence of a gradient system (left) no spatial differentiation is available, as the strength of the magnetic field is homogenous (black bars). However, when a magnetic field gradient is applied, in this example along the x-axis, the variations in magnetic field allow for spatial encoding, essential for image reconstruction. Magnetic field gradients are applied on x-, y-, and z-axis to generate an image.*

The intensity of the MR signal is regulated by a number of parameters that include proton density, T1, T2, and T2* relaxation times, chemical shift and motion. The relative contribution of each parameter can be controlled by modulating the RF pulses, the gradients and the timing applied during data acquisition. These parameters are set in an imaging sequence and are referred to as the pulse sequence or pulse program. The pulse sequence is normally repeated several times along different gradients in order to generate an image.

During data acquisition, the time interval with which the sequence is repeated is known as the repetition time (**TR**). Within a certain repetition, the time between the RF pulse and the echo signal (a collection of such signals that is required to create an image) is known as the echo time (**TE**). Modification of TE and TR times as well as gradient pulses leads to images that are T1, T2 or T2*-weighted.

The echo signal following the pulse sequence is a mixture of different frequencies and phases all at different locations. Through a mathematical process known as a **Fourier Transformation** applied to a collection of echo signals a computer can then reconstruct the image.

2.2.4. MRI of the lung

From a magnetic resonance perspective, the living lung is one of the most difficult organs to image. This is due to the high content of air in the lung that results in a lower proton density and an increase of local air/tissue inhomogeneities that result in very short T2 and T2* relaxation times. At 4.7 T, a magnetic field strength commonly used in animal experiments, T2* of the lung parenchyma is approximately 500 μs. This leads to very low intensity of proton signals from lung parenchyma. Moreover, cardiac and respiratory movements can cause marked image artefacts, particularly in small animals such as rodents where higher cardiac and respiratory rates are present. This can be circumvented by using scan-synchronous ventilation (Gewalt et al., 1993) where respiration is suppressed during acquisition of individual signals. Additionally, imaging is synchronised with the electrocardiogram (ECG). Using this kind of approach, the total acquisition time for one individual image is of 30 to 40 min, not including animal preparation required for ECG recording and artificial ventilation. This type of approach would be difficult to implement in the context of drug discovery (aimed at compound screening) as well as for lung research, as a series of images that cover the entire lung are necessary to understand pathological changes of disease as well as the effects of drugs in disease models.

An approach to address the low parenchymal signal intensity is by using hyperpolarized noble gas isotopes (^{3}He and ^{129}Xe), for a review see (Moller et al., 2002). In this approach, ^{3}He or ^{129}Xe gases are irradiated with an optical laser causing more of these atoms to align themselves in parallel to a static magnetic field, resulting in greater signal intensity than conventional proton MRI. Impressive images from the lung can be obtained after administering these gases, and the approach has been successful in generating information regarding lung ventilation (Chen et al., 2003) and emphysema through measuring the apparent diffusion coefficient (ADC) of ^{3}He (Chen et al., 2000). However, several motives hamper the use of hyperpolarize MRI in lung research. These include: (i) the systems for the generation of hyperpolarized gases are not commercially available; (ii) a complex instrumentation is required for controlling the respiration and delivery of the gases (Chet et al., 2000; Hedlund et al., 2000); (iii) the cost of running and generating hyperpolarised gases is considerably higher than conventional proton MRI; and (iv) more importantly animals need to be artificially ventilated and are often tracheotomized, thus repeated measurements are not possible, depriving MRI of this important asset, non-invasiveness; though, efforts in the development of this application in intact animals have recently been performed in the rat (Stupar et al, 2007).

Beckmann and colleagues introduced an alternative approach to imaging the lung based on conventional proton MRI using gradient-echo sequences that yield T2*-weighted images (Beckmann et al., 2001 b; c). Movement artefacts are suppressed by averaging. Neither cardiac nor respiratory triggering is applied and the animals are able to breathe spontaneously during data acquisition. Using this protocol (for rat lung imaging, gradient-echo sequence with a TR of 5.6 ms, TE of 2.7 ms, flip angle of approximately 15º, and 45 averages resulting in an acquisition time of 59 s per image), the signal from the lung parenchyma is too low to be detected and thus appears black, similarly to background noise. However, this absence of detectable lung parenchyma signals provides a high contrast-to-noise ratio for detection of either fluid secretion, tissue hydration or density changes induced by physiopathologic processes. For instance, signals resulting from edema or mucus

release (Beckmann et al 2001 b; 2002; Tigani et al., 2002) can be easily visualized in the rat (figure 8).

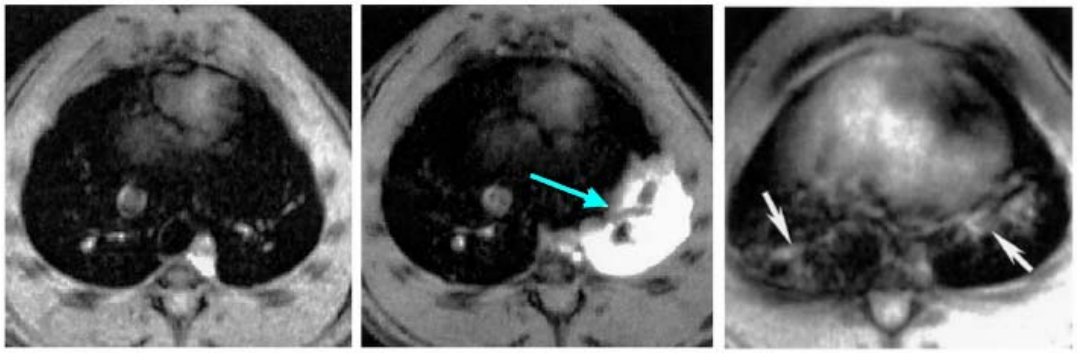

***Figure 8**- Transversal images courtesy of Tigani et al. (2002) showing a baseline image before challenge (left); an image of an actively sensitized rat treated with allergen and imaged 24 h later (middle); and an image of a rat previously treated with endotoxin (right). The blue arrow points at the appearance of a strong even signal that correlated with perivascular oedema observed histologically and an increase in protein concentration in BAL fluid, following allergen challenge. The white arrows point at diffuse signals that correlated with increased goblet cell metaplasia in histological slides and with increased mucin content in BAL fluid, after treatment with endotoxin.*

The MR images that have been generated in this thesis were T2*-weighted and were acquired based on the gradient-echo pulse sequences implemented by Beckmann et al. (2001 b; c; 2002; 2004). The sequences used are described in detail in the manuscript method sections.

3. *Investigated models and proton MRI expectations*

As a result of technical difficulties exposed in the precedent section, proton MRI has only recently been applied to pharmacological studies in the area of respiratory diseases. These recent developments include the non-invasive characterisation in spontaneously breathing rats of lung oedema following allergen challenge in sensitized animals (Beckmann et al., 2001; Tigani et al., 2003); mucus hypersecretion following endotoxin instillation (Beckmann et al, 2002). Based on these observations, one of the objective of the thesis was to further investigate the

potentials of MRI in the comprehension of these models and to explore other models which could give more relevance to MRI use in pharmaceutical research.

The following sections summarize the aspects of respiratory disease and models for which we hypothetized the potentials of MRI in their evaluation, understanding and application in pharmacological research.

3.1. Allergen-induced airway inflammation in sensitized mice

Asthma is a chronic disorder of the lung characterized by a reversible airway obstruction, and involves the interplay of many inflammatory and structural cells, resulting in the interaction of a wide variety of inflammatory mediators that include autacoids, cytokines, chemokines, growth factors, and adhesion molecules. In asthma, these inflammatory mediators are thought to contribute to epithelial cell damage, bronchial hyperresponsiveness, mucus secretion, plasma exudation and oedema of the airway submucosa (Barnes, 1996). Symptomatic attacks of asthma may be caused by several known or unknown factors such as exposure to allergen (Platts-Mills & Wheatley, 1996), viruses (Busse & Gern, 1997), or indoor and outdoor pollutants (Wardlaw, 1993) and each may induce an acute inflammatory response.

Inhaled allergen challenge may be used as a model to understand acute inflammation in asthma. In allergic patients this leads to an early inflammatory allergic reaction and in some cases, this may be followed by a late-phase reaction. The early-phase reaction is initiated after the activation of cells bearing allergen-specific IgE. It is characterized by the rapid activation of airway mast cells (Murray et al., 1985; Liu et al., 1991) and macrophages (Tonnel et al., 1983; Calhoun et al., 1992). Cell types, other than basophils and mast cells, that bear the high-affinity IgE receptor FcεRI (Gounni et al., 1994) may also participate, but it is not known whether they can be activated directly by allergens. The activated cells rapidly release proinflammatory mediators such as histamine (Jarjour et al., 1997), and

reactive oxygen species which induce contraction of the airway smooth muscle, mucous secretion, and vasodilatation. The bronchial microcirculation has a central role in this inflammatory process (Persson et al., 1995). Inflammatory mediators induce microvascular leakage with exudation of plasma into the airways (Greiff et al. 1993; Van-Vyve et al., 1995). Acute plasma protein leakage induces a thickened engorged and edematous airway wall and a resultant narrowing of the airway lumen. In addition, plasma may also traverse the epithelium, pass through the tight junctions, and collect in the airway lumen. Plasma exudation may compromise epithelial integrity, and its presence in the lumen may reduce clearance of mucus (Wanner et al, 1996). Plasma proteins may also promote the formation of viscid luminal plugs of exudates mixed with mucus and inflammatory and epithelial cells. Together, these effects contribute to airflow obstruction. A later phase of inflammatory reaction involves the recruitment and activation of inflammatory cells, such as eosinophils (De Monchy et al., 1985), and CD4+ T cells (Robinson et al., 1993), which subsequently play major roles in the release of proinflammatory mediators (Liu et al., 1991; Smith et al., 1992) and thus in the maintenance of the chronic phase of the response.

Rodents are frequently used in asthma research because they are able to reproduce the global pathological aspects observed in humans following allergen inhalation (Karol, 1994; Canning 2003). In these models, airways inflammation established by allergen administration is commonly assessed by terminal procedures as histology or bronchoalveolar lavage (BAL) fluid analysis.

As previously shown by Beckmann et al. (2001, 2002), lung proton MRI of spontaneously breathing animals provides an efficient alternative tool to assess fluid secretions in the airways in response to either allergen or endotoxin instillation in the rat. Following allergen challenge, this fluid signal has been shown to significantly correlate with the inflammatory parameters in the bronchoalveolar lavage (BAL) fluid (Tigani et al., 2002) and with the perivascular edema quantified by histology (Tigani et al., 2003). Thus, MRI represents a key noninvasive indicator of allergenic inflammation in this rodent model. Besides, this fluid assessment could be of particular interest for diagnostic purposes and for planning and guiding treatment (Beckmann et al., 2001 b).

Thanks to the progress of genetic engineering over the past decade, there has been a shift from the use of rat to murine models of allergenic inflammation for investigations into the molecular basis of asthma and other respiratory disorders. Receptors and intracellular signaling pathways that are subsequently activated can be studied because of the availability of monoclonal antibodies and techniques for targeted gene disruption and gene incorporation for individual mediators, receptors and proteins (Vasquez & Spina, 2000, Chen et al., 2005). Evidently, these essential tools available for the mouse have the potential and proven utility in defining the key events and effector molecules regulating airways inflammation, but also in the drug discovery process.

After allergen provocations in sensitized mice, major characteristics of human asthma including plasma leakage, edema formation and mucus hypersecretion are contributing to luminal airways space narrowing and thus to lung function impairment (Kay, 2001a, 2001b; Bousquet et al., 2000). Worldwide, this model is also routinely used to study the complex mechanism involved in bronchial hyperresponsiveness, another typical feature of human asthma. The way one particular hallmark of airway inflammation is emphasized in the mouse basically determines the differences among several of the murine models described in the literature (Sakai et al., 1999; Haile et al., 1999; Inman et al., 1999; Trifilieff et al., 2000; McCusker et al., 2002; Corteling and Trifilieff, 2004). Among laboratory mouse strains, Balb/c mice are commonly used to study lung inflammation because they develop T helper type 2 cell (Th2)-like response and are highly hyperresponsive. Moreover, they are known to produce high level of antigen-specific IgE and develop a significant airway eosinophilia. Despite their lower levels of antigen-specific IgE and airway responsiveness, C57BL/6 mice are also widely used in purpose to mimic asthma features, especially in studies with a transgenic approach since C57BL/6 is a common genetic background to generate modified mice (Takeda et al., 2001).

Overall, although a wide description in the literature of this murine model of allergic inflammation, up to now, there has been no published information concerning the use of proton MRI in investigation of this mouse model, probably because of technical issues faced with imaging the lung of so small animals.

3.2. Lipopolysaccharide (LPS)-induced mucus hypersecretion in Brown Norway rat airways

Airway mucus hypersecretion is a feature of several lung diseases like asthma, chronic obstructive pulmonary disease (COPD) and cystic fibrosis. It is indicative of poor asthma control and contributes to morbidity and mortality (Rogers 2004). Excess mucus not only obstructs airways but also contributes to airway hyperresponsiveness. Furthermore, asthma might have a specific mucus hypersecretory phenotype. Goblet cell hyperplasia and submucosal gland hypertrophy are shared with COPD (Rogers 2005) which comprises multiple components including pulmonary inflammation, airway remodelling and mucociliary dysfunction. The latter features contribute to the development of chronic, progressive airflow limitation. The mucociliary dysfunction component of COPD is due to mucus hypersecretion coupled with a decrease in mucus transport, and represents an important pathophysiological feature requiring appropriate treatment. There is currently huge research interest in identifying targets involved in inducing mucus abnormalities, which should lead to the rational design of anti-hypersecretory drugs for treatment of airway mucus hypersecretion.

Mucociliary clearance is an important mechanism for removing inhaled particles, secretions and cellular debris from the respiratory tract. In humans and large animals, assessment of mucociliary clearance is most commonly performed using inhaled radiolabeled aerosols and scintigraphy (Figure 9) (Foster and Wagner 2001; Morgan et al 2004).

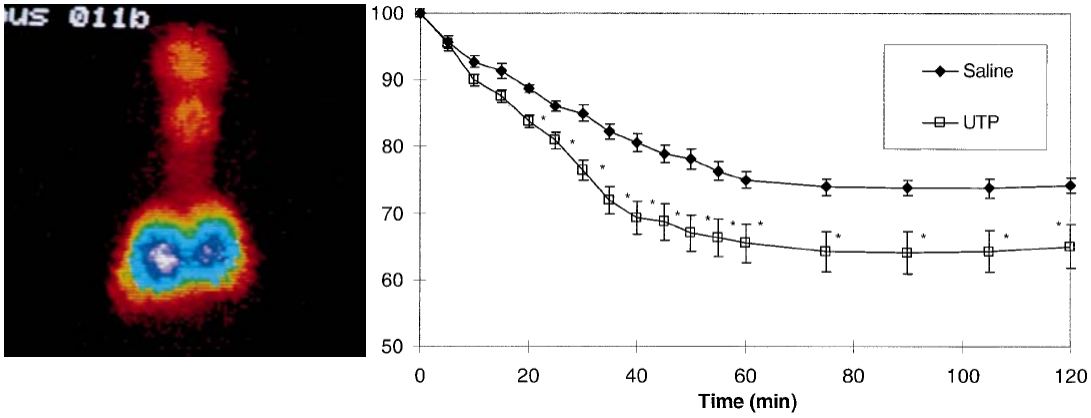

Figure 9 – Left: *Color scintigraphic image of respiratory tract deposition in a mouse after delivery of technetium-labeled sulfur colloid (99mTc-SC) by oropharyngeal aspiration technique. (Foster et al., 2001)* ***Right:*** *Mucociliary clearance rate measured in a Sheep trachea model by inhalation of Technetium-labeled iron oxide particles measured using gamma scintigraphy. (Kellerman et al., 2002)*

In small animals, measurement of the clearance from the lung of fluorescent polystyrene microspheres using serial bronchoalveolar lavage fluid (BAL) is also performed (Coote et al 2004). Evidently, using radioactive materials or performing terminal experiments has its limitations. It would be desirable to have a non-invasive method to measure mucocilliary clearance at high spatial resolution in small rodents. Beckmann et al (2002) have shown previously that magnetic resonance imaging (MRI) can detect a mucus hypersecretory phenotype in Brown Norway (BN) rats after lipopolysaccharide (LPS) challenge. Following challenge of non-sensitised rats with LPS, discontinuous signals of long duration, detectable 8 days after dosing, are detected by MRI in the lung (Figure 10). The only parameter in the BAL fluid that correlates significantly with the MRI signals is the mucus concentration (Beckmann et al 2002; Tigani et al 2002). Histological analysis indicates a substantial and sustained increase in goblet cell number up to 16 days after LPS challenge, and flocculent mucoid material is consistently detected close to the apical surface of the epithelial cells (Beckmann et al 2002). These observations suggest that the long lasting MRI signal following LPS is due to secreted mucus. Nonetheless, the mucus-related signals were of low intensity.

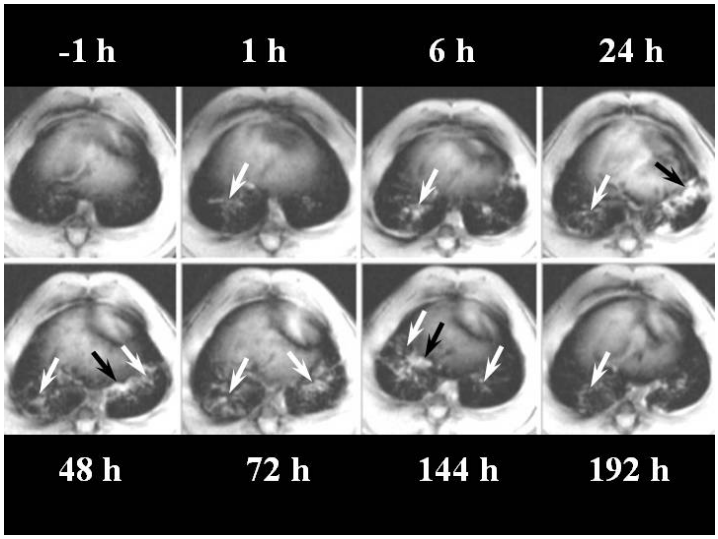

Figure 10 *– Axial sections through the thorax of a single rat in approximately the same position and acquired at various time points following intratracheal challenge with LPS (1 mg/kg). The black and white arrows indicate the two components of the MRI signal detected in the lung, respectively "edema-like" and "mucus-like" signals.*

Thus, in order to improve MRI sensitivity to detect mucus and allow its monitoring, a targeted contrast agent : Gd- and Cy5.5-labeled aminodextrans has been synthesized in house to bind specifically to mucus. Gadolinium is a paramagnetic metal chelate that enhances the proton relaxivity of nearby water molecules and thereby also the signal strength. Additionally, Cy5.5 labeling confers the contrast agent with fluorescent properties which allow its detection by optical imaging modalities.

Adopting this contrast agent, MRI may have the potential to provide a sensitive mean to detect and follow mucus secretion and/or clearance in a rat model of LPS-induced hypersecretion.

3.3. Hypertonicity-induced hydration of the airways secretion in naïve Brown Norway rat

Cystic fibrosis (CF) is a relatively common hereditary disease in Caucasians caused by mutations in the CF transmembrane conductance regulator chloride channel (CFTR) (Deeley et al 2006; Machen 2006; Marcet and Boeynaems 2006). The loss of chloride secretory activity (through CFTR) combined with enhanced Na+ absorption through epithelial sodium channel (ENaC) result in underhydrated mucus, mucostasis and eventual chronic airway infection which result in progressive deterioration of lung function. Therapies that increase the hydration of airway secretions, and hence mucus clearance, should improve lung function in CF patients.

As detailed in the previous section, mucus clearance is an important component of the lung's innate defense against disease, and the ability of the airways to clear mucus is strongly dependent on the volume of liquid on airway surfaces. Indeed, airway surface possesses a mucus component that traps inhaled particles; and a sol layer (airway surface liquid [ASL]) that keeps mucus at an optimum distance from the underlying epithelia, thus affecting the clearance of mucus (Puchelle et al.,1995; Guggino, 2001; Wine, 1999; Knowles & Boucher, 2002; Tarran et al, 2001). In normal airways, the ASL approximates the length of the outstretched cilia (approximately 7µm), whereas the mucus layer varies considerably in height (7 to 70 µm in vivo) (Winters & Yeates, 1997; Jayaraman et al., 2001; Krouse, 2001).

The underlying airway surface epithelium is highly water permeable (Widdicombe et al., 1997; Rahmoune & Shepard, 1995; Sims & Horne, 1997) and is capable of both absorbing Na^+ and secreting Cl^- (Boucher, 1994), which may permit fine tuning of the ASL volume (hydration) to effect efficient mucus clearance, as originally suggested by Kilburn in 1968. The ion and fluid transport through airway epithelia is mediated in part by CFTR, the regulated Cl^- channel that, when mutated, causes the disease cystic fibrosis, and also by the epithelial Na^+ channel ENaC. The latter is composed of three structurally related subunits (α,β,γ) and its activity is regulated by two distinct mechanisms : (i) changes in single channel gating (that is

open probability) or (ii) changes in the number of Na^+ channels expressed in the apical membrane. Besides having an important role in the regulation of the volume of airway surface liquid, ENaC channels are also implicated in the regulation of urinary Na^+ reabsorption, extracellular homeostasis, and control of blood pressure.

Recently, in vitro studies with normal human airway epithelia demonstrated that luminal hypertonic saline increases the volume of ASL, in order to maintain transepithelial isotonicity (Tarran et al., 2001).

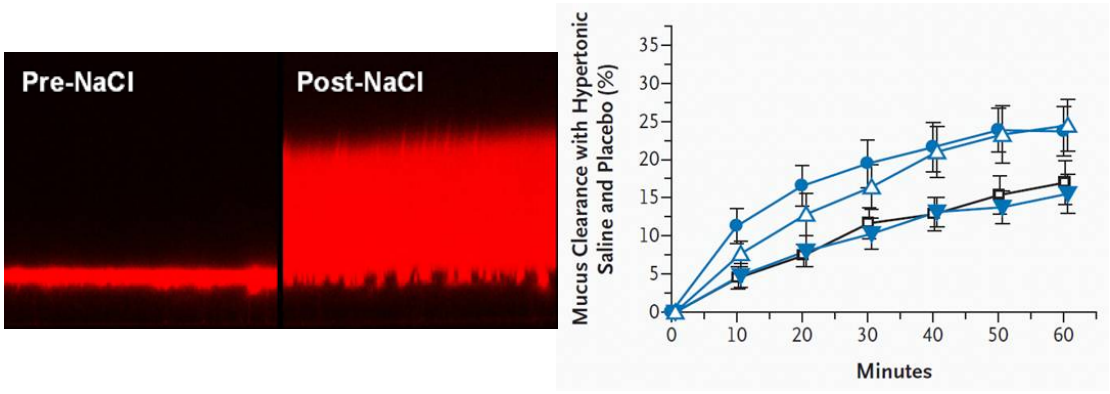

Figure 11 – Left : *Expansion of ASL volume following the addition of 0.9mg NaCl(s) to the apical surface of human bronchic epithelial cells. ASL is labelled with Texas Red Dextran and visualized using confocal microscopy.* ***Right :*** *Inhaled hypertonic saline (7% w/v) acutely improves mucociliary clearance in CF patients when compared with placebo (image courtesy from Donaldson et al., 2006).*

In patients, inhaled HS has been shown to produce short-term stimulation of mucus clearance (Robinson et al. 1997; Donaldson et al. 2006) and to improve lung function (Ballmann and von der Hardt 2002; Eng et al 1996). HS has also been shown to increase mucociliary clearance in healthy subjects and in individuals with asthma or chronic obstructive lung disease (Pavia et al 1978; Daviskas et al 1996). Nevertheless, HS effects were transient and, therefore, of limited therapeutic benefit. Back to in vitro studies, Tarran (2004) demonstrated that slowing the absorption of sodium through epithelium with amiloride, an epithelial sodium-channel (ENaC) blocker, significantly extended the duration of the increase in the volume of airway surface liquid. However, controversial observations have been reported in clinical beneficial evaluation of ENaC blockers (Donaldson et al., 2006; Levin et al., 2006),

suggesting that further studies might help to better understand the mechanism involved in the induced airway surface liquid hydration.

To our knowledge, there is no *in vivo* model available to measure the level of hydration of airways surface liquid. MRI represents a method of choice based on the fact that the technique has been demonstrated to be well suited to quantify fluid signals in the rat lung, in several models of inflammation.

3.4. Bleomycin-induced pulmonary fibrosis in mice

Pulmonary fibrosis, characterized by fibroblast proliferation and extracellular matrix remodeling, is the end result of diverse types of severe lung damage that include usual interstitial pneumonia, desquamative interstitial-pneumonia, non-specific interstitial pneumonia, respiratory bronchiolitis interstitial lung disease, and acute interstitial pneumonia (Lazenby et al., 1990; Katzenstein and Myers 1998; Gross and Hunninhake 2001). In patients with chronic obstructive pulmonary disease (COPD) a patchy alveolar wall fibrosis develops whereas in chronic asthmatics, a fibrotic response occurs predominantly in the lamina reticularis, leading to a thickening of the basement membrane (Brewster et al., 1990; Roche et al., 1989). In both cases the ongoing inflammation-repair cycle leads to permanent structural changes in the airway wall (remodeling) of which fibrosis is a major constituent (Holgate et al., 2000; Jeffery, 2001). However, up to 50% of the cases of pulmonary fibrosis are defined as idiopathic pulmonary fibrosis (Gong et al., 2005). The therapy for idiopathic pulmonary fibrosis is not particularly effective and involves treatment with corticosteroids, antifibrotic agents and other immunosuppressive /cytotoxic agents such as prednisone and cyclophosphamide (Hunninghake and Kalica 1995; International consensus statement 2000; Lasky and Ortiz, 2001).

Scientific progress, most recently in the field of experimental therapy, has relied closely on interpreting data derived from animal modeling. Such models are used to identify the cellular and molecular pathways involved in the lung tissue repair and fibrosis. The simplest strategy to induce experimental pulmonary fibrosis is by directly administrating a profibrotic agent to either wild-type animals or those who

bear a specific genetic modification. Despite an increasing choice of models, there are still good reasons to continue adapting and using on of its earliest examples, the bleomycin (Snider et al., 1978; Thrall et al., 1979; Hay et al., 1991).

Bleomycin is an antibiotic with activity against gram-negative bacteria (Ueda et al., 1983) that also possesses chemotherapeutic properties and is highly efficient in some types of carcinomas. However, bleomycin produces a dose-dependent pulmonary fibrosis in most patients (Gong et al., 2005).

In animal models, the single application of the antibiotic causes an acute inflammatory reaction and fibrotic changes that resemble human fibrotic lung disease both histologically and physiologically (Aso et al., 1976; Thrall et al., 1987; Crouch et al., 1990; Lazenby et al., 1990; Izbicki et al., 2002). In the murine models, C57BL/6 strain were shown to be prone to bleomycin-induced pulmonary fibrosis (Harrison and Lazo, 1998), demonstrating histologic characteristics that bear resemblance to lesions in human fibrotic lung disease, such as parenchymal inflammation, epithelial cell injury and interstitial as well as intra-alveolar fibrosis (Usuki & Fukuda, 1995).

Due to the rapid induction of severe lung injury following bleomycin instillation that leads to pulmonary fibrosis, this model has been regarded by some to mimic closely the forms of human pulmonary fibrosis which follow adult respiratory distress syndrome in patients who have survived into the second week of disease (Coalson, 1982 [book] Fine et al., 1991 [BOOK CHAPTER]), or to typify the Hamman-Rich syndrome (Hamman and Rich, 1935 [book]) rather than the insidious chronic form of human pulmonary fibrosis (Fine et al., 1991). However, it remains true that only *in vivo* models have the potential to recapitulate the complex genetic, biochemical, and environmental interactions that combine to produce pulmonary fibrosis. Thus, the availability of this animal model of pulmonary fibrosis provides the opportunity to investigate novel pharmacological approaches that can be used to treat and prevent this crippling disease (Hay et al., 1991; Lazo et al., 1990; Cortijo et al, 2001).

Nowhere, the most widely used parameters of pulmonary fibrosis in animal models remain the quantitative measurement of lung collagen content and histologic analysis of extracellular matrix deposition (McAnulty et al., 1991) but this method

does not allow for repeated measurements, and requires sacrifice of the animals. Furthermore, histology does not provide information on the entire lung volume. The capacity to non-invasively detect inflammation-related fluid signals and lung tissue density changes could bring proton MRI to become a suitable method for longitudinal monitoring of pulmonary fibrosis in mice.

OBJECTIVES OF THE THESIS

Current methods to evaluate experimental pulmonary diseases in small rodents are generally invasive and terminal. In this contribution, the main objective of the work consisted to illustrate the usefulness of an alternative technique: magnetic resonance imaging (MRI), to obtain anatomical and functional-related information of the lung, with the scope of developing a non-invasive approach for routine testing of drugs in rodent models of airway diseases. With MRI the disease progression can be followed on a same restrained number of animals and a minimal interference with the well-being and physiological status of the animal is achieved.

Thus, the aims of the current work were:

- To develop and evaluate proton MRI capabilities to detect signal changes in the lung of allergen challenged mice, and to provide a quantitative method to correlate these changes with inflammatory status of the lung,
- To illustrate the preceding model in a pharmacological study using transgenic mice,
- To test the potential ability of a contrast agent specific to mucus, to enhance MRI sensitivity in order to detect and follow mucus dynamics,
- To set up and test an *in vivo* model to assess by MRI the level of airways hydration induced by hypertonic instillation and evaluating a possible ENaC-mediated enhancement of this feature in a non-inflammatory model,
- To explore the MRI potential for longitudinal monitoring of a bleomycin-induced fibrosis model in mice.

ORGANISATION OF THE THESIS

The results of this dissertation are presented through several manuscripts and additional data. They correspond to the different models studied to investigate the potential of proton MRI in experimental lung research. First, a murine model of allergen-provoked lung inflammation is primarily described (manuscript 1) in two different strains (additional data) and used as a support for preclinical research in the S1P pharmacology (manuscripts 2 and 3). Then in manuscript 4, we expose the results generated by studying mucus dynamics in a rat model of LPS-induced mucus hypersecretion, using a bi-labeled contrast agent specific to mucus. In manuscript 5, we examined ENaC-mediated effects on a model of hypertonic saline-induced hydration of airway secretions : an *in vivo* model that was set up in this purpose. Finally, in a last section, we describe a preliminary study concerning longitudinal observations imaging a murine model of bleomycin-induced fibrosis.

Manuscript 1 has been accepted for publication in *Radiology*. Results from the manuscripts 2 to 5 will be submitted soon. Of note, additional activities (histology) will need to be pursued to validate the results from manuscript 5 before submission.

This thesis was conducted at and financed by Novartis Institutes for BioMedical Research (NIBR) in Basel, within the departments of Respiratory Diseases Area and Discovery Technologies. Affiliation was with the French Doctoral School “Vie et Santé”, Louis Pasteur University, Strasbourg.

MANUSCRIPT 1

Allergen-induced lung inflammation in actively sensitized mice assessed by MRI

Blé FX, Cannet C, Zurbruegg S, Karmouty Quintana H, Bergmann R, Frossard N, Trifilieff A, and Beckmann N

Allergen-induced Lung Inflammation in Actively Sensitized Mice Assessed with MR Imaging

François-Xavier Blé, Catherine Cannet, Stefan Zurbruegg, Harry Karmouty-Quintana, Reinhard Bergmann, Nelly Frossard, Alexandre Trifilieff, and Nicolau Beckmann

Radiology, 2008, Vol. 248, Pages 834-843

Additional Data

In the perspective of pharmacological investigations using genetically modified animals with C57BL/6 mice background, the objective of the following report was to evaluate if this mouse strain could be used to validate MRI as a relevant non-invasive tool for the investigation of a murine model of allergen-induced airway inflammation. Similarly to the work regarding BALB/c mice presented in the previous chapter, MRI signals detected in the lung of C57BL/6 mice sensitized and challenged with OVA were monitored between and after the allergen provocations and related to bronchoalveolar lavage and histological analysis performed at 24 and 72h after the 4th challenge.

An overview of the data generated by monitoring the allergen-induced lung inflammation model in C57BL/6 mice is provided. Observations are compared with historical results presented in the preceding manuscript using BALB/c mice.

Time course of lung fluid signals assessed by MRI in a murine model of allergen-induced inflammation: A comparison of two strains

ABSTRACT

As in human, in experimental allergic asthma in mice, genetic background is likely to have a major impact on the severity and resolution of the disease.

Comparatively to historical data generated in Balb/c strain, we examined in the lung of actively sensitized C57BL/6 mice plasma leakage- and mucus-related MRI fluid signals between and after multiple ovalbumin challenge. Signals detected by a gradient-echo sequence were compared with the differential cell count and protein

levels in the broncho-alveolar lavage (BAL) fluid, as well as with perivascular and peribronchial edema and mucus observed on lung histological sections.

Despite strain-dependent discrepancies observed in the severity of eosinophilic infiltration and in the course of MRI fluid signals, main features of allergic inflammation including tissue and airway eosinophilia, hypersecretion of mucus, goblet cell hyperplasia and plasma leakage were demonstrated in both strains. Moreover, the volumes of MRI signals detected 24 h after the fourth challenge were comparable in both strains (approximately 40 microliters), and significantly larger than in actively sensitized, saline-challenged mice. As already demonstrated in the BALB/c strain at this time point, the allergen-induced signals detected in C57BL/6 mice were related to both plasma exudation and mucus secretion, respectively confirmed by high level of protein recovered from the BAL and excreted mucus demonstrated by histological analysis.

Overall, the results provided here using MRI as readout of airway secreted fluid in response to allergen provocation constitute the basis for testing compounds in actively sensitized, OVA-challenged C57BL/6 mice.

INTRODUCTION

In the perspective of pharmacological investigations using genetically modified animals, the C57BL/6 strain, which is commonly used as a background to generate transgenic mice, may also be used to study allergen-induced lung inflammation models by MRI. Indeed, strains of mice used in experimental studies of asthma differ in disease profile and in the mechanisms underlying the disease process (Corry et al., 1996; Foster et al., 1996; Herz et al., 1998; Humbles et al.,2004; Rankin et al., 1996; Takeda et al., 2001; Whitehead et al.,2003; Zhang et al., 1997). Despite the fact that BALB/c and C57BL/6 mice differ in the nature and in the underlying mechanisms of the pathophysiology of induced allergic airways disease (Foster et al., 1996; Hamelmann et al., 1999; Humbles et al., 2004; Lee et al., 2004; Takeda et al., 2001), both strains do develop most of the characteristics of asthma, comprising inflammatory cell recruitment to the airways, tissue and airways eosinophilia, extensive production of mucus, airways obstruction, lung edema, and evidence of

increased vascular permeability (Foster et al.,1996; Hussel et al., 1998; MacKenzie et al., 2001; Tumes et al., 2007).

In the present work, fluid signals from multiple MRI acquisitions of sensitized C57BL/6 mice have been followed between and after either ovalbumin (OVA) or saline challenges. The MRI data were then related to post mortem analyses performed at 24 h and 72 h after the last challenge and consisting in differential cell count and protein levels assays of the BAL fluid as well as the demonstration of mucus secretion and of the presence of perivascular and/or peribronchial edema on lung histological sections. Referring to previously described observations in the Balb/c strain, the data generated in this report allowed a comparison of the two strains in our model of allergen-induced lung inflammation, using lung MRI.

MATERIALS AND METHODS

Sensitization and Challenge Protocol

To compare the data generated by studying C57BL/6 with existing results from the model using BALB/c mice, the protocol described in the previous chapter was applied (figure 1). Briefly, 7- to 9-week old female C57BL/6 mice (Janvier, Le Genest-St-Isle, France) were immunized on days 0 and 14 by intraperitoneal injection of 0.2 ml of OVA (250 µg/ml) mixed with aluminum hydroxide (10 mg/ml) in saline. On days 18, 19, 20 and 21, mice were lightly anesthetized with 2% isoflurane (Abbott, Cham, Switzerland) and 100 µg of OVA in 25 µl of saline (SENS/OVA group; n=20 animals) or vehicle (25 µl of saline) (SENS/SAL group; n=12 animals) was administered intranasally (i.n.).

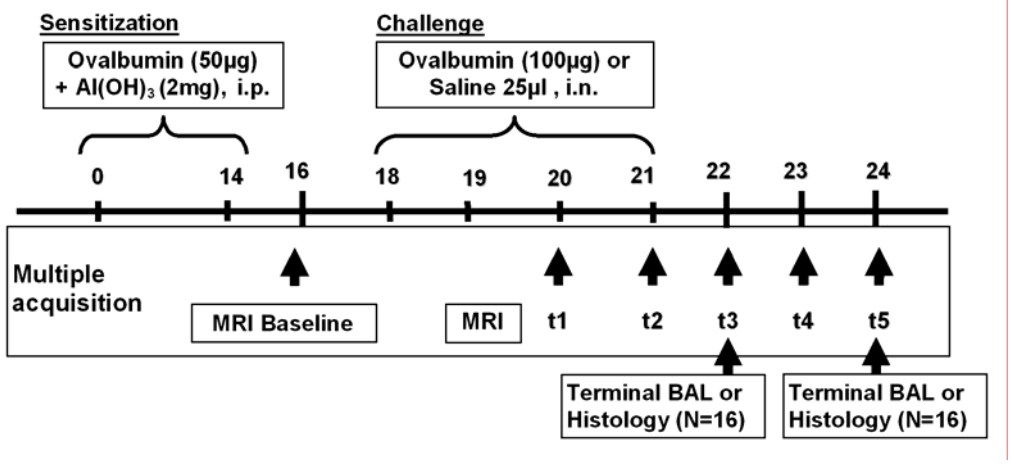

Figure 1 *- Experimental protocol: MR images were acquired 24 h after the 2nd challenge (t1), 24 h after the 3rd challenge (t2), and at various time points after the 4th challenge, namely at 24 h (t3), 48 h (t4) as well as 72 h (t5). Either 24 h or 72 h after the 4th challenge, mice were sacrificed for BAL fluid or histological analyses immediately after the last MRI scan.*

MRI

MRI measurements were carried out in vivo with a Biospec 47/40 spectrometer (Bruker Medical Systems, Karlsruhe, Germany) operating at 4.7 T, equipped with an actively shielded gradient system capable of generating a gradient of 200 mT/m. A birdcage resonator of 32 mm diameter was used for excitation and detection. Gradient-echo images were acquired with the following parameters: repetition time 5.6 ms, echo time 3.5 ms, band width 100 kHz, flip angle of the excitation pulse approximately 10°, matrix size 256 x 128, slice thickness 0.75 mm and field of view 3 x 3 cm^2. A single slice image (acquisition time of 74 s) was obtained by computing the two-dimensional Fourier transform of the averaged signal from 60 individual acquisitions and interpolating the data set to 256 x 256 pixels. The entire lung was covered by 16 consecutive transverse slices. During measurements, mice were anaesthetized with 1.5% isoflurane in a mixture of O_2/N_2O (1:2), administrated via a face cone. Animals were allowed to breath spontaneously, and neither respiratory nor cardiac gating was applied. Body temperature was maintained at 37±1°C by a flow of warm air.

MRI scans of the mouse lung were performed at day 16 for baseline acquisition as well as between (24 h after the 2nd and the 3rd challenge) and at multiple time points (24 h, 48 h and 72 h) after the 4th challenge (Figure 1). In comparison to the

multiple acquisition protocol used with BALB/c mice, the 6 hour time point after the 4th challenge was omitted to allow measurement of all mice in one sole experiment.

Image Analysis

The volume of MRI signals was quantified using a semi-automatic segmentation procedure implemented in the IDL (Interactive Data Language Research Systems, Boulder, Colorado, USA) environment on a Linux system (Beckmann et al. 2001). Images were first weakly lowpass filtered with a Gaussian profile filter and then transformed into a set of four grey level classes using adaptive Lloyd-Max histogram quantitation. The highest grey level class in the transformed images could be extracted interactively by use of a region grower. Contour serving as a growing border was drawn to control region growing manually. Since the signals from extravascular fluid and vessels were of comparable highest intensities, the volume corresponding to the vessels was assessed on baseline images and then could be subtracted from the volumes determined on post-challenge images.

Post-mortem analyses

Animals were killed by intraperitoneal injection of 0.2 ml of pentobarbitone (250 mg/kg), immediately after an MRI acquisition. BAL fluid analysis (n=8 SENS/OVA mice; n=4 SENS/SAL mice) or histology (n=2 SENS/OVA mice; n=2 SENS/SAL mice) was carried out immediately after an MRI acquisition at 24 h or 72 h following the 4th challenge.

- *Bronchoalveolar lavage (BAL) Fluid Analysis*

The trachea was cannulated and the lung lavaged by gently injecting 8 times via the trachea, without any chest massage, 0.5 ml of the BAL solution prepared with (i) Hank's balanced salt solution (HBSS); (ii) Ethylenedaminetetraacetic acid (EDTA) 1mM; (iii) 4-(2-hydroxyethyl)-1-piperazinethanesulphonic acid (HEPES) 0.1M,; (iv) D-glucose anhydrous, 1g and (v) distilled water, 790ml. The BAL fluid obtained by aspiration after the first two lavages was centrifuged (400 *g*, 8 min, 4 °C; Omnifuge 2.0, Heraeus Sepatech, Stuttgart, Germany) and the supernatant was frozen at -80 °C for later protein assay [described in detail in Tigani et al., 2002]. Briefly, protein

levels in the supernatant were measured by a photometric assay, based on the reaction of proteins with an alkaline copper tartrate solution and a Folin reagent. An aliquot from the 6 further lavages was used for total cell count in an automatic cytometer (Cobas Helios 5Diff, Hoffmann-La Roche, Axon Lab, Basel, Switzerland). From each aliquot, a sample containing approximately 50,000 cells was used for cytospin preparation. Cells were stained with Diff-Quik and a differential count of 200 cells (eosinophils, macrophages, neutrophils, lymphocytes) was obtained by observing cytospin slides under a classic light microscope (x100, oil immersion) using standard morphological criteria.

- *Histology*

The trachea was immediately ligated to avoid collapse and the entire lung was removed and immersed in 10% neutral buffered formalin for 72 h. The lungs were then cut longitudinally in order to analyze all lobes. After dehydration of tissues through increasing graded series of ethylic alcohol and processing to paraffin wax, sections were embedded in blocks. Slices of 3 μm thickness were cut so as to observe the main bronchi of each lobe. Slices were stained with hematoxylin and eosin to assess the general morphology, with Verhoeff/Van Gieson‘s method for the demonstration of elastic fibers in arteries and to determine perivascular edema, as well as with Alcian Blue/Periodic Acid Schiff’s (AB/PAS) for demonstrating excreted mucus and mucus-containing goblet cells.

RESULTS

MRI

Transverse MRI sections from two levels through the chests of one actively sensitized mice, acquired at 24 h and 72 h after the last of the four intranasal administrations of OVA, are displayed in figure 2a. Discrete MRI signals, mainly located in the proximal regions of the lung (upper transverse sections on figure 2a) were detected at either 24 or 72 hours after the last OVA challenge. At both time points, MRI signals were of low intensity and widely distributed in the lungs of actively sensitized, OVA-challenged C57BL/6 mice.

The course of volumes of fluid signals for OVA- and saline-challenged C57BL/6 mice assessed from the MR images is displayed with black bars in figure 2b. At all measured time points, a significantly increased signal was observed in OVA-challenged mice when compared to saline-challenged controls. The signal volume increased progressively following successive allergen challenges and reached a maximal value of 39.0±5.4 microliters at 24 h after the 4^{th} challenge. At following time points (48 and 72 h after the 4^{th} challenge) a volume of approximately 30 microliters was maintained. The course of MRI signals for BALB/c mice is presented in the same figure for sake of comparison (white bars). The curves show a clear difference in the early time points, where BALB/c animals demonstrated more prominent signals. However, comparable volumes of signals were quantified 24 h after the 4^{th} challenge in both strains. Finally, at the latest time point, while a tendency to signal decrease was observed for BALB/c mice, volumes of fluid signals were maintained in C57BL/6 animals.

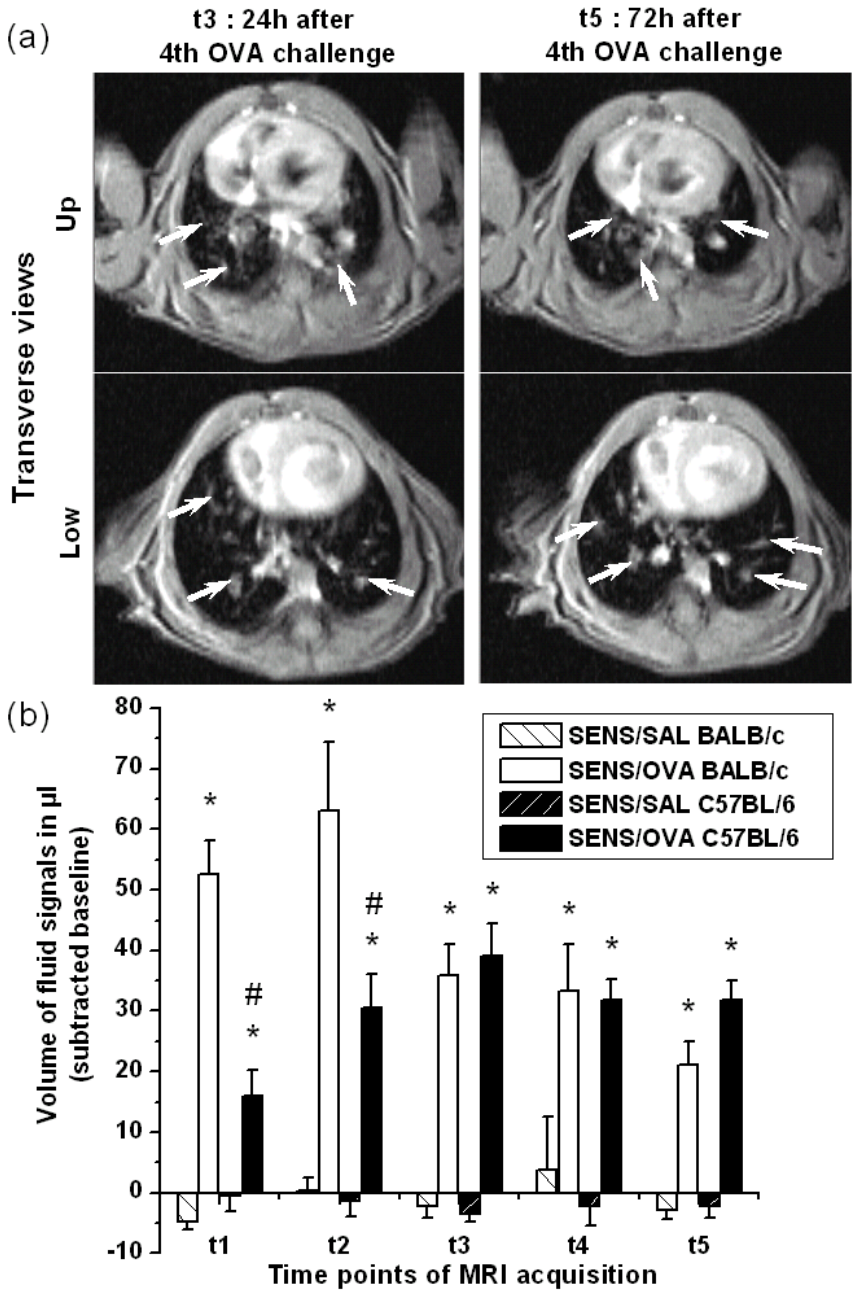

Figure 2 – (a) *Representative MRI transverse sections through the thorax of immunized C57BL/6 mice (N=12), acquired 24 h and 72 h after the last intranasal administration of OVA (100µg in 25 µl of saline, on 4 consecutive days). Arrows indicate fluid signals.* ***(b)*** *Course of volume of MRI signals (mean of the difference post- and pre-challenge ± SEM; N= 8 to 12 mice per group) assessed at different time points between (t1: 24 h after 2nd; t2: 24 h after 3rd) and after challenges (t3: 24 h after 4th; t4: 48 h after 4th; t5: 72 h after 4th) in both BALB/c and C57BL/6 strains. All animals had been actively sensitized to the allergen. SENS/SAL and SENS/OVA mice were challenged with saline and OVA, respectively. The levels of significance are *p<0.05 SENS/SAL vs SENS/OVA and #p<0.05 Balb/c vs C57BL/6*

Post mortem analyses

By analogy to previous observations in BALB/c mice, the total number of cells was significantly higher (P<0.001 SENS/OVA vs SENS/SAL) in BAL fluid samples

from OVA- (2.58±0.27x10^6cells/ml of BAL fluid at 24h; 2.80±0.09x10^6cells/ml of BAL fluid at 72 h) compared to saline-challenged (0.20±0.04x10^6cells/ml of BAL fluid at 24 h; 0.23±0.03x10^6cells/ml of BAL fluid at 72 h), actively sensitized C57/BL6 mice. BAL fluid differential cell count assessed immediately after the MRI acquisitions at 24 and 72 h after the fourth challenge are summarized in figure 3.

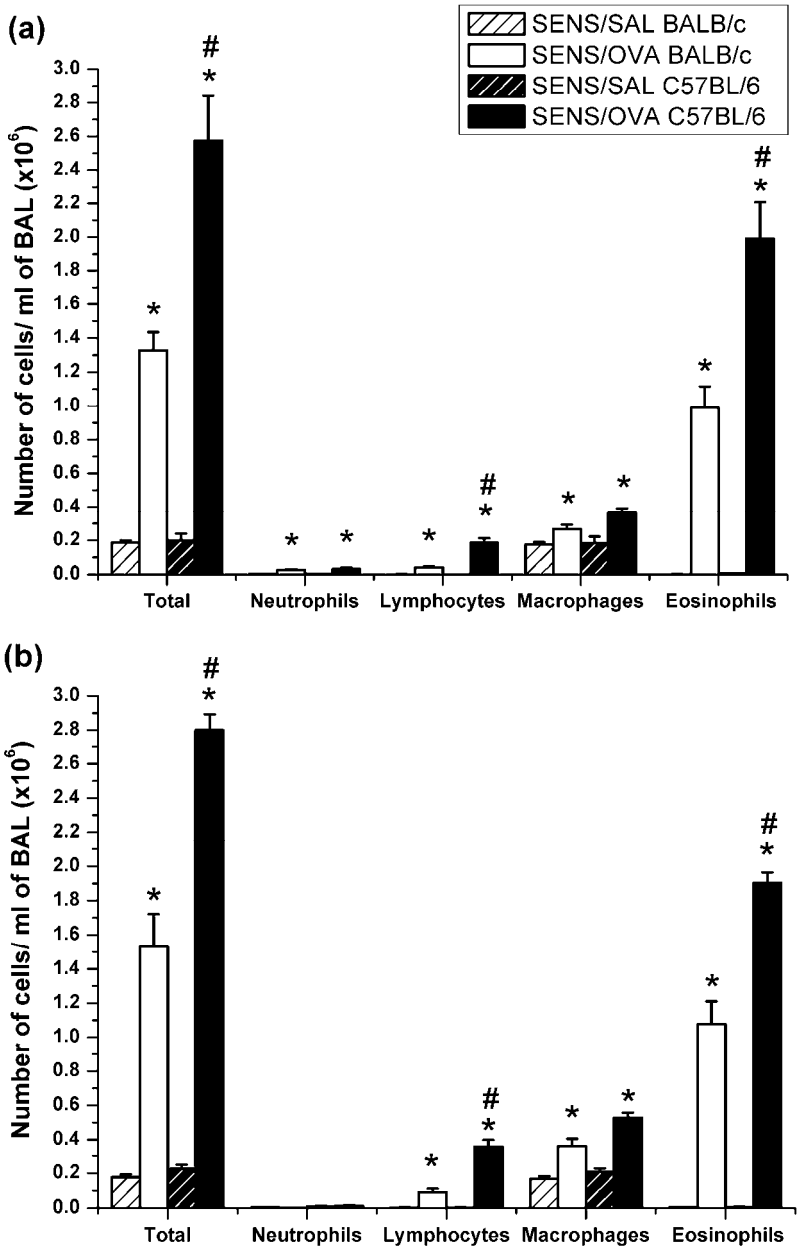

Figure 3 –*Total and differential number of BAL cells established on cytospin preparations from BAL samples recovered* ***(a)*** *24 h and* ***(b)*** *72 h after the 4th challenge. SENS/SAL mice received i.p. immunization and i.n. saline challenges; SENS/OVA mice received i.p. immunization and i.n. ovalbumin challenges as described. Data are expressed as means±SEM (n=6 mice per group and time point), *p<0.001 SENS/SAL vs SENS/OVA; #p<0.001 Balb/c vs C57BL/6.*

Of note, at both time points, the number of eosinophils recovered from the BAL of OVA-challenged mice was significantly augmented in the C57BL/6 compared to the BALB/c strain (24 h: 1.99±0.22 vs 0.99±0.13 x 10^6 cells/ml, P<0.001; 72 h: 1.90±0.06 vs 1.08±0.13 x 10^6 cells/ml, P<0.001). In both strains, in the saline-challenged mice, macrophages constituted the greatest cell type proportion, whereas in the OVA-challenged animals, eosinophilia was predominant at both time points. In analogy to BALB/c mice, neutrophils in the C57BL/6 strain were significantly increased at 24 h (0.03±0.01 x 10^6cells/ml in SENS/OVA vs 0.005±0.001 x 10^6cells/ml in SENS/SAL) but returned to baseline levels 72 h after the last allergen challenge (0.01±0.01 x 10^6cells/ml in SENS/OVA vs 0.01±0.003 x 10^6cells/ml in SENS/SAL). Lymphocytes were also elevated at 24 h (0.019±0.03 x 10^6cells/ml in SENS/OVA C57BL/6 vs 0.002±0.001 10^6cells/ml in SENS/SAL C57BL/6) and were further increased at the subsequent time point (0.36±0.04 x 10^6cells/ml in SENS/OVA C57BL/6 vs 0.003±0.001 x 10^6cells/ml in SENS/SAL C57BL/6). Furthermore, at both time points the lymphocyte levels in SENS/OVA mice were higher in C57BL/6 compared to BALB/c mice (P<0.001). As reported in figure 4, in both strains the protein levels were also significantly higher (P<0.001 SENS/OVA vs SENS/SAL) 24 h after the last allergen challenge when compared to saline instillation, and either maintained in C57BL/6 or slightly reduced in BALB/c mice at 72 h after the 4th challenge.

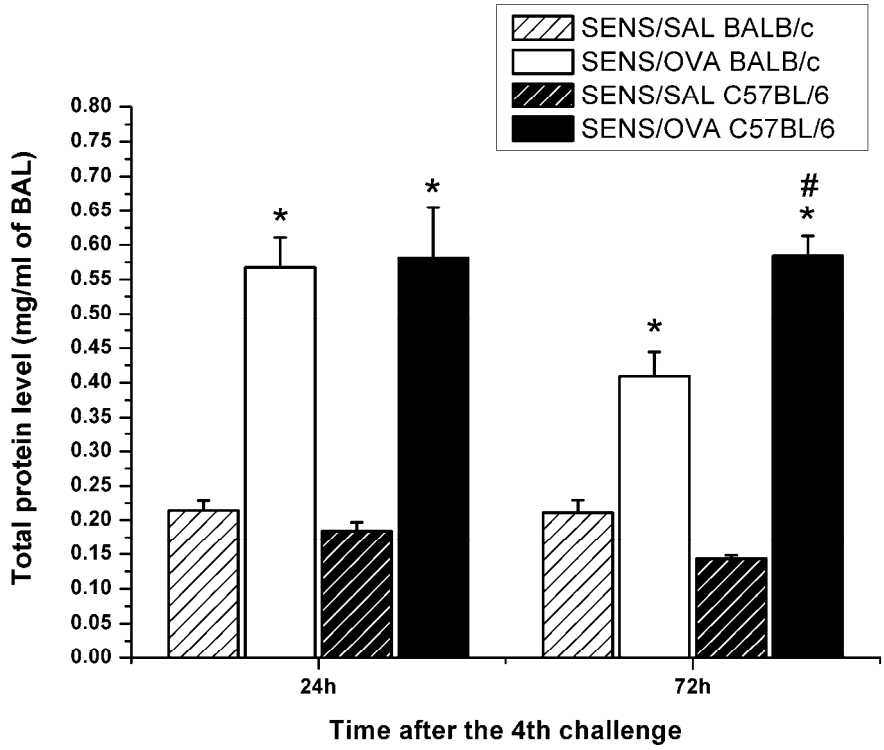

Figure 4 *– Strain and treatment comparison of total protein levels quantified in the BAL fluid recovered at 24 h (left) and 72 h (right) after the 4th challenge. SENS/SAL mice received i.p. immunization and i.n. saline challenges; SENS/OVA mice received i.p. immunization and i.n. ovalbumin challenges as described. Data are expressed as Means±SEM (n=6 mice per group), *p<0.05 SENS/SAL vs SENS/OVA; #p<0.05 Balb/c vs C57BL/6.*

Histological analysis of hematoxylin/eosin-stained lung tissue sections from OVA-challenged animals demonstrated, at 24 h and 72 h following the last challenge, severe peribronchial and perivascular polynuclear cell infiltration (figure 5, black arrow). At both time points, the cellular inflammation was predominantly located in the hilar region, in the vicinity of the first generation airways, but also in more distal regions of the lung when compared to the essentially proximal infiltrate in BALB/c mice. AB/PAS staining revealed clear metaplasia of goblet cells and luminal mucus hypersecretion (figure 5, red arrows) on all lung tissue sections from OVA-challenged mice at 24 h and 72 h. No cell infiltration neither PAS positive cells nor luminal mucus secretion were observed on lung sections from actively sensitized C57BL/6 challenged with saline (Figure 5 , first row).

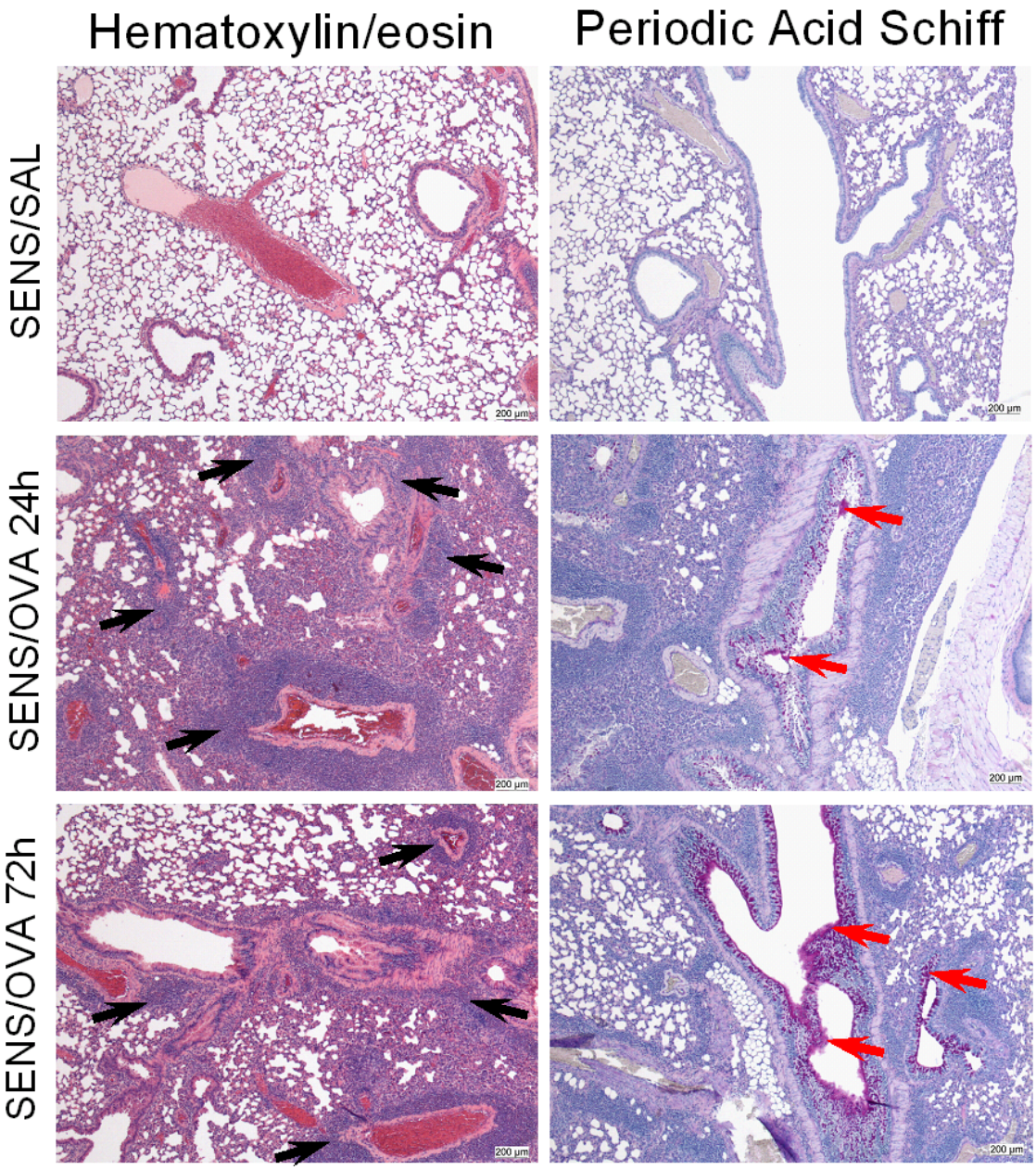

***Figure 5** – Histological sections from the lungs of a SENS/SAL mouse (top, 24 h after last saline challenge) or from SENS/OVA C57BL/6 mice sacrificed 24 h (middle) and 72 h after last OVA challenge (bottom), demonstrating perivascular and peribronchic polynuclear infiltration (black arrows) after hematoxylin and eosin staining (first column) and mucus secretion and goblet cell metaplasia (red arrows) after periodic acid Schiff's staining.*

DISCUSSION

This study demonstrated increased MRI fluid signals in response to allergen challenges in the lungs of sensitized C57BL/6 mice, a similar result as that obtained previously in BALB/c mice. However, this work also highlighted differences

between the two strains in the course as well as in the texture of the MRI signals, mainly at the early time points after allergic provocation. Indeed, while BALB/c had shown localized and prominent volumes of intense signals after the first allergen challenges that slowly decreased until 72 h after the 4th challenge, C57BL/6 demonstrated more discrete and widespread signals increasing between the challenges and stabilizing until the last time point. Thus, the distinction of early and late phases postulated in the BALB/c study and related respectively to plasma leakage and mucus secretion, was not observed in the C57BL/6 strain, and the volumes of MRI signals at 24 h and 72 h after the last OVA challenge did not differ.

Besides considerations of kinetics, the strain differences concerning the texture and the intensity of the MRI signals may be explained by the greater infiltration of pro-inflammatory cells observed in C57BL/6 mice, a results that has also been reported by Atochina et al. (2003). The high density of infiltrated eosinophils in the perivascular and peribronchial regions precluding the emphasis of edema on histological sections might also have reduced the proton mobility in infiltrated plasma and therefore induced a reduction in MRI signal intensity. Compared to the BALB/c strain, the signals in the lungs of allergen-challenged C57BL/6 animals were also more widespread, an observation that could be explained by a more peripheral extent of the eosinophilic infiltration, i.e. in the distal parenchymal regions as previously shown by Takeda et al. (2001). Moreover, in contrast to BALB/c mice, no massive bulk of fluid was detected by MRI in C57BL/6 animals suggesting a lower susceptibility of this strain for prominent edema formation in response to the first allergen challenges. This hypothesis would need further investigations to be confirmed.

Interstingly, C57BL/6 mice are known to be relatively hyporesponsive to non-specific airway stimuli and resistant to development of allergic airway hyperresponsiveness in comparison to other inbred mouse strains (Nicolaides et al., 1997; Takeda et al., 2001; Zhang et al., 1997). Although the exact mechanisms that determine susceptibility or resistance to develop allergic airway hyperresponsiveness remain unclear, airway inflammation is thought to play a role (Broide, 2001; Corrigan & Kay, 1992; De Sanctis et al., 1997; Drazen et al., 1996; Holt et al., 1999; Wills-Karp, 1999). Therefore, it would be interesting to complete the present work

with assessement of airway hyperresponsiveness and to correlate the functional data with inflammatory parameters and with fluid secretions detected by MRI to further investigate the differences between the two strains.

Despite these strain-dependent discrepancies, global features of asthmatic phenotype were observed in both BALB/c and C57BL/6 mice. Indeed, tissue and airway eosinophilia, hypersecretion of mucus, goblet cell hyperplasia and plasma leakage were demonstrated in both strains. Moreover, the volumes of MRI signals detected 24 h after the fourth challenge were comparable in both strains (approximately 40 microliters), and significantly larger than in actively sensitized, saline-challenged mice. As already demonstrated in the BALB/c strain at this time point, the allergen-induced signals detected in C57BL/6 mice were related to both plasma exudation and mucus secretion, respectively confirmed by high level of protein recovered from the BAL and excreted mucus demonstrated by histological analysis.

In conclusion, since major features of airways inflammation observed and characterized in BALB/c were conserved in C57BL/6 mice, the results provided here using MRI as readout of airway secreted fluid in response to allergen provocation constitute the basis for testing compounds in actively sensitized, OVA-challenged C57BL/6 mice by MRI.

REFERENCES

Broide D.H. (2001) Molecular and cellular mechanisms of allergic disease. *J Allergy Clin Immunol*, **108:**S65-S71.

Corrigan C.J., Kay A.B. (1992) T cells and eosinophils in the pathogenesis of asthma. *Immunol Today*, **13:**501-507.

Corry D. B., Folkesson H. G., Warnock M. L., Erle D. J., Matthay M. A., Wiener-Kronish J. P., Locksley R. M. (1996) Interleukin 4, but not interleukin 5 or eosinophils, is required in a murine model of acute airway hyperreactivity. *J. Exp. Med.* **183,** 109–117.

De Sanctis G.T., Itoh A., Green F.H., Qin S., Kimura T., Grobholz J.K., Martin T.R., Maki T., Drazen J.M. (1997) T-lymphocytes regulate genetically determined airway hyperresponsiveness in mice. *Nat Med*, **3:**460-462.

Drazen JM, Arm JP, Austen KF (1996) Sorting out the cytokines of asthma. *J Exp Med*, **183:**1-5.

Foster P. S., Hogan S. P., Ramsay A. J., Matthaei K. I., Young I. G. (1996) Interleukin 5 deficiency abolishes osinophilia, airways hyperreactivity, and lung damage in a mouse asthma model. *J. Exp. Med.* **183,** 195–201.

Hamelmann E., Cieslewicz G., Schwarze J., Ishizuka T., Joetham A., Heusser C., Gelfand E. W. (1999) Anti-interleukin 5 but not anti-IgE prevents airway inflammation and airway hyperresponsiveness. *Am. J. Respir. Crit. Care Med.* **160,** 934–941.

Herz U., Braun A., Ruckert R., Renz H. (1998) Various immunological phenotypes are associated with increased airway responsiveness. *Clin. Exp. Allergy* **28,** 625–634.

Holt P.G., Macaubas C., Stumbles P.A., Sly P.D. (1999) The role of allergy in the development of asthma. *Nature*, **402:**B12-B17.

Humbles A. A., Lloyd C. M., McMillan S. J., Friend D. S., Xanthou G., McKenna E. E., Ghiran S., Gerard N. P., Yu C., Orkin S. H., Gerard C. (2004) A critical role for eosinophils in allergic airways remodeling. *Science* **305,** 1776–1779.

Hussell T., Georgiou A., Sparer T. E., Matthews S., Pala P., Openshaw P. J. (1998) Host genetic determinants of vaccine-induced eosinophilia during respiratory syncytial virus infection. *J. Immunol.* **161,** 6215– 6222.

Lee J. J., Dimina D., Macias M. P., Ochkur S. I., McGarry M. P., O'Neill K. R., Protheroe C., Pero R., Nguyen T., Cormier S. A., Lenkiewicz E., Colbert D., Rinaldi L., Ackerman S. J., Irvin C. G., Lee N. A. (2004) Defining a link with asthma in mice congenitally deficient in eosinophils. *Science* **305,** 1773–1776.

MacKenzie J. R., Mattes J., Dent L. A., Foster P. S. (2001) Eosinophils promote allergic disease of the lung by regulating CD4+ Th2 lymphocyte function. *J. Immunol.* **167,** 3146–3155.

Nicolaides N.C., Holroyd K.J., Ewart S.L., Eleff S.M., Kiser M.B., Dragwa C.R., Sullivan C.D., Grasso L., Zhang L.Y., Messler C.J., Zhou T., Kleeberger S.R., Buetow K.H., Levitt R.C. (1997) Interleukin 9: a candidate gene for asthma. *Proc Natl Acad Sci U S A*, **94:**13175-13180.

Rankin J. A., Picarella D. E., Geba G. P., Temann U. A., Prasad B., DiCosmo B., Tarallo A., Stripp B., Whitsett J., Flavell R. A. (1996) Phenotypic and physiologic characterization of transgenic mice expressing interleukin 4 in the lung: lymphocytic and eosinophilic inflammation without airway hyperreactivity. *Proc. Natl. Acad. Sci. USA* **93,** 7821– 7825.

Takeda K., Haczku A., Lee J. J., Irvin C. G., Gelfand E. W. (2001) Strain dependence of airway hyperresponsiveness reflects differences in eosinophil localization in the lung. *Am. J. Physiol. Lung Cell. Mol. Physiol.* **281,** L394–L402.

Tigani B, Schaeublin E, Sugar R, Jackson AD, Fozard JR, Beckmann N. (2002) Pulmonary inflammation monitored non-invasively by MRI in freely breathing rats. Biochem Biophys Res Commun;**292**:216-221.

Whitehead G. S., Walker J. K., Berman K. G., Foster W. M., Schwartz D. A. (2003) Allergen-induced airway disease is mouse strain dependent. *Am. J. Physiol. Lung Cell. Mol. Physiol.* **285,** L32–L42.

Wills-Karp M. (1999) Immunologic basis of antigen-induced airway hyperresponsiveness. *Annu Rev Immunol*, **17:**255-281.

Zhang Y., Lamm W. J., Albert R. K., Chi E. Y., Henderson Jr W. R., Lewis D. B. (1997) Influence of the route of allergen administration and genetic background on the murine allergic pulmonary response. *Am. J. Respir. Crit. Care Med.* **155,** 661–669.

MANUSCRIPT 2

Intranasal instillation of FTY720 reduces lung MRI fluid signals in a murine model of allergen-induced inflammation: example of a S1P1 agonism

Blé FX, Cannet C, Zurbruegg S, Gérard C, Frossard N, Beckmann N, Trifilieff A

Intranasal instillation of FTY720 reduces lung MRI fluid signals in a murine model of allergen-induced inflammation: example of a $S1P_1$ agonism

Blé FX, Cannet C, Zurbruegg S, Gérard C, Frossard N, Beckmann N, Trifilieff A.

ABSTRACT

The sphingosine 1-phosphate (S1P) receptor agonist FTY720 is an oral immunomodulator that sequesters lymphocytes in secondary lymphoid organs and thereby prevents their migration to sites of inflammation. Moreover, it has been recently suggested that local administration of the compound could have anti-inflammatory effects without causing lymphopenia. We have recently described in an in vivo murine model of allergen-induced inflammation the use of proton magnetic resonance imaging (MRI) to non-invasively assess in the lung plasma leakage- and mucus-related signals, which correlated with inflammatory parameters recovered from the broncho-alveolar lavage (BAL) and with histological analyses (Blé et al., submitted). In the present work we have used this model to investigate the effects of intranasal administration of FTY720 prior to allergen challenges in actively sensitized mice. Budesonide was used as a reference compound. Furthermore, the targeted S1P receptors were identified using $S1P_3$ receptor deletion and $S1P_1$ selective agonist. By evaluating the effects of intranasal administration of FTY720 prior to allergen challenge in actively sensitized mice, we demonstrated that when no systemic effect was observed, the OVA-induced MRI fluid signals were reduced but not the eosinophil infiltration neither the mucus secretory phenotype. Similar results were obtained by evaluating the influence of the selective $S1P_1$ agonist AUY954. In addition, deletion of $S1P_3$ did not compromised FTY720 pretreatment effects and thus showed that $S1P_3$ receptors are not implicated. Our observations suggest that the

reduction of fluid MRI signals, related to plasma leakage and mucus secretion, is mainly explained by the action on endothelial barrier integrity through $S1P_1$ receptors, rather than by an anti-inflammatory effect of the compound. Additionally, we have shown in the present work the usefulness of lung MRI to investigate airway inflammation and its pharmacology.

INTRODUCTION

Inflammatory processes represent a protective response against insults to the organism. They involve the recruitment of many cell types and the production of various inflammatory mediators in attempts to contain and reverse the insult. However, chronic inflammation can lead to irreversible tissue destruction. There is now evidence that sphingosine-1-phosphate (S1P) and its receptors regulate inflammatory processes on several levels. S1P is primarily generated from the cell membrane constituent sphingomyelin via the metabolites ceramide and sphingosine. A variety of inflammatory factors, including interleukine-1, tumor necrosis factor-α and vascular endothelial growth factor, activate S1P to the convert intracellular, pro-apoptotic sphingosine into anti-apoptotic S1P (Chalfant & Spiegel, 2005), and reduces the turn-over and death of pro-inflammatory cells, e.g. of effector T-cells (Goetzl et al., 1999). Furthermore, S1P regulates cell migration and trafficking either by acting as a chemoattractant for migrating cells, or by modulating permeability barriers between different tissues.

The S1P agonist, FTY720, is a novel immunomodulator that sequesters lymphocytes into secondary lymphoid organs, and thereby prevents their migration to sites of inflammation [see Zhang and Schluesener (2007) for a recent review]. Acting through 4 of the 5 G protein-coupled S1P receptors ($S1P_1$, $S1P_{3-5}$), FTY720 is able to modulate cell trafficking and inflammation, as well as endothelial and epithelial barrier function with variable means, depending on the S1P receptor type involved and the targeted cell type/tissue.

We have recently described in an in vivo murine model of allergen-induced inflammation the use of proton magnetic resonance imaging (MRI) to non-invasively assess in the lung plasma leakage- and mucus-related signals, which correlated with

inflammatory parameters recovered from the broncho-alveolar lavage (BAL) and with histological analyses (Blé et al., submitted). Contributing to the functional impairment of the lung, plasma leakage and mucus hypersecretion are important features of airways inflammation, directly influenced by the degree of the inflammatory response and by the barriers integrity in the lung tissues. Being able to quantify the volume of interstitial and luminal fluids in a non-invasive manner constitutes an advantage to investigate in vivo the effects of anti-inflammatory drugs and of barrier-protective compounds.

In this work we have used this model to investigate the effects of intranasal administration of FTY720 prior to allergen challenges of actively sensitized mice. Budesonide was used as a reference compound. Signals detected by MRI were related to differential cell count in the bronchoalveolar lavage fluid and the blood as well as to the cell infiltrate and epithelial mucus hypersecretory phenotype demonstrated by histological analyses. Furthermore, the targeted S1P receptors were identified using $S1P_3$ receptor deletion and $S1P_1$ selective agonist.

MATERIALS AND METHODS

Animals

Seven- to 9-week-old C57BL/6 female mice (Janvier, Le Genest-St-Isle, France) were used throughout the study. They were housed in a temperature- and humidity-controlled environment, with free access to standard mouse chow and tap water.

For generation of $S1P_3$ knock-out mice, ES cells derived from the 129/OlaHsd mouse substrain were used to generate chimeric mice. F1 mice were generated by breeding with C57BL/6 females. F2 homozygous mutants were produced by intercrossing F1 heterozygous males and females. Experiments were carried out with the approval of the Veterinary Authority of the City of Basel (license number 1989).

Allergen Sensitization and Challenge

Ovalbumin (OVA, 250 µg/ml; Fluka, Buchs, Switzerland) was mixed (30 minutes on ice) in a blender with aluminum hydroxide (10 mg/ml) in saline and injected intraperitoneally on days 0 and 14 (0.2 ml per animal). On day 18 mice were lightly anesthetized with 2 % isoflurane (Abbott, Cham, Switzerland) and 100 µg of OVA in

25 µl of saline or vehicle (25 µl of saline) was administered intranasally (i.n.) via a micropipette (12.5 µl per nostril). Animals were allowed to recover immediately after. This procedure was repeated on days 19, 20 and 21.

Drug Treatment

Glucocorticosteroid budesonide (Sicor, Milan, Italy) was dissolved in DMSO (2 % final concentration) and diluted with saline. FTY720 obtained from Novartis Pharmaceuticals (Basel, Switzerland) was dissolved in distilled water. The selective $S1P_1$ agonist AUY954 (Pan et al., 2006) obtained from Novartis Pharmaceuticals (Basel, Switzerland) was dissolved in 2 % DMSO in saline. Animals were lightly anaesthetized and budesonide (3 mg/kg), FTY720 (0.003, 0.01, 0.03 or 0.1 mg/kg), AUY954 (0.003 or 0.01 mg/kg) or their corresponding vehicles were administered intranasally, in a volume of 25 µl (12.5 µl per nostril), 30 minutes before each intranasal OVA challenge. The number of mice per group was 8.

MRI

At baseline (on day 16) and 24 h after the last OVA challenge, measurements were carried out in vivo with a Biospec 47/40 spectrometer (Bruker Medical Systems, Karlsruhe, Germany) operating at 4.7 T, equipped with an actively shielded gradient system capable of generating a gradient of 200 mT/m. A birdcage resonator of 32 mm diameter was used for excitation and detection. Gradient-echo images were acquired with the following parameters: repetition time 5.6 ms, echo time 3.5 ms, band width 100 kHz, flip angle of the excitation pulse approximately 10°, matrix size 256 x 128, slice thickness 0.75 mm and field of view 3 x 3 cm^2. A single slice image (acquisition time of 74 s) was obtained by computing the two-dimensional Fourier transform of the averaged signal from 60 individual acquisitions and interpolating the data set to 256 x 256 pixels. The entire lung was covered by 16 consecutive transverse slices.

During measurements, mice were anaesthetized with 1.5% isoflurane in a mixture of O2/N2O (1:2), administrated via a face cone. Animals were allowed to breathe spontaneously, and neither respiratory nor cardiac gating was applied. Body temperature was maintained at 37±1°C by a flow of warm air.

Image Analysis

The volume of MRI signals was quantified using a semi-automatic segmentation procedure implemented in the IDL (Interactive Data Language Research Systems, Boulder, Colorado, USA) environment on a Linux system (Beckmann et al., 2001). Images were first weakly lowpass filtered with a Gaussian profile filter and then transformed into a set of four grey level classes using adaptive Lloyd-Max histogram quantification. The highest grey level class in the transformed images could be extracted interactively by use of a region grower. Contour serving as a growing border was drawn to control region growing manually. Since the signals from extravascular fluid and vessels were of comparable highest intensities, the volume corresponding to the vessels was assessed on baseline images and then could be subtracted from the volumes determined on post-challenge images.

Peripheral Blood Lymphocyte Depletion Assay

Immediately after MRI acquisition, C57BL/6 mice were maintained under anaesthesia (isoflurane 3 % v/v). About 500 µl of blood were sampled by retro-orbital bleeding in ethylenediaminetetraacetic acid(EDTA)-coated Eppendorf tubes and subjected to hematology analysis. Absolute and differential leukocyte counts, including lymphocyte counts, were obtained with the Technicon H1-E analyzer (Bayer Diagnostics, Zurich, Switzerland).

Post-Mortem Analyses

Mice were killed by intraperitoneal injection of 0.2 ml of pentobarbitone (250 mg/kg).

- Bronchoalveolar Lavage (BAL) Fluid Analysis

The trachea was cannulated and the lung washed out by gently injecting 8 times via the trachea, without any chest massage, 0.5 ml of a BAL solution prepared with (i) Hank's balanced salt solution (HBSS); (ii) Ethylenedaminetetraacetic acid (EDTA) 1mM; (iii) 4-(2-hydroxyethyl)-1-piperazinethanesulphonic acid (HEPES) 0.1M,; (iv) D-glucose anhydrous, 1g and (v) distilled water. An aliquot from BAL fluid was used for total cell count in an automatic cytometer (Sysmex, Norderstedt, Germany). From each aliquot, a sample containing approximately 50,000 cells was used for

cytospin preparation. Cells were stained with Diff-Quik and a differential count of 200 cells (eosinophils, macrophages, neutrophils, lymphocytes) was obtained by observing cytospin slides under a classic light microscope (x100, oil immersion) using standard morphological criteria.

- Histology

Histology has been performed on 2 mice, that were not subject to BAL, per group receiving the highest dose of each tested compound and its vehicle. Immediately after a lethal injection of pentobarbitone, the trachea was ligated to avoid collapse and the entire lung was removed and immersed in 10 % neutral buffered formalin for 72 h. The lung was then cut longitudinally in order to analyze all lobes. After dehydration of tissues through increasing graded series of ethylic alcohol and processing to paraffin wax, sections were embedded in blocks. Slices of 3 µm thickness were cut in order to observe the main bronchi of each lobe. Slices were stained with hematoxylin and eosin to assess the general morphology, with Verhoeff/Van Gieson‘s method for the demonstration of elastic fibers in arteries and to determine perivascular edema, as well as with Alcian Blue/Periodic Acid Schiff’s (AB/PAS) method for demonstrating excreted mucus and mucus-containing goblet cells.

RESULTS

Effect of intranasal budesonide pre-treatment on allergen-induced lung inflammation and MRI fluid signals

To verify whether anti-inflammatory treatment might affect fluid signals detected by MRI in the lungs, budesonide, a glucocorticosteroid widely used to treat human asthma, was tested in the model. Figure 1 shows representative MR images of the chests of actively sensitized, compound- or vehicle-treated mice. The images were acquired 24 h after the last OVA or saline challenges. Fluid signals, which had been demonstrated earlier to reflect plasma leakage and mucus secretion in this murine model (Blé at al., submitted), were apparent in the lungs of vehicle-treated, OVA-challenged mice, whereas, less signals were present after treatment with budesonide. No fluid signals were present in the lungs of saline-challenged animals.

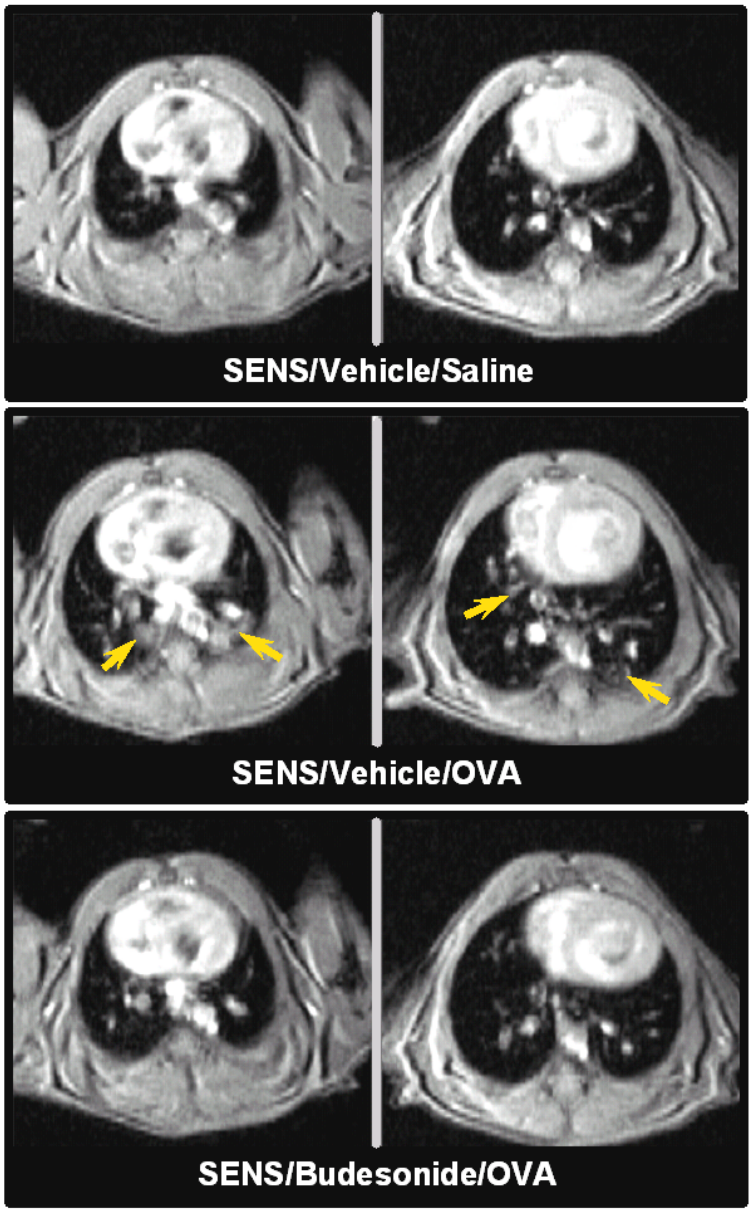

Figure 1 – *Representative MRI transverse sections through the thorax of actively sensitized C57BL/6 mice, acquired 24 h after the last intranasal challenge. SENS/Vehicle/Saline mice (N=8) were treated with the vehicle (2% DMSO in saline) before saline-challenge; SENS/Vehicle/OVA mice (N=8) were treated with the vehicle (2% DMSO in saline) before ovalbumin-challenge, SENS/Budesonide/OVA mice (N=8) were treated with budesonide (3 mg/kg) before ovalbumin-challenge Arrows indicate fluid signals.*

Quantification of the MRI signals showed that, compared to vehicle pre-treatment, budesonide led to an approximately 80 % reduction of the fluid signals detected by MRI in vivo (figure 2a). The reduced number of infiltrated eosinophils recovered from the BAL (Figure 2b) and the decreased inflammatory features observed on histological sections (data not shown) confirmed the local anti-inflammatory

effectiveness of the corticosteroid. In addition, no effect was observed on the number of circulating lymphocytes (figure 2c).

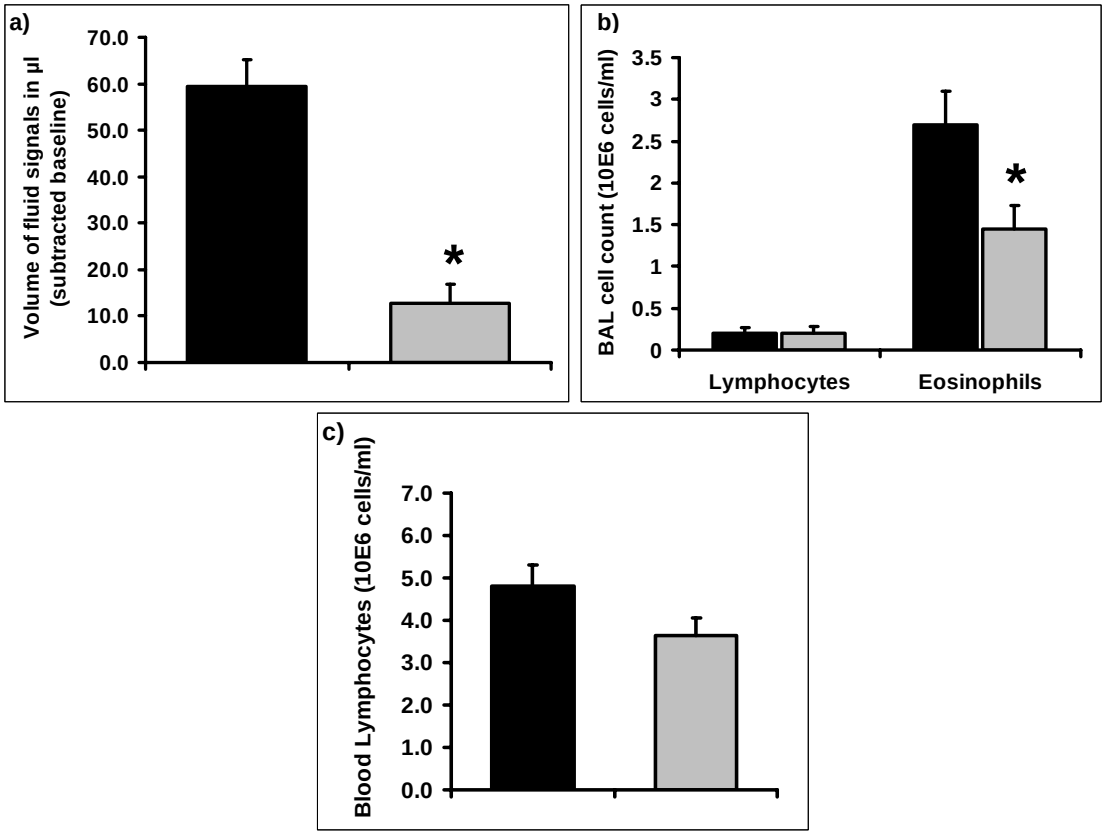

Figure 2 *- Effects of intranasal pretreatment with budesonide (3 mg/kg, grey bar, n=8) or its vehicle (2% DMSO with saline, black bars, n=8) on allergen-induced MRI fluid signals (a), BAL fluid lymphocytes and eosinophils (b), and circulating lymphocytes (c). *P>0.05 vehicle vs budesonide.*

Effect of intranasal pretreatment of FTY720 on allergen-induced lung inflammation.

Figure 3 shows representative lung MR images acquired 24 h after multiple OVA challenges in mice pretreated with FTY720 0.1 mg/kg or its vehicle. Reduced fluid signals were detected in the lungs of FTY720-treated OVA-challenged mice in comparison to mice that received vehicle. For doses from 0.003 to 0.1 mg/kg, FTY720 administered intranasally 30 min prior to each OVA challenge reduced by approximately 50% the signals detected by MRI in the lungs 24 h after the last allergen challenge (Figure 4a). In addition, the compound dose-dependently diminished the circulating lymphocytes with a significant inhibition observed from the dose of 0.03 mg/kg (Figure 4c). However, only at the highest dose (0.1 mg/kg)

FTY720 was able to significantly decrease the number of eosinophils and lymphocytes in the BAL fluid (Figure 4b).

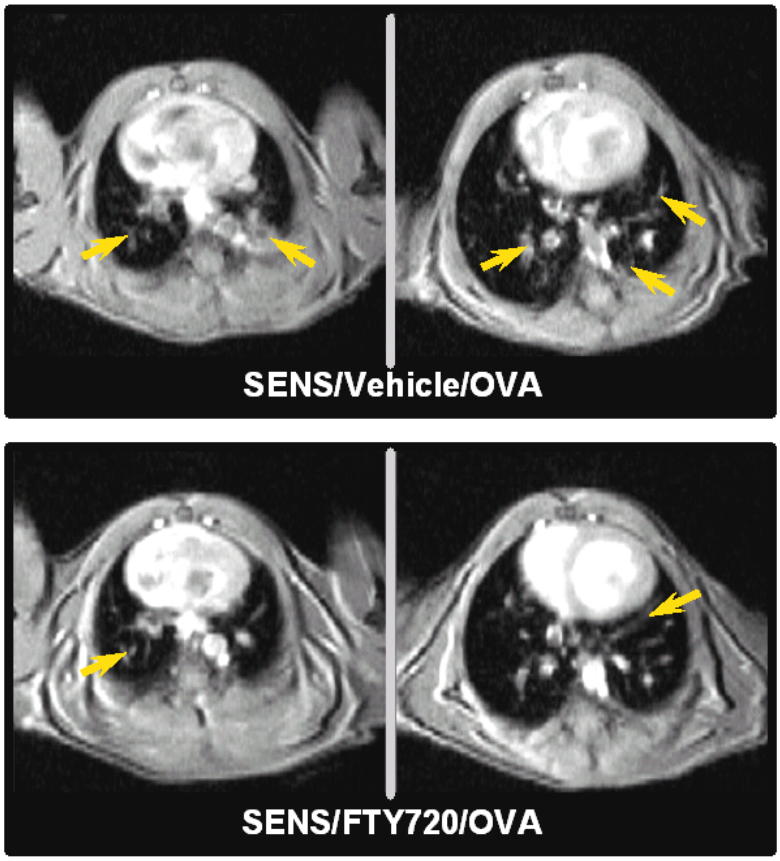

Figure 3 *- Representative MRI transverse sections through the thorax of C57BL6 mice (N=8 per group), acquired 24 h after the last intranasal challenge. SENS/Vehicle/OVA mice were treated with the vehicle (distilled water) before ovalbumin-challenge and SENS/FTY720/OVA mice were treated with FTY720 (0.1 mg/kg) before ovalbumin-challenge. Arrows indicate fluid signals.*

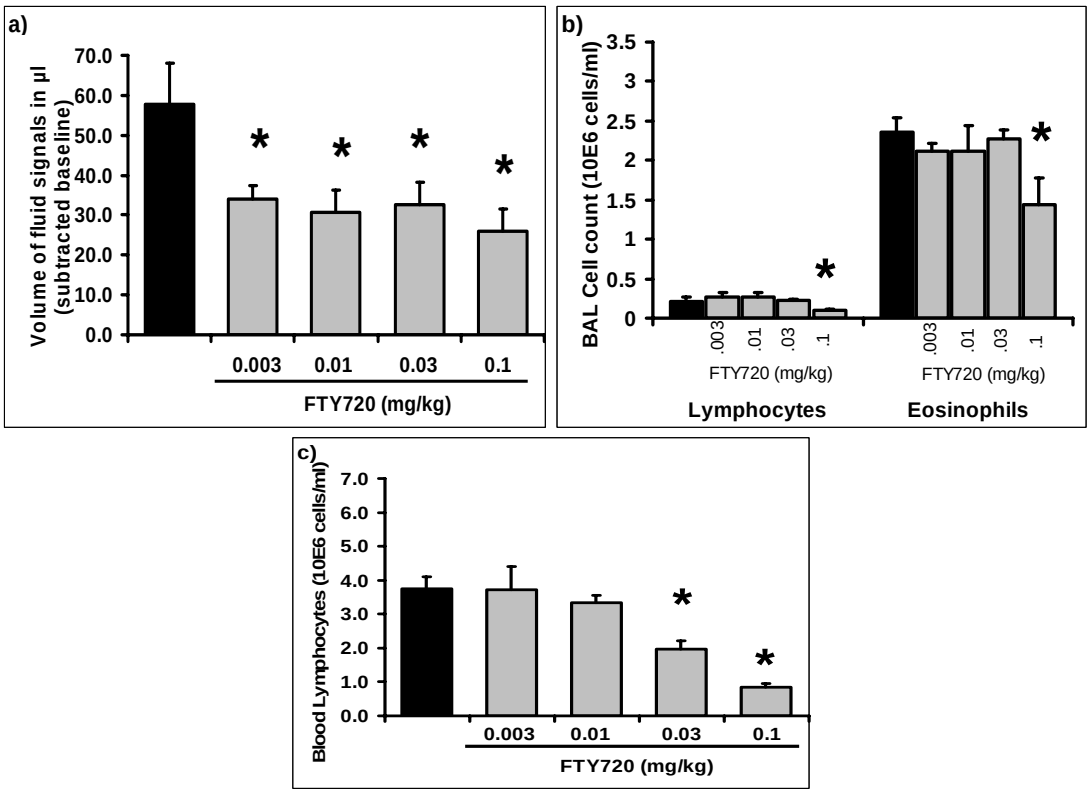

Figure 4 *- Effects of intranasal pretreatment with FTY720 at doses from 0.003 to 0.1 mg/kg (grey bar, n=6 to 8 per group) or its vehicle (saline 0.9%; Black bar, n=6 to 8) on allergen-induced MRI fluid signals (a), BAL fluid lymphocytes and eosinophils (b), and circulating lymphocytes (c).*P>0.05 vehicle vs FTY720*

At this dose, histological analysis revealed a slight amelioration of the general inflammatory status of the lung in comparison to the vehicle-treated mice. Indeed, the sections corresponding to OVA-challenged animals pretreated with 0.1 mg/kg of FTY720 demonstrated moderate to marked perivascular and peribronchial infiltration with inflammatory cells (Figure 5), no to slight peribronchial edema, hyperplasia of goblet cells and the presence of slight to marked mucus in the bronchial lumen.

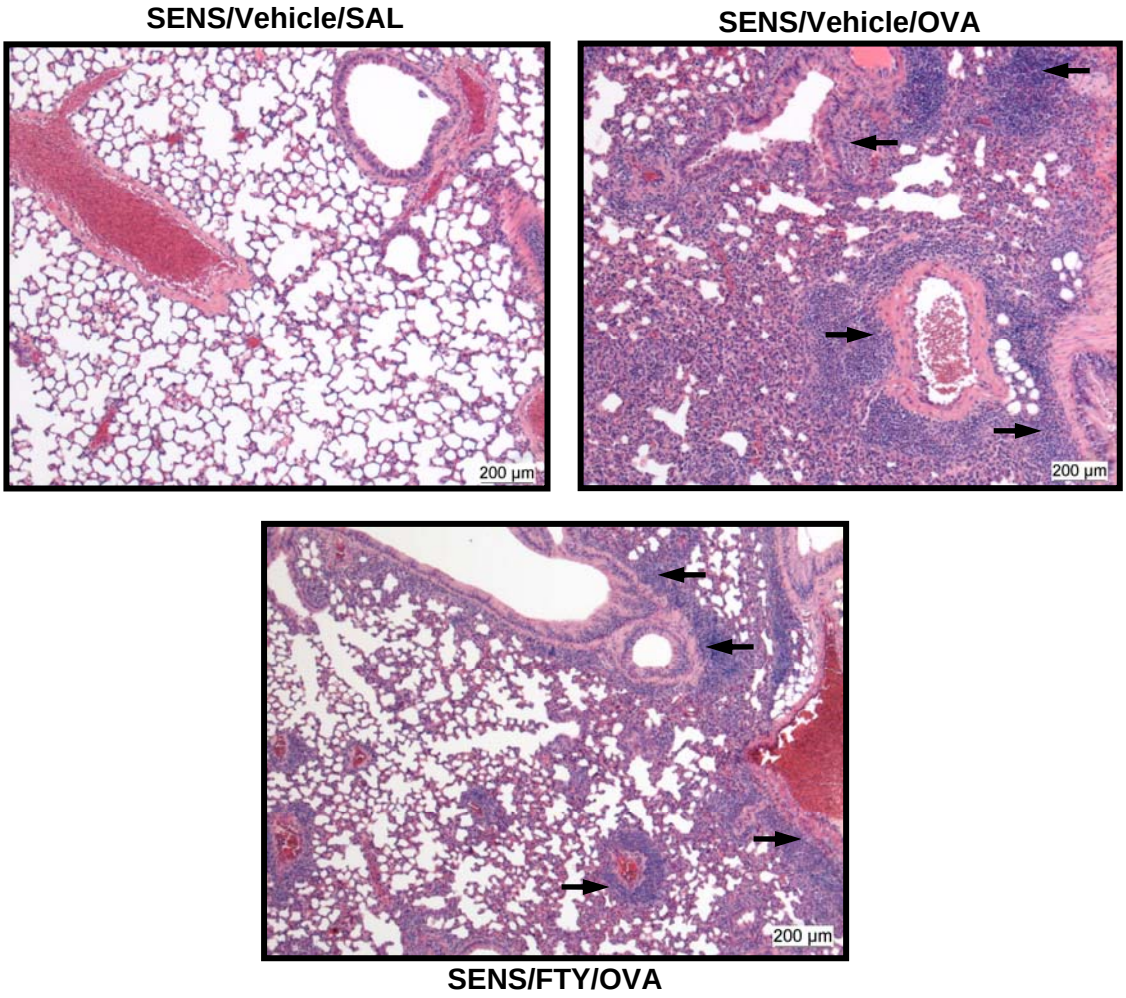

Figure 5 – *Representative histological sections from the lung of actively sensitized mice sacrificed 24h after last challenge, and that received different treatment : vehicle pretreatment and either saline- (up left) or ovalbumin challenged (up right), and FTY720 (0.1 mg/kg) pretreatment and OVA challenge (bottom). Black arrows indicate perivascular and peribronchial polynuclear infiltration after hematoxylin/eosin staining (N=2 per group)*

Effect of intranasal pretreatment of FTY720 on allergen-induced lung inflammation in $S1P_3$-deficient mice.

To answer the question whether $S1P_3$ receptors were implicated in the effects described above, we compared the effects of FTY720 in allergen-challenged wild type (WT) and in $S1P_3$-deficient mice (Figure 6). The $S1P_3$ deficiency had no significant effect on the ovalbumin challenges-induced increase in MRI signal and BAL inflammatory cell infiltration. Similarly, no difference was observed in the blood lymphocyte counts (Figure 5). Intranasal administration of FTY720 prior to allergen challenge induced blood lymphopenia and also a decrease of allergen-

induced MRI fluid signals, in both WT and $S1P_3$ deficient mice. Moreover, histological analysis demonstrated that in both WT and $S1P_3$ deficient mice, pretreatment with FTY720 (0.1 mg/kg) had the same ability to reduce the perivascular and peribronchial cell infiltration, as well as the mucus hypersecretory phenotype (data not shown).

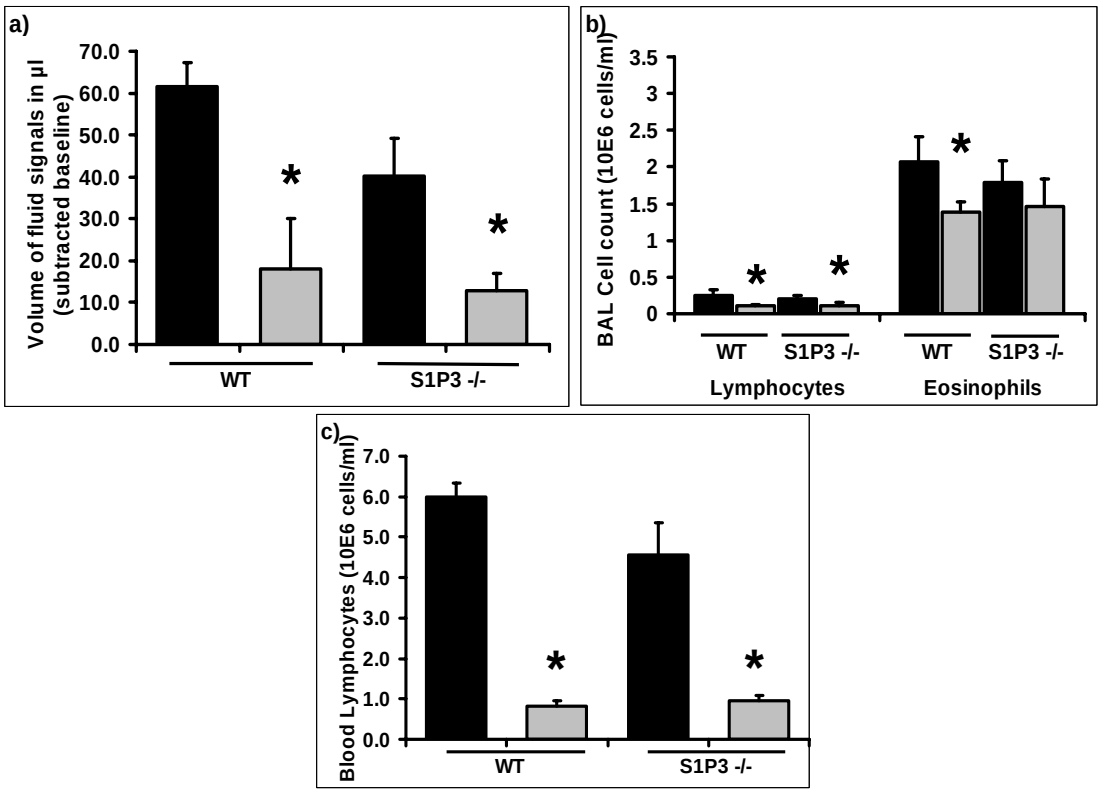

Figure 5 *Effects of intranasal pretreatment with FTY720 (0.1 mg/kg; grey bars, n=6) and its vehicle (black bars, n=6) on allergen-induced MRI fluid signals (a), BAL fluid lymphocytes and eosinophils (b), and circulating lymphocytes (c) in S1P3 knock-out mice and their WT littermates. *P>0.05 refers to Student's t test vehicle vs FTY720.*

Effect of intranasal selective $S1P_1$-agonist: AUY954, on allergen-induced lung inflammation in C57BL/6 mice.

The doses of AUY954 were chosen based on recently published results showing a 4-fold less efficacy on human $S1P_1$ receptors in comparison to FTY720 (Pan et al., 2006). As shown in figure 6, intranasal administration of the $S1P_1$ selective agonist, AUY954 at doses 0.003 and 0.01 mg/kg prior to ovalbumin challenges reduce the MRI fluid signal in response to allergen by about 50 % of that observed in the

vehicle-treated mouse. At both doses, AUY954 had no effect on the infiltrated cells in the BAL nor on the circulating lymphocytes.

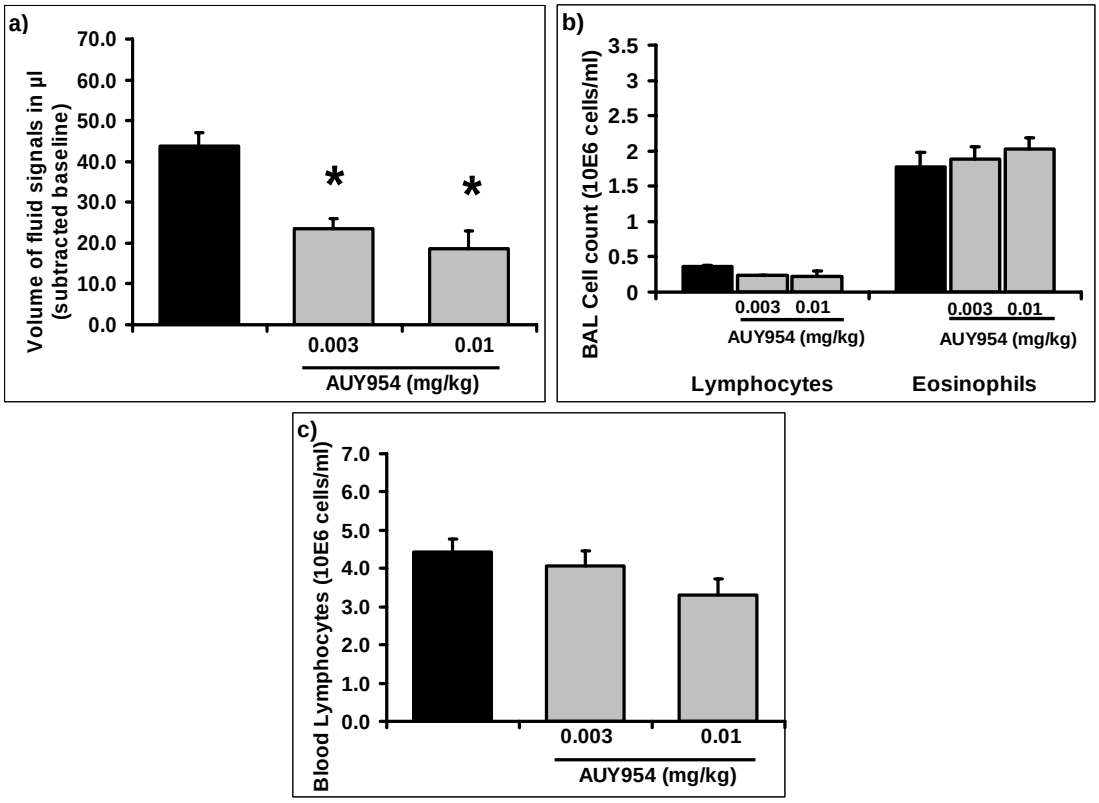

Figure 6 *Effects of intranasal pretreatment with AUY954 (0.003 and 0.01 mg/kg, grey bars; n=8 per group) and its vehicle (black bars; n=8 per group) on allergen-induced MRI fluid signals (a), BAL fluid lymphocytes and eosinophils (b), and circulating lymphocytes (c). *P>0.05 refers to Student's t-test vehicle vs AUY954.*

DISCUSSION

The methods available for the evaluation of the activity of potential anti-inflammatory treatments for lung diseases, particularly in small animal models, are limited and generally invasive. They basically rely on the determination of inflammatory parameters in BAL fluid samples (Kirby et al., 1987) and in induced sputum (Pavord et al., 1997), or on the histological analysis of bronchial biopsies or tissue sections (Jeffery et al., 1989). We have demonstrated recently that MRI provides a relevant mean to assess a signal associated with the lung inflammation induced in sensitized mice by multiple challenges with OVA (Blé et al., submitted). In this work we have demonstrated that FTY720, given locally to the airways and

acting on the $S1P_1$ receptor, is a potent inhibitor of allergen-induced plasma leakage at doses that have no effect on cellular inflammation.

In confirmation with our previous findings (Blé et al., submitted), instillation of OVA resulted in intense MRI signals in the lungs of allergen-sensitized mice. In addition, these signals were shown to be significantly reduced by pretreatment with a standard corticosteroid, budesonide. The inhibition of the allergen-induced increase in the MRI signals was concomitant with an observed reduction of airway inflammatory cell infiltration, plasma leakage indicators and of the mucus hypersecretory phenotype. These data obtained in the mouse are analogous to previous results obtained in a rat model of allergen-induced pulmonary inflammation (Tigani et al, 2002; 2003), indicating that in the mouse, the effects of anti-inflammatory drugs are also non-invasively quantifiable by MRI.

FTY720 has been shown to be effective as an oral drug for treatment of experimental asthma induced by adoptive transfer of Th2 cells (Sawicka et al., 2003). The systemic immunodeficiency caused by S1P receptor-mediated inhibition of lymphocyte egress from the lymph node medulla was probably responsible for the observed reduction of the inflammatory response to allergen. More recently, with the aim of minimizing systemic side effects, Lambrecht et al. (2007) investigated the effect of intratracheal administration of FTY720 in a murine model of asthma, and were able to suppress Th2-related eosinophilic airway inflammation without causing lymphopenia. The authors postulated that the effectiveness of local treatment was achieved by inhibition of the lung dendritic cells capacity to interact with allergen-specific Th2 cells in lymph nodes. Contrasting with these observations, our data suggested that, when applied intranasally, FTY720 reduced eosinophilic airway inflammation only when the levels of circulating lymphocytes were decreased. The discrepancy between these studies might be explained by the different routes of administration (intranasal versus intratracheal) and/or the mouse strains employed.

Of note, in the present study, even at doses that did not lead to systemic immunosuppression, FTY720 potently decreased the volume of MRI signals detected in response to allergen challenge. Relying on the fact that MRI fluid signals detected in this murine model reflect both plasma leakage and mucus secretion (Blé et al.,

submitted), it is conceivable that even without displaying anti-inflammatory effects as revealed histologically and by BAL fluid analysis, FTY720 at low doses could have affected the lung barrier integrity. Indeed, it has been shown that S1P can modulate the lung barrier permeability and plasma exudation (Sanchez et al., 2003; Peng et al., 2004; McVerry & Garcia, 2005). $S1P_1$ and $S1P_3$ receptors play opposing roles in the modulation of the lung barrier integrity. On one hand, activation of the $S1P_3$ receptors, expressed on the airways epithelium, can increase the epithelial junction disruption (Gon et al., 2005). On the other hand, the $S1P_1$ receptors expressed on the endothelium has been demonstrated to be protective against vascular leakage *in vivo* (Sanna et al., 2006).

The fact that FTY720 had the same effects on the MRI signals in wildtype and $S1P_3$-deficient mice challenged by OVA suggests that the activity of this compound is not mediated via the $S1P_3$ receptor. Furthermore, in mice challenged with saline, treatment with FTY720 did not induce any MRI signals (data not shown). Nevertheless, according to Gon et al. (2005), deletion of $S1P_3$ receptors abolishes the transient disturbance of epithelial tight junctions integrity induced by local exogenous $S1P_3$ receptor agonists. Interestingly, the $S1P_3$ deletion led to a small (albeit not significant) reduction of MRI fluid signals induced by allergen provocation in vehicle-pretreated knockout animals. Thus, it cannot be excluded that the $S1P_3$ receptor has a minor contribution to fluid signals detected in response to multiple allergen challenges.

Similarly to that observed for FTY720, the selective $S1P_1$ agonist AUY954 potently reduced allergen-induced MRI signals.This strongly suggest that the inhibition of the MRI signal observed with FTY720 is $S1P_1$-mediated, probably by counteracting plasma leakage at the level of the endothelium (Sanna et al., 2006). At the doses used, AUY954 did not influence the number of BAL inflammatory cells nor the number of circulating lymphocytes. This probably reflects a low systemic concentration of the compound at the doses used.

We have shown in the present work the usefulness of lung MRI to investigate airway inflammation and its pharamacology. By evaluating the effects of intranasal administration of FTY720 prior to allergen challenge in actively sensitized mice, our

observations suggest that the reduction of fluid MRI signals, related to plasma leakage and mucus secretion, is mainly explained by the action on endothelial barrier integrity through $S1P_1$ receptors, rather than by an anti-inflammatory effect of the compound. In addition, deletion of $S1P_3$ did not compromise FTY720 pretreatment effects and thus imply that $S1P_3$ receptors are not implicated. Nevertheless, when pharmacological tools for $S1P_4$ and $S1P_5$ receptors would be available, further investigation would be necessary to confirm that these FTY720-sensitive receptors are not also implicated in the effect observed in our murine model of airway inflammation.

ACKNOWLEDGEMENTS

The support from Daniel Wyss and Barbara Nuesslein-Hildesheim is gratefully acknowledged. The receipt of an award by the 3R Research Foundation (Münsingen, Switzerland) is gratefully acknowledged by NB (project 82/02).

REFERENCES

Beckmann N, Tigani B, Ekatodramis D, Borer R, Mazzoni L, Fozard JR. Pulmonary edema induced by allergen challenge in the rat: noninvasive assessment by magnetic resonance imaging. *Magn Reson Med.* 2001;45(1):88-95.

Blé FX, Cannet C, Zurbruegg S, Karmouty-Quintana H, Bergmann R, Frossard N, Trifilieff A, Beckmann N. Allergen-induced lung inflammation in actively sensitized mice assessed by MRI. *Radiology.* Submitted.

Chalfant CE, Spiegel S. Sphingosine 1-phosphate and ceramide 1-phosphate: expanding roles in cell signaling. *J Cell Sci*. 2005;118(Pt 20):4605-12. Review.

Goetzl EJ, Kong Y, Mei B. Lysophosphatidic acid and sphingosine 1-phosphate protection of T cells from apoptosis in association with suppression of Bax. *J Immunol*. 1999;162(4):2049-56.

Gon Y, Wood MR, Kiosses WB, Jo E, Sanna MG, Chun J, Rosen H. S1P3 receptor-induced reorganization of epithelial tight junctions compromises lung barrier integrity and is potentiated by TNF. *Proc Natl Acad Sci U S A.* 2005;102(26):9270-5.

Jeffery PK, Wardlaw AJ, Nelson FC, Collins JV, Kay AB. Bronchial biopsies in asthma. An ultrastructural, quantitative study and correlation with hyperreactivity. *Am Rev Respir Dis*. 1989;140(6):1745-53.

Kirby JG, O'Byrne PM, Hargreave FE. Bronchoalveolar lavage does not alter airway responsiveness in asthmatic subjects. *Am Rev Respir Dis*. 1987;135(3):554-6.

McVerry BJ, Garcia JG. In vitro and in vivo modulation of vascular barrier integrity by sphingosine 1-phosphate: mechanistic insights. *Cell Signal.* 2005;17(2):131-9.

Pan S, Mi Y, Pally C, Beerli C, Chen A, Guerini D, Hinterding K, Nuesslein-Hildesheim B, Tuntland T, Lefebvre S, Liu Y, Gao W, Chu A, Brinkmann V, Bruns C, Streiff M, Cannet C, Cooke N, Gray N. A monoselective sphingosine-1-phosphate receptor-1 agonist prevents allograft rejection in a stringent rat heart transplantation model.*Chem Biol*. 2006;13(11):1227-34.

Pavord ID, Pizzichini MM, Pizzichini E, Hargreave FE. The use of induced sputum to investigate airway inflammation.*Thorax*. 1997;52(6):498-501.

Peng X, Hassoun PM, Sammani S, McVerry BJ, Burne MJ, Rabb H, Pearse D, Tuder RM, Garcia JG. Protective effects of sphingosine 1-phosphate in murine endotoxin-induced inflammatory lung injury. *Am J Respir Crit Care Med.* 2004;169(11):1245-51.

Sanchez T, Estrada-Hernandez T, Paik JH, Wu MT, Venkataraman K, Brinkmann V, Claffey K, Hla T. Phosphorylation and action of the immunomodulator FTY720 inhibits vascular endothelial cell growth factor-induced vascular permeability. *J Biol Chem.* 2003;278(47):47281-90.

Sanna MG, Wang SK, Gonzalez-Cabrera PJ, Don A, Marsolais D, Matheu MP, Wei SH, Parker I, Jo E, Cheng WC, Cahalan MD, Wong CH, Rosen H. Enhancement of capillary leakage and restoration of lymphocyte egress by a chiral S1P1 antagonist in vivo. *Nat Chem Biol.* 2006;2(8):434-41.

Tigani B, Cannet C, Zurbrugg S, Schaeublin E, Mazzoni L, Fozard JR, Beckmann N. Resolution of the oedema associated with allergic pulmonary inflammation in rats assessed noninvasively by magnetic resonance imaging. *Br J Pharmacol.* 2003;140(2):239-46.

Tigani B, Schaeublin E, Sugar R, Jackson AD, Fozard JR, Beckmann NPulmonary inflammation monitored noninvasively by MRI in freely breathing rats. *Biochem Biophys Res Commun*. 2002;292(1):216-21.

Zhang Z, Schluesener HJ. FTY720: a most promising immunosuppressant modulating immune cell functions. *Mini Rev Med Chem.* 2007; 7:845-850.

MANUSCRIPT 3

A S1P2 antagonist inhibits allergen-induced increase in MRI fluid signals in mouse via a non mast cell-dependent mechanism

Blé FX, Cannet C, Zurbruegg S, Gérard C, Frossard N, Beckmann N, and Trifilieff A

A $S1P_2$ antagonist inhibits allergen-induced increase in MRI fluid signals in mouse via a non mast cell-dependent mechanism

Blé FX, Cannet C, Zurbruegg S, Gérard C, Frossard N, Beckmann N, Trifilieff A.

ABSTRACT

Recent in vitro evidence suggest the involvement of the sphingosine-1-phosphate (S1P) type 2 receptor in allergen-induced mast cell activation. In this study, we have used a mouse model of allergen-induced airway inflammation, plasma leakage- and mucus-related MRI signal and study the effect of JTE-013, a selective $S1P_2$ receptor antagonist. The implication of mast cells in this murine model of asthma was demonstrated by mast cell granule depletion with compound 48/80 (C48/80) that results in reduction of the formation MRI fluid signals in response to allergen challenge. JTE-013 was able to significantly reduce the fluid signals detected by MRI but only in non depleted mast cells animals. However, JTE-013 ha no effect on the degranulation status of the mast cells induced by ovalbumin challenge. Taken together, the present results show that in our in vivo murine model, despite failing to inhibit mast cell degranulation JTE-013 had preventive effect on fluid accumulation in the lung, an effect that may be explained by an enhanced vascular barrier function through the endothelial $S1P_2$ receptor.

INTRODUCTION

Mast cells and their released products contribute to the development of allergic respiratory disorders. Cross linking of the high affinity receptor for IgE (FcεR1) on mast cells induces their activation and the release of a panel of preformed or newly synthesized mediators including histamine, tryptase, prostaglandins, leukotrienes, and platelet activating factor, which can provoke the acute phase allergic reaction in the lung including airway microvascular leakage, mucosal edema, as well as mucus hypersecretion leading to airway obstruction (Galli & Costa, 1995; Mencia et al., 1983).

Sphingosine-1-phosphate (S1P) is a bioactive sphingolipid metabolite known to regulate diverse biological functions of various cell types, from proliferation and survival to migration and secretion. This mediator exerts its action as a result of activation of G protein-coupled receptors named $S1P_{1-5}$ (Rosen & Goetzl, 2005). S1P has been demonstrated as an important regulator of allergen-induced mast cell activation using bone marrow-derived mouse mast cells in vitro (Jolly et al., 2004; Prieschl et al., 1999). In addition, investigations involving S1P2-deficient mice and antisense oligonucleotides have suggested that this receptor was responsible for the S1P effects on mast cell (Jolly et al., 2004). A shortcoming of these two studies is that both involved the use of ex vivo differentiated mast cells and in vitro activation assays.

We recently described in an in vivo murine model of allergen-driven airway inflammation the assessement plasma leakage and mucus secretion by MRI (Blé et al., 2007). As the extent to which mast cells contribute to airway inflammation seems to be highly dependent on the specific experimental model being investigated (Hamelmann et al.,1999; Korsgren et al.,1997; Martin et al., 1993; Mehlhop et al.,1997; Takeda et al., 1997, Williams & Galli, 2000), in the present work we *(i)* aimed at verifying whether mast cells play a role in the formation of allergen-induced signals detected by MRI and *(ii)* investigated in our model the effects of the S1P2 antagonist, JTE-013, that could implicate mast cell dependent mechanisms.

MATERIAL AND METHODS

Animals

Seven- to 9-week old female C57/BL6 mice (Janvier, Le Genest-St-Isle, France) were used throughout the study. They were housed in a temperature- and humidity-controlled environment, with free access to standard mouse chow and tap water. Experiments were carried out with the approval of the Veterinary Authority of the City of Basel (license number 1989).

Allergen Sensitization and Challenge

Ovalbumin (OVA, 250 µg/ml; Fluka, Buchs, Switzerland) was mixed (30 minutes on ice) in a blender with aluminum hydroxide (10 mg/ml) in saline and injected (0.2 ml per animal, intraperitoneally) on days 0 and 14. On day 18 mice were lightly anesthetized with 2% isoflurane (Abbott, Cham, Switzerland) and 100 µg of OVA in 25 µl of saline (SENS/OVA group) or vehicle (25 µl of saline) (SENS/SAL group) was administered intranasally (i.n.) via a micropipette (12.5 µl per nostril). Animals were allowed to recover immediately after. The same procedure was repeated on days 19, 20 and 21.

Depletion of mast cell granule

Chronic treatment with compound 48/80 (C48/80) leads to depletion of mast cell granule contents (Jaffery et al., 1994). Compound 48/80 (Sigma-Aldrich, Munich, Germany) was dissolved in 0.1 mL of 0.9% NaCl and injected i.p. twice daily as follows: 0.5 mg/kg on day 15, 1.0 mg/kg on day 16, 2.0 mg/kg on day 17, 3.0 mg/kg on day 18, and 4.0 mg/kg on day 19. This protocol was modified from previous work by Oldenburg and Mustafa (2004).

Drug treatment

The pyrazolopyridine derivative, JTE-013 (Tocris, Bristol, UK), is a specific $S1P_2$ antagonist (Osada et al, 2002). The compound was dissolved in a combination of polyethylene glycol 200 and saline (1:1) and sonicated for 10 minutes. Mice were anesthetized with 2% isoflurane (Abbott, Cham, Switzerland) and JTE-013 at doses of 1, 3 or 10 mg/kg or its vehicle was administered intranasally (2x 12.5µl/nostril) 30 minutes prior to each OVA challenge.

MRI

Under baseline conditions (on day 14) and 24 h after the last OVA challenge, measurements were carried out in vivo with a Biospec 47/40 spectrometer (Bruker Medical Systems, Karlsruhe, Germany) operating at 4.7 T, equiped with an actively shielded gradient system capable of generating a gradient of 200 mT/m. A birdcage resonator of 32 mm diameter was used for excitation and detection. Gradient-echo images were acquired with the following parameters: repetition time 5.6 ms, echo time 3.5 ms, band width 100 kHz, flip angle of the excitation pulse approximately 10°, matrix size 256 x 128, slice thickness 0.75 mm and field of view 3 x 3 cm^2. A single slice image (acquisition time of 74 s) was obtained by computing the two-dimensional Fourier transform of the averaged signal from 60 individual acquisitions and interpolating the data set to 256 x 256 pixels. The entire lung was covered by 16 consecutive transverse slices (Blé et al., 2007).

During measurements, mice were anaesthetized with 1.5% isoflurane in a mixture of O_2/N_2O (1:2), administrated via a face cone. Animals were allowed to breathe spontaneously, and neither respiratory nor cardiac gating was applied. Body temperature was maintained at 37±1°C by a flow of warm air.

Image Analysis

The volume of MRI signals was quantified using a semi-automatic segmentation procedure implemented in the IDL (Interactive Data Language Research Systems, Boulder, Colorado, USA) environment on a Linux system (Beckmann et al. 2001). Images were first weakly lowpass filtered with a Gaussian profile filter and then transformed into a set of four grey level classes using adaptive Lloyd-Max histogram quantitation. The highest grey level class in the transformed images could be extracted interactively by use of a region grower. Contour serving as a growing border was drawn to control region growing manually. Since the signals from extravascular fluid and vessels were of comparable high intensity, the volume corresponding to the vessels was assessed on baseline images and then could be subtracted from the volumes determined on post-challenge images to provide with differential volume as displayed on the figures.

Post-Mortem Analyses

Animals were killed by intraperitoneal injection of 0.2 ml of pentobarbitone (250 mg/kg), immediately after the last MRI acquisition.

- Bronchoalveolar Lavage Fluid Analysis

The trachea was cannulated and the lung lavaged by gently injecting via the trachea 8 times 0.5 ml of a bronchoalveolar lavage (BAL) solution prepared with (i) Hank's balanced salt solution (HBSS); (ii) Ethylenedaminetetraacetic acid (EDTA) 1mM; (iii) 4-(2-hydroxyethyl)-1-piperazinethanesulphonic acid (HEPES) 0.1M,; (iv) D-glucose anhydrous, 1g and (v) distilled water. An aliquot from BAL fluid was used for total cell count in an automatic cytometer (Sysmex Corporation, Kobe, Japan). From each aliquot, a sample containing approximately 50,000 cells was used for cytospin preparation. Cells were stained with Diff-Quik and a differential count of 200 cells (eosinophils, macrophages, neutrophils, lymphocytes) was obtained by observing cytospin slides under a classic light microscope (x100, oil immersion) using standard morphological criteria.

- Histology

The trachea was immediately ligated to avoid collapse and the entire lung was removed and immersed in 10% neutral buffered formalin for 72 h. The lungs were then trimmed longitudinally in order to analyze all lobes. After dehydration of tissues through increasing graded series of ethylic alcohol and processing to paraffin wax, sections were embedded in blocks. Slices of 3 μm thickness were cut in order to observe the main bronchi of each lobe. Slices were stained with hematoxylin and eosin to assess the general morphology and cell infiltration, as well as with Alcian Blue/Periodic Acid Schiff's (AB/PAS) for demonstrating excreted mucus and mucus-containing goblet cells.

Toluidine blue was applied to lung sections for mast cell granules staining. Only mast cells showing identifiable nuclei were considered for counting. Degranulated and non-degranulated mast cells were counted on the whole longitudinal lung section.

RESULTS

To answer the question of whether mast cells were implicated in the interstitial and luminal fluid accumulation induced by allergenic provocation, we evaluated the effect of a chronic pretreatment with C48/80 on lung fluid signals detected by MRI after multiple allergen challenge in sensitized mice. Figure 1 illustrates the volume of fluid signals evaluated in the lung of sensitized mice challenged with saline and OVA, with or without C48/80 pretreatment. In both pretreatment conditions, fluid signals, which had been demonstrated earlier to reflect plasma leakage and mucus secretion in this murine model (Blé et al., 2007), were detected in the lungs of OVA-challenged mice, whereas, no extravascular signals were present in the lungs of sensitized but saline-challenged mice. However, OVA-induced fluid signals detected by MRI were significantly decreased in mice pretreated with C48/80 (P=0.023).

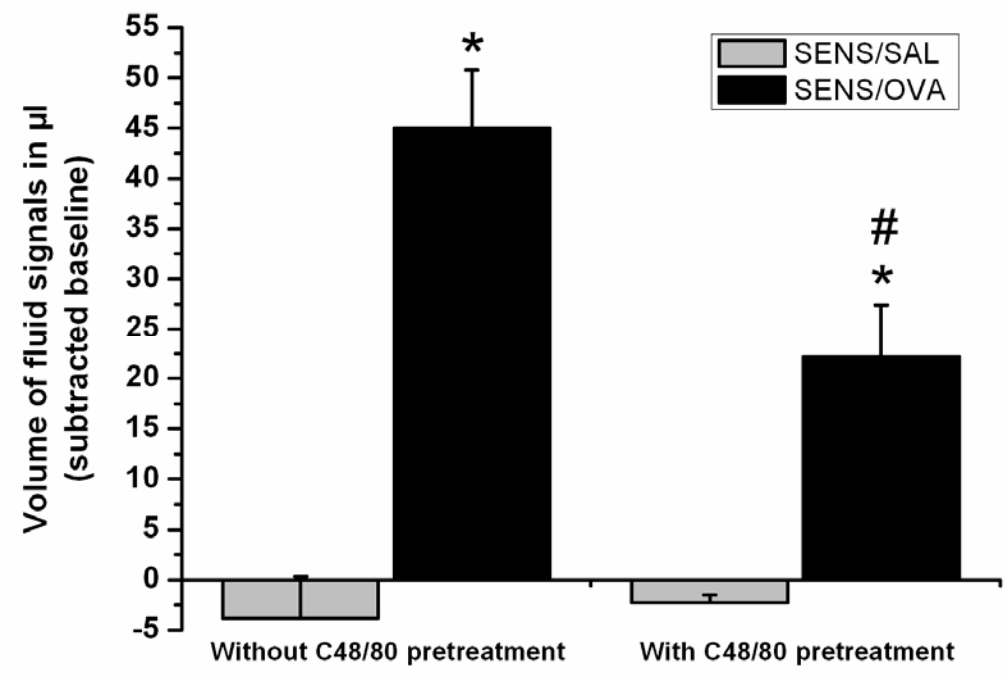

Figure 1 *- Lung fluid signal volumes determined from MR images of actively sensitized mice challenge with saline or OVA in the presence (SENS/SAL N=8; SENS/OVA N=8) or absence of C48/80 pretreatment (SENS/SAL N=4; SENS/OVA N=4). Data are expressed as means ± sem.*p<0.05 indicates statistical significance determined by Student's t-test comparisons between the SENS/SAL and SENS/OVA groups.* $^{\#}$ *p<0.05 refers to a comparison between SENS/OVA animals pre-treated or not with C48/80.*

In contrast, no significant differences were observed between the total and differential cell count in the BAL fluid recovered from OVA-challenged mice pretreated or not with C48/80 (macrophages : 0.49±0.11 10^6 cell/ml without C48/80

versus 0.50±0.10 10^6 cell/ml with C48/80; eosinophils : 1.09±0.16 10^6 cell/ml without C48/80 versus 0.83±0.30 10^6 cell/ml with C48/80). Moreover, C48/80 pretreated animals did not demonstrate changes in the amount of mucus secretion shown on PAS-stained lung sections (Figure 2) or in the severity of interstitial cell infiltration revealed by hematoxylin eosin staining, in comparison to lung sections from control mice.

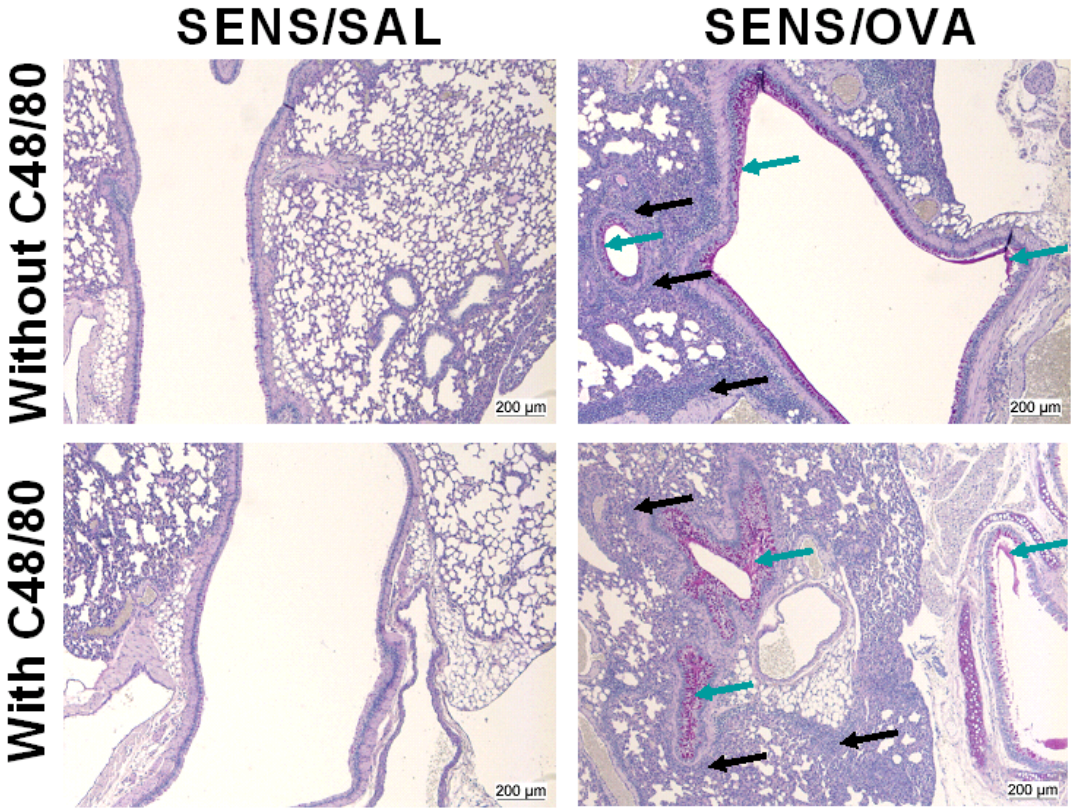

Figure 2 – *AB/PAS-stained histological sections from the lungs of actively sensitized mice challenged with saline (left; SENS/SAL) or OVA (right; SENS/OVA), in the presence or absence of C48/80 pretreatment. Green arrows indicate mucus load and goblet cell metaplasia, black arrows : perivascular and peribronchial cellular infiltration. Mice were sacrificed 24 h after last challenge.*

Additionally, lung histological sections stained with toluidine blue were used to show the proportion of degranulated mast cells. On the lung sections from each group, a relatively low number of mast cells (21±10 for SENS/SAL; 21±9 for SENS/OVA; 16±5 for SENS/SAL pretreated with C48/80; 19±4 for SENS/OVA pretreated with C48/80) were found in the peribronchic area and in the hilus region. Results from the mast cell counting are summarized in Table 1. Sensitized mice challenged with saline showed a large proportion of non-degranulated mast cells

(91%). After either OVA challenge, C48/80 alone or in combination with OVA an increased proportion of degranulated mast cells was observed in the lungs of sensitized mice. Chronic administration of C48/80 effectively induces mast cell degranulation in the airways.

Table 1 – *Counting of degranulated and non-degranulated mast cells on toluidine blue- stained lung sections from actively sensitized saline-challenged (SENS/SAL) and OVA-challenged (SENS/OVA) mice sacrificed 24h after last challenge, in the presence (SENS/SAL N=4; SENS/OVA N=4) or absence of C48/80 pretreatment (SENS/SAL N=2; SENS/OVA N=2). Data are expressed as means±SEM.*

Treatment		Number of non-degranulated mast cells 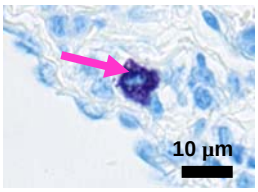	Number of degranulated mast cells 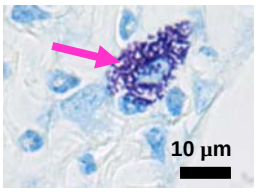	Proportion of degranulated mast cells (in %)
Without C48/80 pretreatment	SENS/SAL	**19±9**	**2±1**	**9.4±0.3**
	SENS/OVA	**11±8**	**10±1**	**55.8±19.2**
With C48/80 pretreatment	SENS/SAL	**6±2**	**10±4**	**59.4±7.7**
	SENS/OVA	**10±2**	**9±2**	**48.5±2.3**

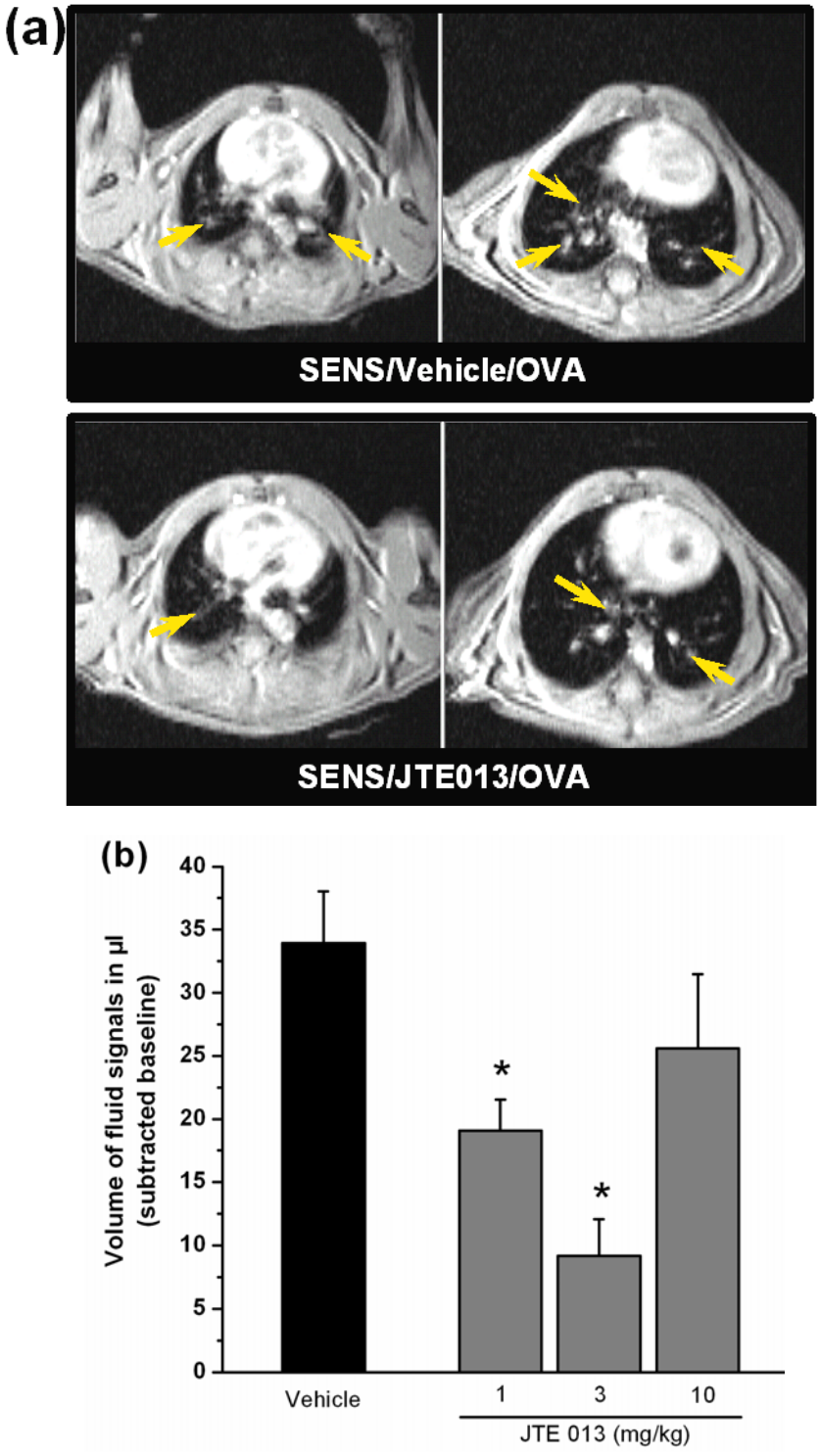

Figure 3 (a) *Representative MRI transverse sections acquired 24 h after the 4th allergen challenge through the chest of ovalbumin-immunized and -challenged mice pretreated with either vehicle (SENS/Vehicle/OVA) or JTE-013 3 mg/kg (SENS/JTE013/OVA). Arrows indicate fluid signals.* ***(b)*** *Lung fluid signal volumes determined from MR images at 24 h after the 4th allergen challenge in mice pretreated with JTE-013 at doses 1 mg/kg (N=8), 3 mg/kg (N=12) and 10 mg/kg (N=12) or its vehicle (N=12) instilled intranasally 30 minutes before OVA challenges. Data are expressed as means ± sem.* indicates p<0.05 statistical significance determined by Student's t-tests (JTE013 vs Vehicle treatment).*

The effect of JTE-013 (1, 3 and 10 mg/kg) or its vehicle (Polyethylene glycol in saline 1:1) has been tested to verify whether the intranasal administration of the S1P2 antagonist had an effect on the fluid signals elicited by multiple allergen provocation. Figure 3a shows representative MRI sections through the chest of OVA-sensitized and -challenged mice treated with vehicle or with JTE-013 at 3 mg/kg. MRI fluid signals elicited by multiple allergen challenges and localized in the proximal regions of the lung were clearly decreased when mice were pretreated with JTE-013. Figure 3b shows the volumes of MRI signals detected in the lung of mice that were treated with the vehicle or JTE-013 at three doses prior to OVA challenges. A volume of 33.9±4.4 µl was quantified in the vehicle group and a significant reduction of this volume was observed in the groups of mice pretreated with JTE-013 1mg/kg (19.1±2.5 µl, $p<0.001$ vs vehicle group) and 3mg/kg (9.2±2.9 µl, $p<0.001$ vs vehicle group). However, when given at 10 mg/kg no more inhibition was observed (Figure 3b). At all the doses tested, JTE-013 had no significant effect on the BAL inflammatory cells content (data not shown).

The next step was the evaluation of JTE-013 in mice that have been treated with C48/80. JTE-013 at a dose of 3 mg/kg or the vehicle were administered after chronic pretreatment with C48/80. Figure 4 illustrates the volumes of fluid signals detected by MRI in the lungs of C48/80 pretreated mice that received vehicle or JTE-013 prior to allergen. For comparison, the same experiment regarding JTE-013 treatment was repeated on mice that had not been pretreated with C48/80 before OVA challenges. A significantly reduced volume of MRI signals was observed in C48/80 pretreated mice that received further vehicle treatment (14.0±3.7 µl for C48/80 pretreated mice vs 35.0±3.7 µl for vehicle treated animals without C48/80 pretreatment, $p<0.001$). In contrast, JTE-013 treatment had no effect on the MRI signals detected in the lungs of C48/80 pretreated mice.

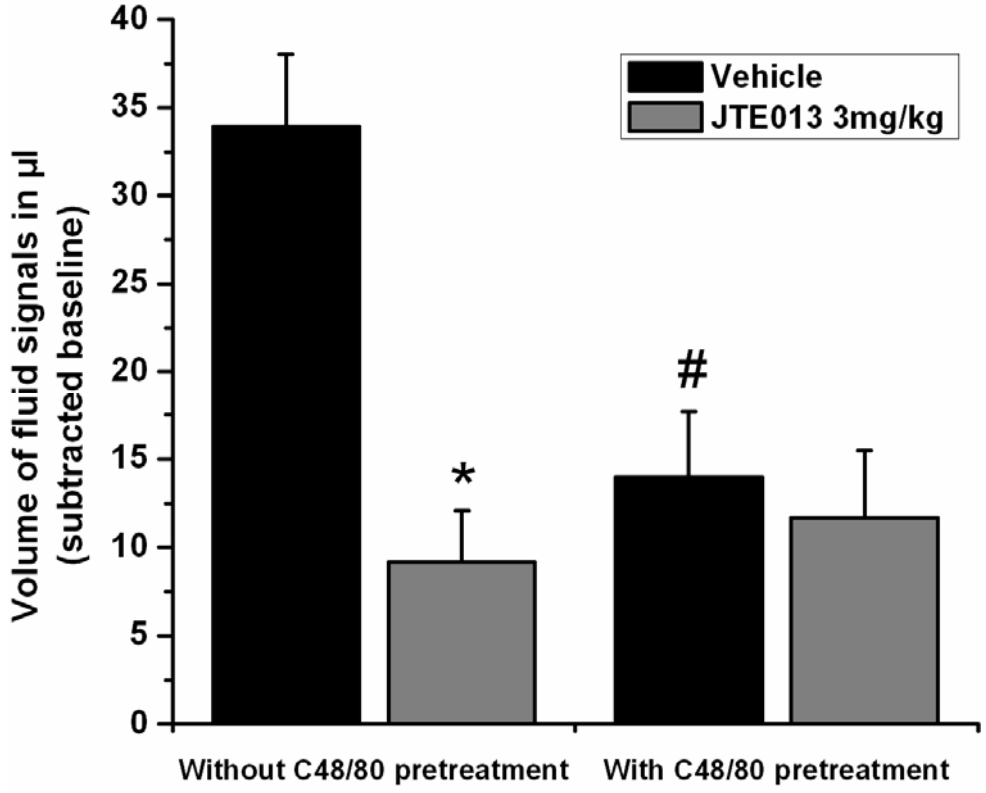

Figure 4 *- Lung fluid signal volumes determined from MR images at 24 h after the 4th allergen challenge in C48/80 pretreated mice instilled intranasally with JTE-013 (3 mg/kg; N=8) or its vehicle (N=8) 30 minutes before OVA challenges. Data obtained from an analogous experiment performed on mice that had not been subjected to C48/80 pretreatment are also shown (JTE013 N=12; Vehicle N=12). Data are expressed as means ± sem.* indicates statistical significance (p<0.05) determined by Student's t-test on mice that had not been pretreated with C48/80 but received either JTE013 or its vehicle. # indicates statistical significance (p<0.05) determined by Student's t-test on vehicle-treated animals that had received C48/80 pretreatment or not.*

No significant differences were observed between the differential cell counts in the BAL fluid of mice pretreated with C48/80 with respect to those obtained from animals that had not received C48/80. Also, no differences between these groups were found on histological lung sections stained with PAS and hematoxylin-eosin, respectively regarding mucus secretion and interstitial cell infiltration (data not shown).

The proportions of degranulated mast cell that were estimated on toluidine blue-stained sections from the lung of ovalbumin-challenged mice treated with vehicle or JTE-013, and pretreated with C48/80 or not, are represented in Table 2. In both groups of mice that received chronic pretreatment with C48/80, a great proportion of degranulated mast cells was observed (67.7±3.3% in vehicle treated mice, 70.0±2.0% in JTE-013 treated mice), indicating the efficiency of chronic C48/80 administration

to deplete mast cells with their granules. Of note, when no C48/80 was administered, mice that were pretreated with JTE-013 did not show any reduction of the proportion of degranulated mast cells. These results indicates that, though JTE-013 induced a reduction of MRI fluid signals, the intranasal instillation of this compound prior to allergen challenge did not attenuate ovalbumin-induced mast cell degranulation (table 2).

Table 2 – *Counting of degranulated and non-degranulated mast cells on toluidine blue- stained lung sections from actively sensitized ovalbumin-challenged instilled intranasally with JTE-013 3 mg/kg, or its vehicle 30 minutes before ovalbumin challenges in the presence (JTE013 N=4; Vehicle N=4) or absence of C48/80 pretreatment(JTE013 N=4; Vehicle N=4). Data are expressed as mean ± sem.*

Treatment		Number of non-degranulated mast cells	Number of degranulated mast cells	Proportion of degranulated mast cells (in %)
Without C48/80 pretreatment	Vehicle	**7±2**	**9±3**	**54.6±2.4**
	JTE013	**9±3**	**17±3**	**66.5±10.0**
With C48/80 pretreatment	Vehicle	**6±1**	**12±1**	**67.7±3.3**
	JTE013	**8±3**	**17±5**	**70.0±2.0**

DISCUSSION

Tissue mast cells can be activated to release potent mediators of inflammation by antibody-dependent mechanisms, and can respond to very low doses of specific antigen (Galli, 1997; Turner & Kinet, 1999). Although mast cells would appear to be well suited to amplify local inflammatory responses to antigen challenge as suggested in this report, there is considerable debate about the importance of these cells in the expression of the features of chronic asthma in murine models (Corry et al., 1998; Galli, 1997; Hamelmann et al., 1999; Korsgren et al., 1997; Kung et al., 1995; Mehlhop et al., 1997). For example, it has been previously shown that airway hyperreactivity to methacholine can be induced in mice by IgE (Hamelmann et al.,

1999; Martin et al., 1993) and mast cell–dependent mechanisms (Martin et al., 1993). However, airway hyperreactivity and airway eosinophilia [characteristics of the chronic inflammation associated with asthma (Barnes, 1999; Corry & Kheradmand, 1999; Turner & Kinet, 1999)], can also be elicited in mouse models in the absence of mast cells (Kung et al., 1995;Takeda et al., 1997). Brightling et al. (2003) suggested that whether mast cells play a critical role in the development of features of asthma is dependent upon the asthma model under investigation.

In the present report, we used an in vivo murine model of airway inflammation in which C57BL/6 mice were actively immunized and challenged with OVA to examine the putative role of mast cells in the formation of allergen-induced signals detected by MRI. These signals have been previously demonstrated to be associated to plasma leakage and mucus secretion (Blé et al., 2007), both important features of airway inflammation. Our results showed that chronic administration of C48/80 has effectively depleted mast cells from their granule content, confirming earlier observations by Jaffery et al. (1994). Additionally, the mast cell degranulation observed in allergen-challenged mice that were not pretreated with C48/80, and the reduced volume of signals detected in the lungs of OVA-challenged mice that had been pretreated with C48/80 suggest that, in the present model, activation of mast cells by allergen challenge is implicated in the mechanism leading to the formation of prominent fluid signals in the lung. The residual volume of fluid signal detected in OVA-challenged mice pretreated with C48/80 (figure 1) indicates that mast cells participate in the inflammatory response but are not the only element orchestrating it. Interestingly, no significant changes in the eosinophil infiltration were detected in BAL fluid samples and on histological lung sections from OVA-challenged mice that were pretreated with C48/80. These findings are in line with other published observations showing that there is no mast cell-dependent contribution to eosinophil recruitment in response to allergen provocation (Kobayashi et al., 2000; Takeda et al., 1997; Williams & Galli, 2000). Therefore, our data support the hypothesis that, in the present murine model of asthma, mast cells constitute an amplifier of one important feature of antigen-dependent inflammation, namely interstitial and/or luminal fluid secretions that are detected by MRI, while not affecting pro-inflammatory cell infiltration.

Once the implication of mast cells in our model had been established, we tested the effects of local instillation of the $S1P_2$ receptor antagonist, JTE-013, on allergen-induced fluid signals since $S1P_2$ receptor has been previously suggested to be required for mast cell degranulation (Jolly et al., 2004). A statistically significant reduction of MRI fluid signals was observed when mice were treated with JTE-013 at doses of 1 and 3 mg/kg before allergen challenge. Moreover, the dose of 3 mg/kg JTE-013 had no significant effect in comparison to vehicle when animals were pretreated with C48/80, i.e., when mast cell granules were depleted. So far, our observations would indicate that JTE-013 may inhibit a mast cell-dependent mechanism, a result that would be in line with findings by Jolly et al. (2004) showing that antisense oligonucleotides for $S1P_2$ specifically inhibited IgE-induced mast cell degranulation in vitro. However, the fact that no reduction of the proportion of degranulated mast cells has been observed on toluidine blue-stained lung sections indicated that local administration of JTE-013 prior to allergen had no beneficial effects on mast cell degranulation in vivo.

Although further investigations would be necessary to understand why JTE-013 did not directly inhibit mast cell degranulation in our murine model, the possibility that S1P2 antagonism might influence other mechanisms than mast cell degranulation needs to be considered. The vascular permeability could be a possible contributor since a variety of potent mediators released by antigen-activated mast cells, including histamine, serotonin (in rodents), leukotriene C4 and certain cytokines (Bradding et al., 1995), are capable of inducing mucosal edema. Of note, rodents have large amounts of preformed serotonin in the granules of their mast cells. Serotonin is secreted abundantly during the allergic response and its relevance for increased vascular permeability is established (Evans et al., 1988; Hele et al., 1999). Moreover, proinflammatory mediators also released by activated mast cells have the potential to stimulate inflammatory effectors which are themselves able to release vasoactive substances. As an example, the lipid-derived mediator platelet activating factor released by mast cells has the potential to stimulate serotonin release by platelets and thus enhance plasma exudation from the lung vasculature. In addition, sphingosine-1-phosphate (S1P) was recently added to the list of proinflammatory bioactive lipids released by IgE-activated mast cells (Jolly et al. 2002) and its

involvement in endothelial barrier function has been demonstrated (McVerry & Garcia, 2005; Singleton et al., 2006). Interestingly, in a recent publication Sanchez et al. (2007) investigated the effects of the blockade of S1P2 receptor on vascular permeability in an ex vivo model of perfused rat lung. In this study, they were able to show that inhibition of S1P2 receptor signaling by JTE-013 resulted in decreased vascular permeability and H_2O_2-induced lung edema. These findings are in line with our hypothesis postulating that a direct effect of JTE-013 on endothelial S1P2 receptor may prevent the loss of vascular barrier integrity induced by degranulated mast cell products.

In conclusion, we have shown in a mast cell-dependent murine model that, following treatment with the S1P2 receptor antagonist, JTE-013, the reduction of allergen-elicited fluid signals detected by MRI in the lung was not due to inhibition of mast cell degranulation. A direct effect of the compound on vascular S1P2 receptors implicated in the endothelial barrier integrity could be a more likely mechanism. It would be important to test other S1P2 antagonists to verify whether this could be a generalized mechanism for this class of compounds.

ACKNOWLEDGEMENTS

The support from Daniel Wyss is gratefully acknowledged. The receipt of an award by the 3R Research Foundation (Münsingen, Switzerland) is gratefully acknowledged by NB (project 82/02).

REFERENCES

Barnes PJ. Therapeutic strategies for allergic diseases. *Nature.* 1999; 402(Suppl):B31-B38

Beckmann N, Tigani B, Ekatodramis D, Borer R, Mazzoni L, Fozard JR. Pulmonary edema induced by allergen challenge in the rat: noninvasive assessment by magnetic resonance imaging. *Magn Reson Med.* 2001;45(1):88-95.

Blé FX, Cannet C, Zurbruegg S, Karmouty-Quintana H, Bergmann R, Frossard N, Trifilieff A, Beckmann N. Allergen-induced lung inflammation in actively sensitized mice assessed by MRI. *Radiology.* Submitted.

Bradding P, Okayama Y, Howarth PH, Church MK, Holgate ST. Heterogeneity of human mast cells based on cytokine content. *J Immunol.* 1995;155(1):297-307.

Corry DB & Kheradmand F. Induction and regulation of the IgE response. *Nature* 1999; 402(Suppl):B18-B23

Corry DB, Grunig G, Hadeiba H, Kurup VP, Warnock ML, Sheppard D, Rennick DM, Locksley RM. Requirements for allergen-induced airway hyperreactivity in T and B cell deficient mice. *Mol. Med*. 1998;4:344-355

Galli SJ. Complexity and redundancy in the pathogenesis of asthma: reassessing the roles of mast cells and T cells. *J. Exp. Med.* 1997;186:343-347

Galli SJ & Costa JJ. Mast cell leukocyte cytokine cascades in allergic inflammation. *Allergy*. 1995; 50:851-862.

Eum SY, Norel X, Lefort J, Labat C, Vargaftig BB, Brink C. Anaphylactic bronchoconstriction in BP2 mice: interactions between serotonin and acetylcholine. *Br J Pharmacol* 1999; 126:312–6.

Evans TW, Rogers DF, Aursudkij B, Chung KF & Barnes PJ. Inflammatory mediators involved in antigen-induced airway microvascular leakage in guinea-pigs. *Am. Rev. Respir. Dis.* 1988;138: 395−399.

Hamelmann E, Tadeda K, Oshiba A, Gelfand EW. Role of IgE in the development of allergic airway inflammation and airway hyperresponsiveness – a murine model. *Allergy* 1999; 54: 297–305.

Hele DJ, Birrell MA, Foster M, Webber SE & Belvisi MG. Regional variation in microvascular leakage induced by ovalbumin, 5-HT, histamine and leukotriene D4 in the airways of the sensitised Brown Norway rat. *Eur. Resp. J.* 1999;14: 158s.

Jaffery G, Coleman JW, Huntley J & Bell E. Mast cell recovery following chronic treatment with compound 48/80. *International Archives of Allergy and Immunology.* 1994;105: 274-280.

Jolly PS, Bektas M, Olivera A, Gonzalez-Espinosa C, Proia RL, Rivera J, Milstien S, Spiegel S. Transactivation of sphingosine-1-phosphate receptors by FcepsilonRI triggering is required for normal mast cell degranulation and chemotaxis. *J Exp Med* 2004; 199: 959-970.

Jolly PS, Rosenfeldt HM, Milstien S, Spiegel S. The roles of sphingosine-1-phosphate in asthma. *Mol. Immunol.* 2002;38(16-18):1239-45.

Kobayashi T, Miura T, Haba T, Sato M, Serizawa I, Nagai H, Ishizaka K. An essential role of mast cells in the development of airway hyperresponsiveness in a murine asthma model. *J. Immunol.* 2000;164:3855-3861

Korsgren M, Erjefalt JS, Korsgren O, Sundler F, Persson CG. Allergic eosinophil-rich inflammation develops in lungs and airways of B-cell deficient mice. *J Exp Med* 1997; 185: 885–92.

Kung TT, Stelts D, Zurcher JA, Jones H, Umland SP, Kreutner W, Egan RW, Chapman RW. Mast cells modulate allergic pulmonary eosinophilia in mice. *Am. J. Respir. Cell Mol. Biol.* 1995;12:404-409

MacVerry BJ, Garcia JG. In vitro and in vivo modulation of vascular barrier integrity by sphingosine 1-phosphate: mechanistic insights. *Cell Signal*. 2005;17(2):131-9.

Martin TR, Takeishi T, Katz HR, Austen KF, Drazen JM, Galli SJ. Mast cell activation enhances airway responsiveness to methacholine in the mouse. *J Clin Invest* 1993; 91: 1176–82.

Mehlhop PD, van de Rijn M, Goldberg AB et al. Allergen induced bronchial hyperreactivity and eosinophilic inflammation occur in the absence of IgE in a mouse model of asthma. *Proc Natl Acad Sci USA* 1997; 94: 1344–9.

Mencia-Huerta JM, Lewis R, Razin E, Austen KF. Antigen-initiated release of platelet-activating factor (PAF acether) from mouse bone marrow-derived mast cells sensitized with monoclonal IgE. *J Immunol*. 1983; 131:2958-2963.

Nagai H, Yamaguchi S, Maeda Y, Tanaka H. Role of mast cells, eosinophils and IL-5 in the development of airway hyperresponsiveness in sensitized mice. *Clin Exp Allergy* 1996; 26:642–7.

Oldenburg PJ, Mustafa SJ. Involvement of mast cells in adenosine-mediated bronchoconstriction and inflammation in an allergic mouse model. *J Pharmacol Exp Ther.* 2005;313(1):319-24.

Osada M, Yatomi Y, Ohmori T, Ikeda H, and Ozaki Y. Enhancement of sphingosine 1-phosphate-induced migration of vascular endothelial cells and smooth muscle cells by an EDG-5 antagonist. *Biochem Biophys Res Commun*. 2002; 299, 483–487

Prieschl EE, Csonga R, Novotny V, Kikuchi GE, Baumruker T. The Balance between Sphingosine and Sphingosine-1-phosphate Is Decisive for Mast Cell Activation after Fc{isin} Receptor I Triggering. *The Journal of Experimental Medicine* 1999; 190: 1-8.

Rosen H ,Goetzl EJ Sphingosine 1-phosphate and its receptors: an autocrine and paracrine network. *Nat Rev Immunol* 2005; 5: 560-570.

Sanchez T, Skoura A, Wu MT, Casserly B, Harrington EO and Hla T. Induction of vascular permeability by the sphingosine-1-phosphate receptor–2 (S1P2R) and its downstream effectors ROCK and PTEN. *Arterioscler. Thromb. Vasc. Biol.* 2007;27;1312-1318

Singleton PA, Dudek SM, Ma SF, Garcia JG. Transactivation of sphingosine 1-phosphate receptors is essential for vascular barrier regulation. Novel role for hyaluronan and CD44 receptor family. *J Biol Chem*. 2006;281(45):34381-93.

Takeda K, Hamelmann E, Joetham A et al. Development of eosinophilic airway inflammation and airway hyperresponsiveness in mast cell deficient mice. *J Exp Med* 1997; 186: 449–54.

Turner H, Kinet JP. Signaling through the high-affinity IgE receptor FcRI. *Nature*. 1999;402(Suppl):B24-B30

Williams CMM, Galli SJ. Mast cells can amplify airway reactivity and features of chronic inflammation in an asthma model in mice. *J Exp Med* 2000; 192: 455–62.

MANUSCRIPT 4

In vivo assessments of mucus dynamics in the lungs using a Gd-Cy5.5-bilabeled contrast agent

Blé FX, Schmitd P, Kneuer R, Cannet C, Gérard C, Karmouty Quintana H, Zurbruegg S, Gremlich HU, and Beckmann N

In vivo assessments of mucus dynamics in the lungs using a Gd-Cy5.5-bilabeled contrast agent

François-Xavier Blé[¶,§,#] BSc MSc, Phillip Schmitd[¶] BSc MSc PhD, Rainer Kneuer[¶] BSc MSc PhD, Catherine Cannet[¶] BSc MSc, Harry Karmouty Quintana[¶] BSc MSc PhD, Stefan Zurbruegg[¶] BSc, Hans-Ulrich Gremlich[¶] BSc MSc PhD and Nicolau Beckmann[¶,1] BSc MSc PhD

Novartis Institutes for BioMedical Research

[¶]Discovery Technologies and [§]Respiratory Diseases Department, CH-4056 Basel, Switzerland

[#]University Louis Pasteur-Strasbourg-1, Faculty of Pharmacy, F-67401 Illkirch Cedex, France.

[1] Correspondence to: Nicolau Beckmann, PhD

Novartis Institutes for BioMedical Research

Discovery Technologies, Analytics and Imaging Sciences Unit

Forum 1, Novartis Campus

WSJ-386.2.09

CH-4002 Basel – Switzerland

Tel.: +41-61-3249576; Fax: +41-61-3243889

e-mail: nicolau.beckmann@novartis.com

The receipt of an award by the 3R Research Foundation (Münsingen, Switzerland) is gratefully acknowledged by NB (project 82/02).

ABSTRACT

It has been shown previously that MRI can detect in the lungs of lipopolysaccharide (LPS)-challenged rats signals reflecting secreted mucus (Beckmann et al., 2002; Tigani et al., 2002). As these signals are of low intensity, we examined here the feasibility of improving the MRI mucus detection by using a contrast agent, NVP-BCR249/250, a Gd- and Cy5.5-labeled aminodextran aimed at binding specifically to mucus. Administration of the contrast agent either as powder or solution led to a significant increase of signals 24 h after endotoxin. The signals remained increased for about 24 h after the probe administration. Histology revealed that NVP-BCR249/250 was bound specifically to mucus. Secondly, we tested in this model uridine triphosphate (UTP) which is known to increase the rate of mucus clearance in patients suffering from chronic bronchitis or from cystic fibrosis. Within one hour from its administration, UTP (60 mM) in physiological saline applied simultaneously with the probe at 24 h after LPS resulted in a larger signal increase than that observed when only the contrast agent had been instilled. Despite the acceleration of the clearance of labeled mucus by UTP illustrated by the decreased probe-specific signals, the therapeutic effect of the compound was questionable since the course of MRI signals showed that the overall fluid content 24 h after UTP and later was the same for UTP- and vehicle-treated rats. This fact suggests that when examining compounds aimed at influencing the mucus dynamics it is essential to get a global view of fluid dynamics in the lungs rather than of mucociliary clearance only. Thanks to the use of the contrast agent NVP-BCR249/250, we showed here that MRI detects the resultant effect of mucus release/clearance balance. Thus, the present method provides a good strategy to assess the effects of compounds affecting mucociliary clearance from the whole lung *in vivo*, information that may support mucokinetic-based investigations.

INTRODUCTION

Mucociliary clearance is an important mechanism for removing inhaled particles, secretions and cellular debris from the respiratory tract. Dysfunctions in airway clearance are associated with the accelerated loss of lung function in patients with obstructive lung diseases as chronic obstructive pulmonary disease (COPD), asthma, cystic fibrosis and bronchiectasis. Airway mucus hypersecretion is a further important characteristic of these lung conditions [see Cazzola et al., 2007; Danahay and Jackson, 2005; Livraghi and Randell, 2007; Morcillo and Cortijo, 2006 for recent reviews]. A better understanding of the disease pathogenesis is required to identify specific therapeutic targets which, in turn, should lead to the rational design of drugs for treatment of obstructive pulmonary diseases (Kelly, 2007; Rogers and Barnes, 2006; Rowe and Clancy, 2006).

In humans and large animals, assessment of mucociliary clearance is most commonly performed using inhaled radiolabeled aerosols and scintigraphy (Foster and Wagner, 2001; Morgan et al., 2004). Studies regarding the clearance from the lung of fluorescent polystyrene microspheres using serial analyses bronchoalveolar lavage (BAL) fluid are performed in small animals (Coote et al., 2004). Evidently, using radioactive materials or performing terminal experiments represent major limitation in research. It would be desirable to have a non-invasive method to measure mucociliary clearance at high spatial resolution in small rodents.

It has been reported previously that magnetic resonance imaging (MRI) can detect a mucus hypersecretory phenotype in the rats after lipopolysaccharide (LPS) challenge (Beckmann et al., 2002). Following intratracheal administration of LPS to naïve Brown Norway (BN) rats, discontinuous MRI signals of long duration were observed in the lungs up to 16 days after dosing. The parameter in the BAL fluid that correlated significantly with the MRI signals was the mucus concentration (Beckmann et al., 2002; Tigani et al., 2002). Histological analysis indicated a substantial and sustained increase in goblet cell number up to 16 days after LPS challenge, and flocculent mucoid material was consistently detected close to the apical surface of epithelial cells (Beckmann et al., 2002). These observations clearly indicate that the long lasting MRI signal following LPS was due to secreted mucus.

Since dextran is a polysaccharide that competes with mucous glycoproteins for hydrogen bonding sites (Feng et al., 1999), we verified in the present work whether our contrast agent NVP-BCR249/250, a Gd- and Cy5.5-labeled aminodextran was able to bind specifically to mucus. Then, we examined the feasibility of improving the MRI mucus detection by using the contrast agent NVP-BCR249/250, a Gd- and Cy5.5-labeled aminodextran in LPS-challenged rats the. Finally, the probe was adopted to study MRI signal dynamics in the presence or absence of uridine triphosphate (UTP) which is known to increase the rate of mucus clearance in healthy humans as well as in patients suffering from chronic bronchitis or cystic fibrosis (Johnson et al., 2002; Kellerman, 2002; Roomans, 2003).

MATERIALS AND METHODS

Animals

Male Brown Norway (BN) rats, weighing 270-300 g, were supplied by IFFA CREDO (L'Arbresle, France). Upon arrival animals were kept at an ambient temperature of 22 ± 2°C under a 12 h normal phase light-dark cycle and fed with pellets (Nahr- und Futtermittel AG, Gossau, Switzerland) for at least one week before starting the experiments. Drinking water was freely available.

Experiments were carried out with the approval of the Veterinary Authority of the City of Basel (license number 1989).

LPS Challenge

Animals were anesthetised with 3% isoflurane (Abbott, Cham, Switzerland) and LPS from Salmonella typhosa (Sigma, Dorset, UK; 1 mg/kg dissolved in 0.2 ml saline) was administered intra-tracheally (i.t.) and the animals allowed to recover.

Contrast Agents (NVP-BCR250 and NVP-BCR249)

- Synthesis and characterization

NVP-BCR250: Aminodextran10 (425 mg, 0.042 mmol; MW: 10.000 Da; Molecular Probes, Invitrogen, Basel, Switzerland) was dissolved over a period of 2 h

(swelling) in $NaHCO_3$ (0.1 M, 15 ml) and adjusted to pH 9 by Na_2CO_3 (0.1 M). After adding Cy5.5-NHS (1.1 eq., 46.9 mg, 0.046 mmol) dissolved in $NaHCO_3$ (0.1 M, 0.5 ml) the resulting mixture was stirred for 15 min at room temperature. pSCN-Bn-DOTA (6 eq., 177 mg, 0.253 mmol; Macrocyclics) was dissolved in $NaHCO_3$ (0.1 M, 5 ml) adjusted to pH 9 by Na_2CO_3 (0.1 M) and added to the reaction mixture that was stirred additional 18h at room temperature. Part of the reaction mixture (0.2 ml) was purified by size exclusion chromatography (sephadex, bidest. water). After lyophilization the labeling ratio of the DOTA-ligand was determined by ^{1}H-NMR. The adduct was purified by ultrafiltration (MWCO 5.000, PES, 5 x $NaHCO_3$, 0.1 M) until the filtrate appeared colorless. The buffer was exchanged (2 x citrate buffer, 0.1 M, pH 8) and after dissolving Gadolinium chloride hexahydrate (5 eq., 78.4 mg, 0.211 mmol; Sigma) in citrate buffer (0.1 M) and adjusting to pH 8 by NaOH (1 M) the reaction mixture was stirred for 72h at room temperature. Purification was carried out by ultrafiltration (MWCO 5.000, PES, 5 x citrate buffer, 0.1 M; pH 8, 5 x bidest. water) until the filtrate was free of unbound gadolinium ions (xylenol orange test at pH 6). Elemental analysis showed labeling of 4.49% Gd/mol: 4 x Gd per molecule. Cy5.5 ratio was determined by an UV-absorbance concentration assay at wavelength maximum of the dye: 0.75 x Cy5.5 per molecule.

NVP-BCR249 was synthesized as described above for BCR250 starting from aminodextran70 (MW: 70.000 Da; Molecular Probes). Elemental analysis: 4.42% Gd/mol: 24 x Gd per molecule. UV determined Cy5.5 ratio: 0.55 x Cy5.5 per molecule.

- Powder and dissolved formulation

As the vehicle (0.9% NaCl) itself is known to induce MRI signal enhancement in the rat lung (data not shown) it was decided first to apply the contrast agent as a dry powder. NVP-BCR250 milling led to particles that were small enough (90% under 5µm) (Figure 1) to be applied i.t. by the 5 milliliter-syringe jet through a 1.6 mm diameter cannula.

NVP-BCR249 was dissolved in physiological saline (20 mg/ml) when synchronously administrated with the tested-drug or -vehicle solution.

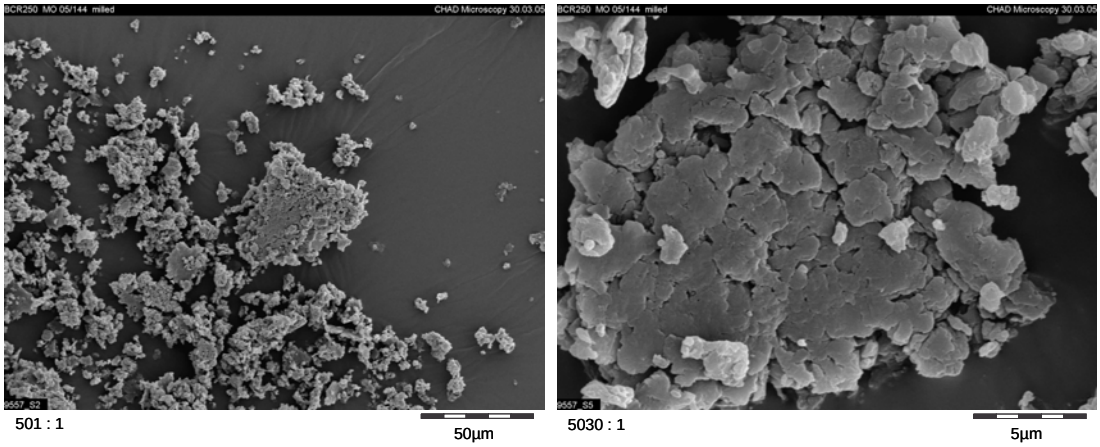

Figure 1 *– Electron microscopy of milled NVP-BCR250 at two different magnifications.*

- Ex Vivo Imaging

Phantom studies were made with human sputum that was incubated 30 minutes in contrast agent-solutions (1 ml). After three washings with bidestilled water (15 ml overall) the sputum was stored in 0.9% NaCl and stable for days. Phantoms containing mucus and contrast agents with different labeling properties or control solutions were compared under daylight, by magnetic resonance imaging and by near infrared fluorescence imaging.

- Drug administration

As uridine 5'-triphosphate (UTP) may enhance the secretion of mucus in addition to its clearance (Kim and Lee 1991; Kim et al 1996) and aiming to guarantee the same distribution of the compound and of the contrast agent in the lung, the probe was administered at the same time as UTP. Thus, UTP (60 mM; Sigma-Aldrich, Buchs, Switzerland) was dissolved in physiological saline (vehicle) with or without added NVP-BCR249. Aliquots (200 µl) of the solutions were sprayed i.t. 24 h after LPS challenge.

MRI

Measurements were carried out with a Biospec 47/40 spectrometer (Bruker, Karlsruhe, Germany) operating at 4.7 T. A gradient-echo sequence with repetition time 5.6 ms, echo time 2.7 ms, band width 100 kHz, flip angle of the excitation pulse approximately 15º, field of view 6x6 cm2, matrix size 256x128 and slice thickness 1.5 mm was used throughout the study. A single slice image was obtained by

computing the 2DFT of the averaged signal from 60 individual image acquisitions and interpolating the data set to 256x256 pixels. There was an interval of 530 ms between individual image acquisitions, resulting in a total acquisition time of 75 s for a single slice. A birdcage resonator of 7 cm diameter was used for excitation and detection. During MRI measurements, rats were anesthetized with 2 % isoflurane in a mixture of O_2/N_2O (1:2), administered via a face mask, and placed in supine position. The body temperature of the animals was maintained at 37 °C by a flow of warm air.

Image Analysis

The volume of fluid signals was quantified using a semiautomatic segmentation procedure implemented in the IDL (Interactive Data Language Research Systems, Boulder, Colorado, USA) environment (version 5.1) on a Linux system. The procedure was extensively described in Beckmann et al (2001). Segmentation parameters were the same for all analyzed images, chosen to segment regions corresponding to high intensity signals. Because the fluid signals and those from vessels were of comparable intensities, the volume corresponding to the vessels was assessed on baseline images and then subtracted from the volumes determined on post-treatment images.

Histology

Immediately following an MRI session, rats were killed by an overdose of pentobarbital (250 mg/kg i.p.). After being removed from the thorax, lungs were immersed in 10% neutral formalin buffer for 72 h. After fixation, transverse sections were cut through the median part of the left, the right apical, the median and the caudal lobes, dehydrated through increasing graded series of ethylic alcohol, and processed into paraffin wax overnight. Three serial slices of 3 µm thickness were cut from each section. Following stainings were then applied: (i) hematoxylin/eosin to assess general morphology; (ii) PAS/Alcian blue reaction to detect mucus and goblet cells. One slice was left unstained for the detection of Cy5.5 by confocal microscopy.

Near-Infrared Fluorescence (NIRF) Imaging

NIRF images were acquired from isolated lungs, harvested immediately after an MRI session. For fluorescence excitation, three laser diodes operating at 660 nm with a power of 10 mW/cm2 were used. The fluorescent light emitted from the lung samples was detected by a charge-coupled device (CCD) camera (Hamamatsu Photonics, Schüpfen, Switzerland) equipped with a focusing lens system (macro lens 60 mm, 1:2.8, Nikon). The CCD featured low noise and low dark signal, enabling low light level detection as well as long integration times. The matrix size of the images was 532×256 pixels. A hard filter was used for selecting the wavelength at detection (700 nm). Data acquisition (i.e. integration) times ranged from 0.5 to 2.0 s depending on the intensity of fluorescence. The experiment was controlled by a PC using the Siemens SYNGO® software.

Statistics

ANOVA (with the Bonferroni method) and Student's t-test comparisons were performed for the volume of fluid signals determined by MRI using the SigmaStat 3.1 (©2003 Systat Software, Inc., Point Richmond, CA) software package.

RESULTS

The characterization of the contrast agent abilities was first stepped by the ex-vivo experiment in which phantoms containing mucus and contrast agents with different labeling properties or control solutions were tested under different imaging modalities (Figure 2). Among different contrast agents NVP-BCR249 showed best labeling properties, as illustrated in figure 2 by a clear enhancement of the signal rising from BCR249-labelled mucus under both magnetic resonance and near infrared fluorescence imaging modalities. Thus, NVP-BCR249 was suggested for in vivo studies.

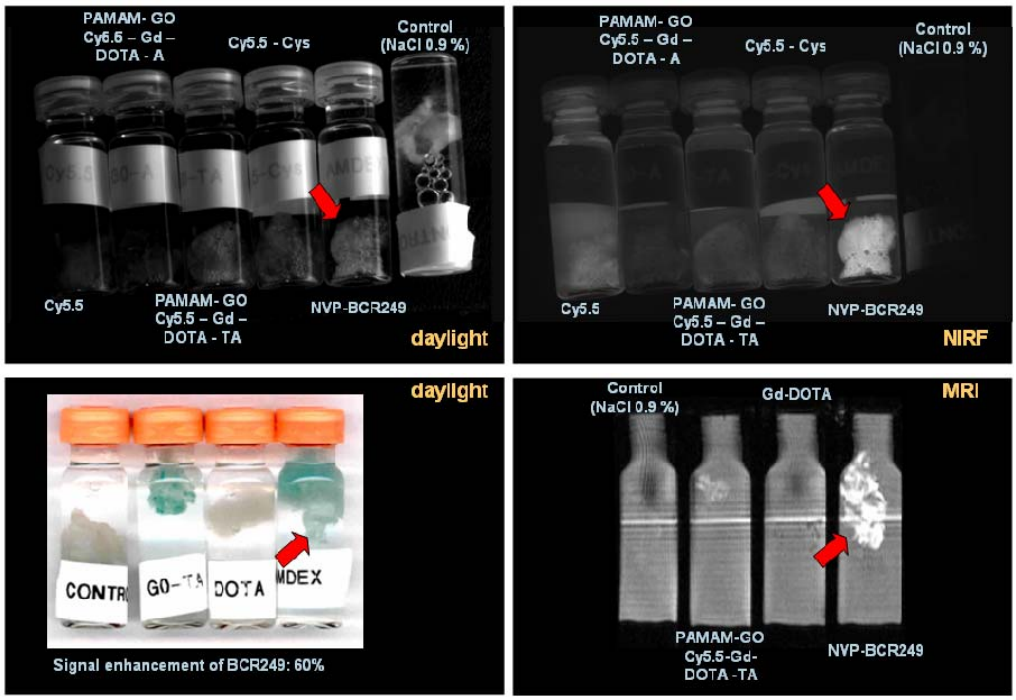

Figure 2 *– NIRF (top row) and MR imaging(right bottom) of labeled mucus by different contrast agents. Red arrows indicate BCR249-labeled mucus for which clear signal enhancement was observed.*

Figure 3 shows representative MRI transverse sections through the thoracic region of a BN rat before and at various times following i.t. exposure to LPS (1 mg/kg). In agreement with previous studies (Beckmann et al., 2002; Tigani et al., 2002), a discrete signal of weak intensity was detected by MRI at 24 h following LPS. Intra-tracheal administration of NVP-BCR250, the contrast agent in powder form, at this time point resulted in a significant increase of MRI signals until 24 h later (Figure 3). Histology demonstrated that the agent bound specifically to mucin that had been secreted or was present in goblet cells (Figure 4). Similar enhancement of MRI signals was observed when NVP-BCR249, the agent in solution form, was given 24 h post-LPS (Figure 5). The increased signal was still detected 24 h later and at this time point, NIRF confirmed the presence of the contrast agent in the isolated lungs from the same animal (Figure 5).

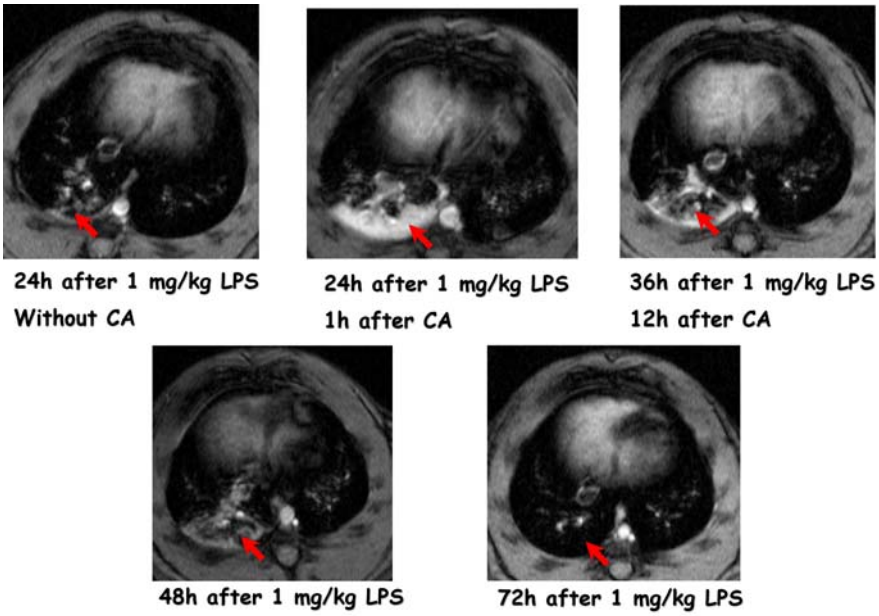

Figure 3 *– Representative prominent MRI signal increase in the lung of BN rat, induced by NVP-BCR250 (CA, 20 mg/kg) applied i.t. as a powder, 24h after intratracheal LPS instillation (1 mg/kg).*

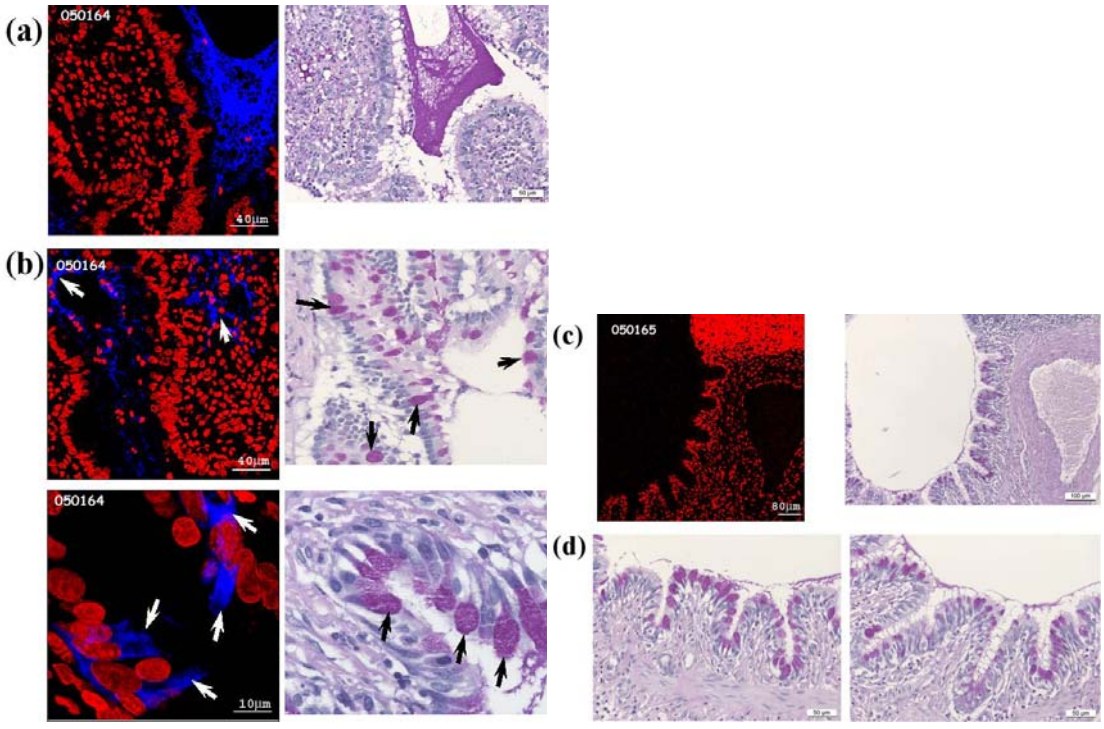

Figure 4 *- Confocal microscopy (mucus: blue; nuclei: red) and PAS/Alcian blue (mucus: violet; nuclei: blue) stained sections of lungs from LPS-challenged rats. (a) Confocal microscopy (left) demonstrates that NVP-BCR250 bound specifically to mucus. (b) NVP-BCR250 also marked mucus present in goblet cells. (c) No mucus was labeled when vehicle was administered. (d) The number of goblet cells was the same in LPS-challenged rats treated with NVP-BCR250 (left) or vehicle (right).*

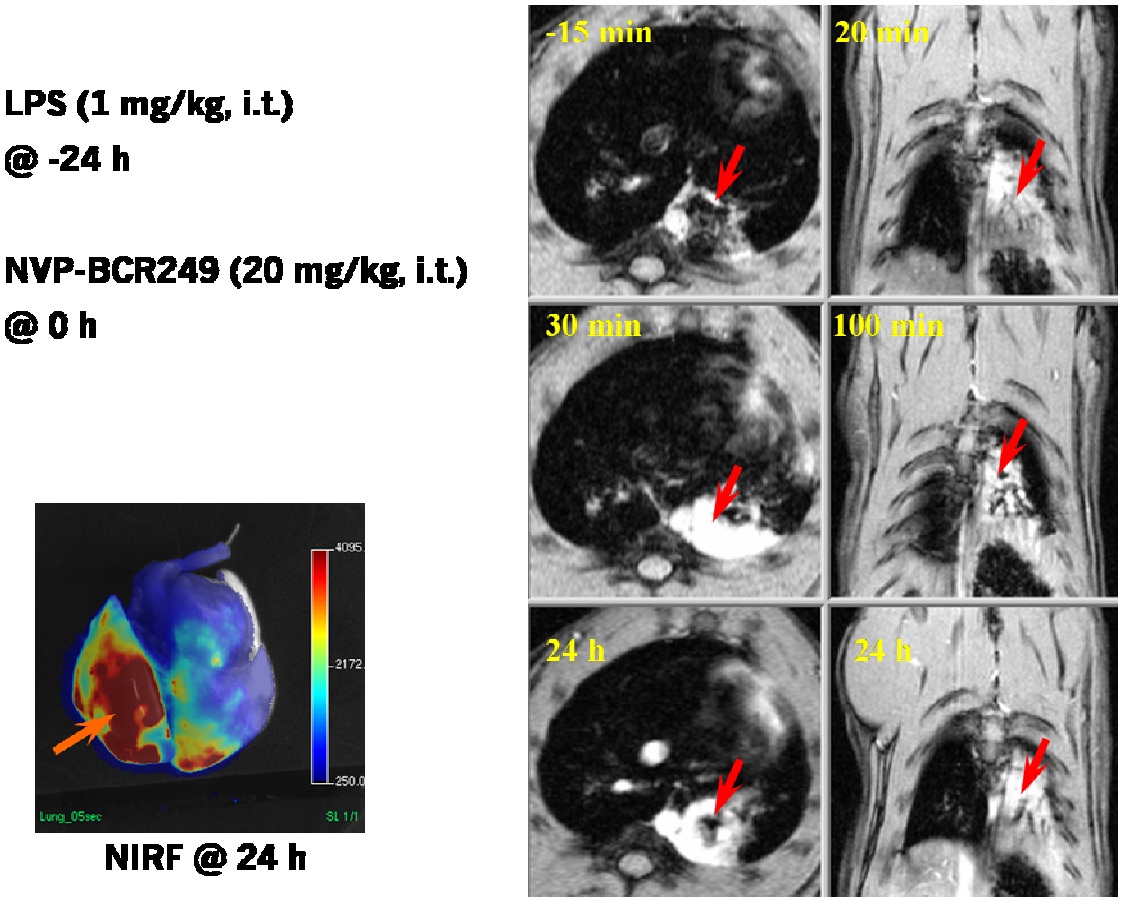

Figure 5 *- Intra-tracheal administration of NVP-BCR249 in solution (0.2 mL) led to prominent increase in the intensity of MRI signals induced by LPS, which persisted for 24 h after contrast agent delivery. The presence of the contrast agent predominantly in the left lobe, where the initial response has been detected by MRI, was confirmed by NIRF. The NIRF image was acquired from isolated lungs harvested from the animal immediately after the MRI session.*

Figure 6 illustrates the course of MRI signals detected in the lungs of LPS-challenged rats that received NVP-BCR249 or its vehicle (saline) at 24 h after endotoxin exposure. Intra-tracheal administration of the agent led to a prominent increase in signal volume in the first hour following its delivery. Six hours later, the signal volume had decreased to pre-contrast agent administration levels, probably because of mucus clearance. Nonetheless, the signal volumes were still significantly augmented 24 h after LPS when compared to those signals observed after the solvent instillation (Figure 6).

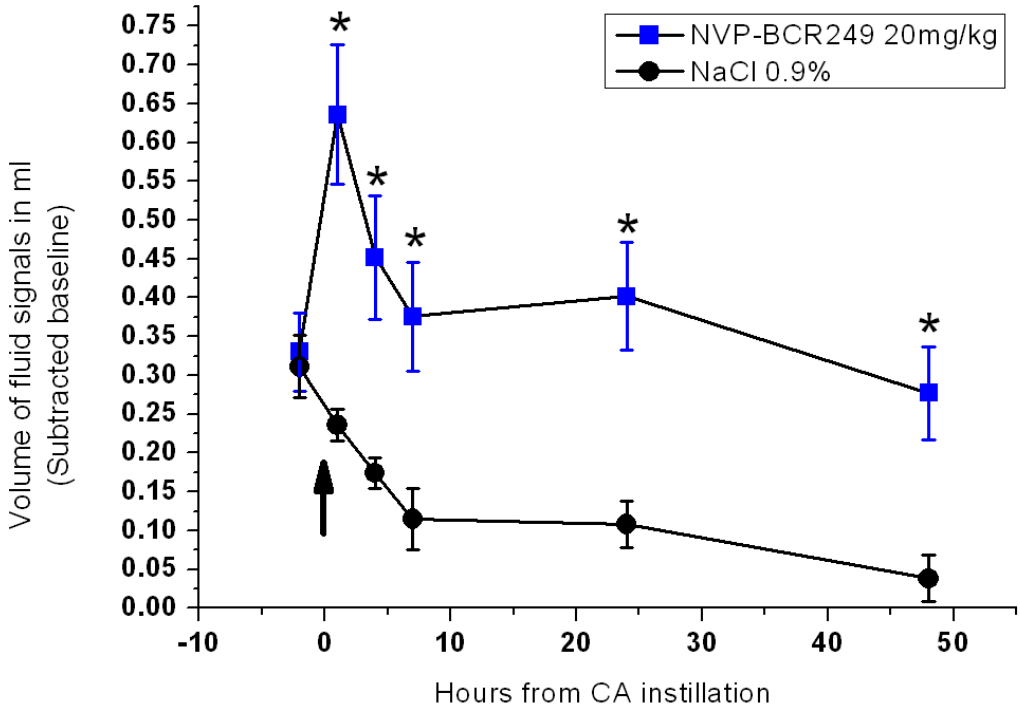

Figure 6 *- Volume (mean±sem, n=7 in each group) of MRI signals detected in the lungs of naïve BN rats following LPS (1 mg/kg) administration as a spray. The contrast agent NVP-BCR-249 (CA, 0.2 ml) or its vehicle (0.2 ml of NaCl 0.9%) was sprayed i.t. 24 h after LPS (Black arrow).*p<0.05 indicates statistical significance determined by Student's t-test comparisons between the CA and vehicle instilled rats.*

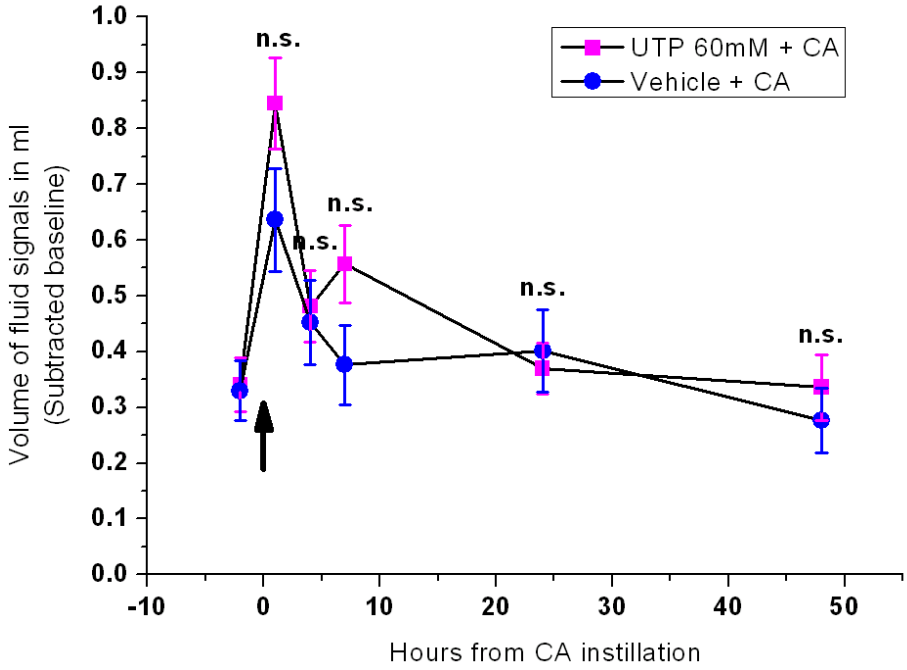

Figure 7 *- Volume (mean±sem, n=7 in each group) of MRI signals detected in the lungs of naïve BN rats following LPS (1 mg/kg) administration as a spray. UTP (60 mM) or its vehicle (saline, 0.2 ml) was sprayed i.t. together with the mucus CA (BCR-249) 24 h after LPS. n.s. : no significant difference determined by Student's t-test comparisons between the UTP and vehicle treated rats.*

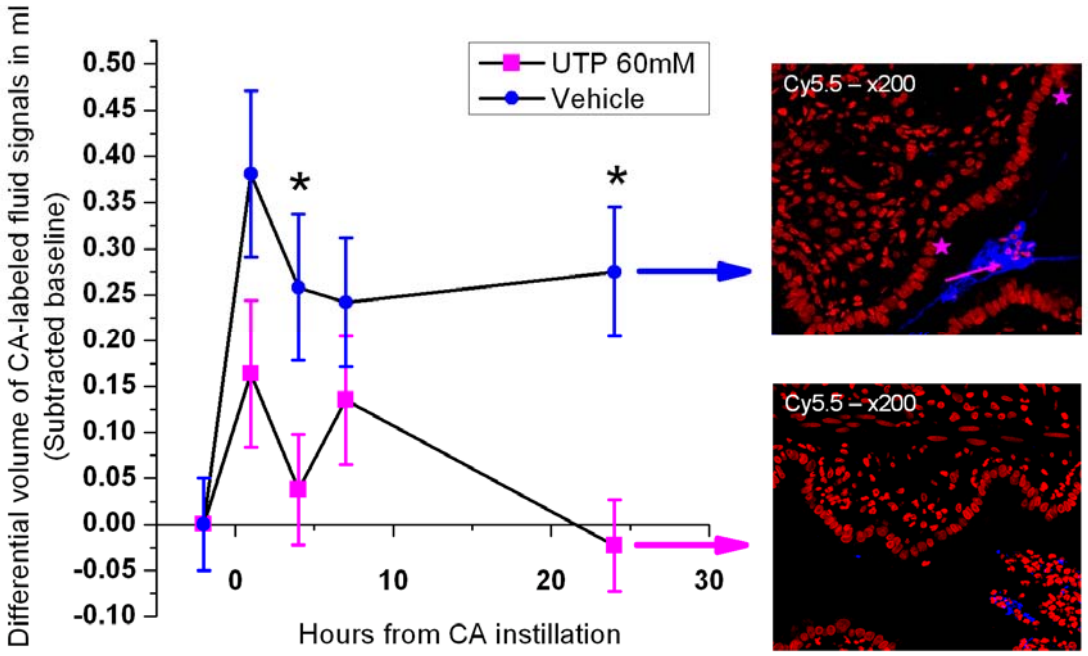

Figure 8a *- Kinetics of mucus labeled by the CA NVP-BCR249, administered together with UTP or its vehicle (saline), 24 h following LPS challenge. These curves are the result of subtractions between the data presented in figure 7 and those generated in the same conditions but without the contrast agent. Confocal microscopy (blue: mucus) confirmed the lower content of labeled mucus in UTP-treated rats suggested by the MRI data.*

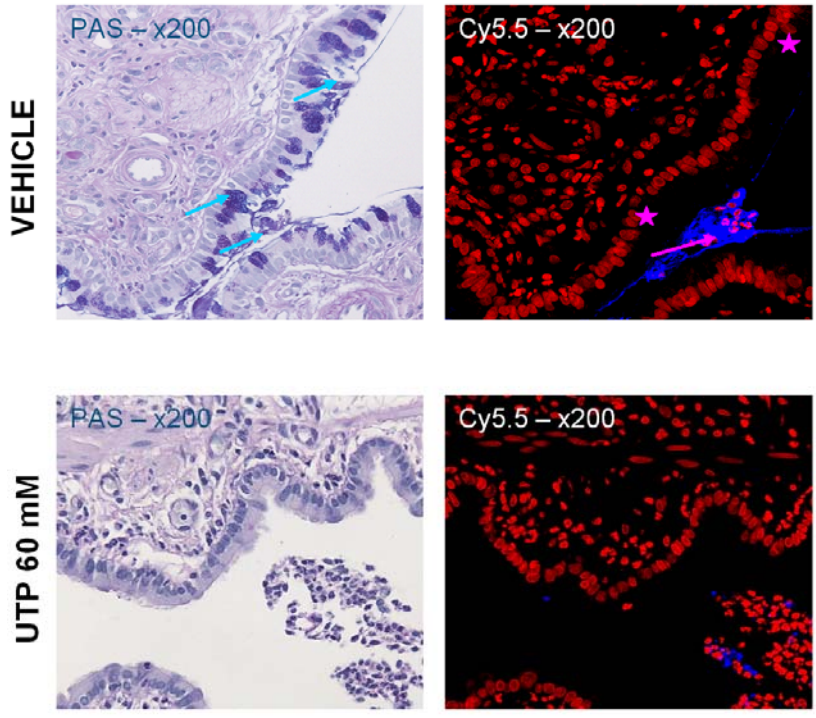

Figure 8b *- (Top) Histological analysis demonstrating a massive presence of mucus in goblet cells (blue arrows in the PAS section) and of labeled mucus (blue region in the confocal microscopic image) at 24 h after vehicle treatment (25 h after LPS). (Bottom) Twenty four hour after UTP (60mM) administration, goblet cells were empty (PAS section) and the airways lumen devoid of labeled mucus (confocal microscopic image).*

To avoid potential interferences arising from an additional instillation of liquid in the lung, UTP was dosed simultaneously to contrast agent instillation. The course of signals detected by MRI in the lungs of BN rats following the administration of UTP or its vehicle together with the contrast agent, at 24 h after endotoxin, is summarized in figure 7. Within the first hour following its administration, UTP induced an increase in the global fluid volume in the lung (mucus, surfactant, secretion hydration). The fluid resorption was then enhanced but, compared to vehicle treatment, there was no beneficial effect of UTP on global fluid volume even 48 h after dosing. This is better illustrated by the dynamics of mucus labeled by the contrast agent (figure 8a), obtained by subtracting from the curves of figure 6a data obtained in the same condition but without contrast agent addition. Because the contrast agent binds specifically to mucus, it can be assumed that the subtraction of fluid signals obtained without the probe from signals detected in the presence of the agent provides a means to measure the kinetics of contrast agent-labeled mucus in the lung. With this approach, it can be seen that UTP had an early effect (significant 4 h after its administration) on the clearance of labeled-mucus whereas the vehicle-instilled animals demonstrated maintained probe-specific signals until 24 h (figure 8). Histological analysis confirmed that UTP administration led to emptying of goblet cells and to an accelerated clearance of labeled mucus from the airways lumen (Figure 8b).

DISCUSSION

The present results show that, in LPS-instilled BN rats, our contrast agent NVP-BCR249/250, a Gd- and Cy5.5-labeled aminodextran bound specifically to mucus. These findings are in agreement with Feng et al. (1999) observations suggesting that the polysaccharide dextran competes with mucous glycoproteins for hydrogen bonding sites. The instillation of NVP-BCR249/250 in rats with mucus hypersecretory phenotype induced a prominent and durable increase of MRI sensitivity to detect mucus. Thanks to its combined fluorescent and paramagnetic properties, our probe NVP-BCR249/250 allowed for multimodal examination of the mucus dynamics in the whole lung. Indeed, the MRI readouts were straightforward validated by near infrared imaging and fluorescent-based histological technique i.e. confocal microscopy. Careful histological examination revealed that not only secreted mucus, but also mucin in goblet cells was labeled by the contrast agent. This suggests that the time course of MRI signals in the lungs of LPS-challenged animals following administration of the contrast agent did not only reflect mucus clearance, but also the resolution of mucus plugging. It is also conceivable that NVP-BCR249/250 is only slowly cleared from the lung, thus contributing to enhance the signal from continuously secreted mucus.

The clearance of particles from the airways is a complex process. Upon inhalation, particles deposited on airway epithelium are cleared by various mechanisms. Depending on their initial site of deposition, a fast- and a slow-clearance phase have been observed in particle retention experiments. The fast-clearance phase has traditionally been interpreted as tracheobronchial whereas the slow-clearance phase is commonly attributed to mechanical clearance from the alveolar region (ICRP 1994). While general agreement supports that mucociliary transport is the principal clearance mechanism in the tracheobronchial region during the first 24 h after exposure, experimental data from bolus inhalation studies indicated the existence of a slow bronchial clearance phase (Stahlhofen et al., 1990). Recent assessments of mucociliary clearance in the human tracheobronchial tree suggested that these findings might be partly explained by a delayed clearance from

peripheral bronchiolar airways in an asymmetric lung structure (Asgharian et al., 2001).

Tracheal mucociliary clearance velocities in rats display a wide range of values, presumably because of differences in the techniques used for measurements. Values found in the literature range between 1.9 and 8.1 mm/min (Felicetti et al., 1981; Giordano and Morrow, 1972; Patrick and Stirling, 1977). Anesthesia may influence (decrease) mucociliary transport. A comparison of these values with the rates of MRI signal resolution suggests that what we detected with MRI were events related to the delayed clearance phase.

The impairment of MCC in the airways is central to the pathophysiology of various respiratory disorders (Wanner 1977). The functional relationships among the ciliated surface epithelium, the mucous (gel) layer, and the underlaying perciliary fluid (sol) layer constitute the basic interactions that promote mucociliary transport (Fulford and Blake, 1986). Therefore, the disruption of any single component of this naturally occurring defense system can contribute to mucociliary dysfunction.

Exogenous nucleotides have been shown to modulate several physiological activities that are vital to the mucociliary apparatus. Adenosine triphosphate (ATP) and UTP have been shown to induce chloride secretion and water movement into the airway surface liquid (Jiang et al., 1993; Knowles et al., 1991; Mason et al., 1991) which hydrates mucus and optimizes perciliary fluid viscosity, both crucial for an efficient ciliary beating (Boucher, 1992). Other studies demonstrated the direct stimulatory effects of UTP on ciliary beat frequency (Wong and Yeates, 1992), as well as increased submucosal gland secretion (Merten et al., 1993) and goblet cell degranulation (Kim and Lee 1991; Lethem et al., 1993) induced by UTP. The combination of these effects should enhance MCC in the airways. Previous in vivo studies with ATP (Laurenzi et al., 1968) and, more recently, UTP (Olivier et al., 1996) confirm this hypothesis.

In our study, administration of UTP led to a distinct signal increase within one hour. Based on previous results showing that MRI non-invasively detects LPS-induced mucus hypersecretion (Beckmann et al., 2002; Tigani et al., 2002), we hypothesize that the signal increase observed following UTP was due to the opening

of goblet cells and concomitant release of mucus. This was confirmed by histological analysis, as there was less contrast agent-labeled mucus in the lungs of UTP- than vehicle-treated animals (figure 6c). These observations are consistent with the view that increased mucus secretion is often coupled with increased mucus clearance (Kishioka et al., 2003). This may be a protective response of the lung. Despite the acceleration of the clearance of labeled mucus by UTP, the therapeutic effect of the compound is questionable. Indeed, the MRI signal course displayed in figure 6b shows that the overall fluid content 24 h after UTP and later was the same for UTP- and vehicle-treated rats, suggesting no beneficial effect of the compound.

In summary, our results indicate the advantage of using MRI and the probe NVP-BCR249/250 for labeling specifically mucus: the technique provides at the same time a global view on overall fluid dynamics, as well as specific information on the mucus dynamics. Both informations may be fundamental in gaining insights into the therapeutic value of compounds aiming at influencing the dynamics of mucus in the lung.

ACKNOLEDGEMENTS

We gratefully acknowledge the support from several colleagues from Development: Milling processes were performed by A. Baumberger and W. Wirth (CHAD/PPO); electron microscopy by D. Märtin and K. Paulus (CHAD/ARD), and Brigitte Greiner (CHAD/Tox). Comments by H. Danahay from RDTA Horsham are gratefully acknowledged.

REFERENCES

Asgharian B, Hofmann W, Miller FJ (2001) Mucociliary clearance of insoluble particles from the tracheobronchial airways of the human lung. J Aerosol Sci; 32:817–832.

Beckmann N, Tigani B, Sugar R, Jackson AD, Jones G, Mazzoni L, Fozard JR (2002) Noninvasive detection of endotoxin-induced mucus hypersecretion in rat lung by MRI. Am J Physiol Lung Cell Mol Physiol; 283:L22-L30.

Boucher RC (1992). Drug therapy in the 1990s. What can we expect for cystic fibrosis? Drugs; 43:431-439.

Cazzola M, Donner CF, Hanania NA (2007) One hundred years of chronic obstructive pulmonary disease (COPD). Respir Med; 101:1049-1065.

Coote K, Nicholls A, Atherton HC, Sugar R, Danahay H (2004) Mucociliary clearance is enhanced in rat models of cigarette smoke and lipopolysaccharide-induced lung disease. Exp Lung Res; 30:59-71.

Danahay H, Jackson AD (2005). Epithelial mucus-hypersecretion and respiratory disease. Curr Drug Targets Inflamm Allergy; 4:651-664.

Felicetti SA, Wolff RK, Muggenburg BA (1981). Comparison of tracheal mucous transport in rats, guinea pigs, rabbits, and dogs. J Appl Physiol; 51: 1612–1617.

Feng W, Garret H, Speert DP, King M (1998) Improved clearability of cystic fibrosis sputum with dextran treatment *in vitro.* Am J Respir Crit Care Med; 157: 710-714.

Feng W, Nakamura S, Sudo E, Lee MM, Shao A, King M (1999) Effects of dextran on tracheal mucociliary velocity in dogs *in vivo.* Pulm Pharmacol Ther; 12: 35-41 .

Foster WM, Wagner, EM (2001) Bronchial edema alters ^{99m}Tc-DTPA clearance from the airway surface in sheep. J Appl Physiol; 91:2567-2573.

Giordano AM, Morrow PE (1972) Chronic low-level nitrogen dioxide exposure and mucociliary clearance. Arch Environ Health; 25: 443–449.

International Commission on Radiological Protection (ICRP) (1994). *Human Respiratory Tract Model for Radiological Protection*. ICRP Publication 66, Annals of the ICRP 24, 1–3. Elsevier Science, Oxford.

Jiang C, Finkbeiner WE, Widdicombe JH, McCray PB Jr, Miller SS (1993). Altered fluid transport across airway epithelium in cystic fibrosis. Science; 262:424-427.

Johnson FL, Donohue JF, Shaffer CL (2002) Improved sputum expectoration following a single dose of INS316 in patients with chronic bronchitis. Chest; 122:2021-2029.

Kellerman DJ (2002) P2Y(2) receptor agonists: a new class of medication targeted at improved mucociliary clearance. Chest; 121(5 Suppl):201S-205S.

Kelly HW (2007) Non-corticosteroid therapy for the long-term control of asthma. Expert Opin Pharmacother; 8:2077-2087.

Kim KC, Lee BC (1991). P2 purinoceptor regulation of mucin release by airway goblet cells in primary culture. Br J Pharmacol; 103:1053-1056.

Kim KC, Park HR, Shin CY, Akiyama T, Ko KH (1996). Nucleotide-induced mucin release from primary hamster tracheal surface epithelial cells involves the P2u purinoceptor. Eur Respir J; 9:542-548.

Kishioka C, Okamoto K, Kim JS, Rubin BK (2003) Hyperosmolar solutions stimulate mucus secretion in the ferret trachea. Chest; 124:306-313.

Knowles MR, Clarke LL, Boucher RC (1991). Activation by extracellular nucleotides of chloride secretion in the airway epithelia of patients with cystic fibrosis. N Engl J Med; 325:533-538.

Laurenzi GA, Yin S, Guarneri JJ (1968). Adverse effect of oxygen on tracheal mucus flow. N Engl J Med; 279:333-339.

Lethem MI, Dowell ML, van Scott M, Yankaskas JR, Egan T, Boucher RC, Davis CW (1993). Nucleotide regulation of goblet cells in human airway epithelial explants: normal exocytosis in cystic fibrosis. Am J Respir Cell Mol Biol; 9:315-322.

Livraghi A, Randell SH (2007) Cystic fibrosis and other respiratory diseases of impaired mucus clearance. Toxicol Pathol; 35:116-129.

Mason SJ, Paradiso AM, Boucher RC (1991). Regulation of transepithelial ion transport and intracellular calcium by extracellular ATP in human normal and cystic fibrosis airway epithelium. Br J Pharmacol; 103:1649-1656.

Merten MD, Breittmayer JP, Figarella C, Frelin C (1993). ATP and UTP increase secretion of bronchial inhibitor by human tracheal gland cells in culture. Am J Physiol; 265 (Lung Cell. Mol. Physiol. 9): L479-L484.

Morcillo EJ, Cortijo J (2006) Mucus and MUC in asthma. Curr Opin Pulm Med; 12:1-6.

Morgan L, Pearson M, de Iongh R, Mackey D, van der Wall H, Peters M, Rutland J (2004) Scintigraphic measurement of tracheal mucus velocity in vivo. Eur Respir J; 23:518-522.

Olivier KN, Bennett WD, Hohneker KW, Zeman KL, Edwards LJ, Boucher RC, Knowles MR (1996). Acute safety and effects on mucociliary clearance of aerosolized uridine 5'-triphosphate +/- amiloride in normal human adults. Am J Respir Crit Care Med; 154:217-223.

Patrick G, Stirling C (1977) Measurement of mucociliary clearance from the trachea of conscious and anesthetized rats. J Appl Physiol; 42: 451–455.

Rogers DF, Barnes PJ (2006) Treatment of airway mucus hypersecretion. Ann Med; 38:116-125.

Roomans GM (2003) Pharmacological approaches to correcting the ion transport defect in cystic fibrosis. Am J Respir Med; 2:413-431.

Rowe SM, Clancy JP (2006) Advances in cystic fibrosis therapies. Curr Opin Pediatr; 18:604-613.

Rogers DF (2004) Airway mucus hypersecretion in asthma: an undervalued pathology? Curr Opin Pharmacol; 4:241-250.

Rogers DF (2005) Mucociliary dysfunction in COPD: effect of current pharmacotherapeutic options. Pulm Pharmacol Ther;18:1-8.

Stahlhofen W, Köbrich R, Rudolf G, Scheuch G (1990) Short-term and long-term clearance of particles from the upper human respiratory tract as a function of particle size. J Aerosol Sci; 21 (suppl. 1):S407–S410.

Tigani B, Schaeublin E, Sugar R, Jackson AD, Fozard JR, Beckmann N (2002) Biochem Biophys Res Commun; 292:216-221.

Wong LB, Yeates DB (1992). Luminal purinergic regulatory mechanisms of tracheal ciliary beat frequency. Am J Respir Cell Mol Biol; 7:447-454.

MANUSCRIPT 5

ENaC-mediated effects assessed by proton MRI in a rat model of hypertonic-induced hydration of airways

Blé FX, Cannet C, Zurbruegg S, Danahay H, Collingwood S and Beckmann N

ENaC-mediated effects assessed by proton MRI in a rat model of hypertonic-induced hydration of airways

François-Xavier Blé[¶,§,#] BSc MSc, Catherine Cannet[¶] BSc MSc, Stefan Zurbruegg[¶] BSc, Henry Danahay[§] BSc MSc PhD, Steve Collingwood[§] BSc MSc PhD and Nicolau Beckmann[¶,1] BSc MSc PhD

Novartis Institutes for BioMedical Research
[¶]Global Imaging Group and [§]Respiratory Diseases Department CH-4056 Basel, Switzerland
[#]University Louis Pasteur-Strasbourg-1, Faculty of Pharmacy, F-67401 Illkirch Cedex, France.

[1] Correspondence to: Nicolau Beckmann, PhD
Novartis Institutes for BioMedical Research
Global Imaging Group
Forum 1, Novartis Campus
WSJ-386.2.09
CH-4002 Basel – Switzerland
Tel.: +41-61-3249576; Fax: +41-61-3243889
e-mail: nicolau.beckmann@novartis.com

The receipt of an award by the 3R Research Foundation (Münsingen, Switzerland) is gratefully acknowledged by NB (project 82/02).

***Nota Bene*: For confidentiality reasons the substance "Compound A" was not structurally identified.**

ABSTRACT

Recent data indicate a clinical benefit of nebulized hypertonic saline (HS) in cystic fibrosis (CF) patients, with a proposed mechanism involving sustained increase in airway surface liquid (ASL) volume. However, the effects of HS are transient and, therefore, of limited therapeutic benefit. Administration of epithelial sodium channel (ENaC) blockers prior to HS is being pursued as a strategy to improve the duration of action of HS (Burrows et al 2006). In the present study we demonstrate the usefulness of MRI to non-invasively follow the fluid dynamics in the lungs of spontaneously breathing rats that were treated with compounds that interact directly or indirectly with ENaC, administered before HS.

We examine in this model, fluid dynamics in the lung of rats pre-treated under different experimental conditions that may interact directly or indirectly with ENaC : amiloride (0.03, 0.3 and 3 mg/kg), Compound A (0.1, 1, 10 and 100 µg/kg), aprotinin (1 µg/kg) or ethylisopropyl amiloride (EIPA) (3 mg/kg). Pre-treatment with the ENaC blocker, amiloride (0.03, 0.3 and 3 mg/kg), or with compound A (0.1, 1, 10 and 100 µg/kg), an ENaC blocker of higher potency than amiloride, at 20 min prior to HS led to a dose-dependent formation of fluid signals in the lungs. For the highest doses, signals were detected by MRI up to 4 h after HS, indicating that compound A was approximately 30 times more potent than amiloride. The broad spectrum protease inhibitor, aprotinin (1 µg/kg), administered 2 h prior to HS, led to similar effects as amiloride or compound A in the first hour following HS. However, fluid signals persisted over a longer time interval: at 6 h after HS, the volume of signals was approximately 40% of that detected at 30 min post-HS administration. Interestingly, extensive fluid signals were also detected in the lungs of rats treated 20 min prior to HS with ethylisopropyl amiloride (EIPA) (3 mg/kg), a compound that is structurally related to amiloride and with low affinity to bronchial ENaC in vitro but suggested to inhibit Na^+ transport through alveolar epithelium (Yue & Matalon 1997). The MRI fluid signals observed in EIPA-pretreated rats were of different appearance and distribution than those observed previously suggesting that EIPA effectively targets other ENaC channels than the classical airways channels inhibited by amiloride and the other compounds tested.

Providing a non-invasive readout of the fluid dynamics in the whole lung in situ, MRI may provide complementary information to that obtained using in vitro or ex vivo models currently supporting ENaC-related drug investigations.

INTRODUCTION

Cystic fibrosis (CF) is a relatively common hereditary disease in Caucasians caused by mutations in the CF transmembrane conductance regulator chloride channel (Deeley et al 2006; Machen 2006; Marcet and Boeynaems 2006). Morbidity and mortality in CF result primarily from chronic airway infection, which leads to progressive deterioration of lung function.

Prior clinical studies supported the efficacy of various inhaled hyperosmolar agents in CF (Eng et al 1996; Robinson et al 1996,1997,1999). More recent clinical studies have demonstrated that nebulized hypertonic saline (HS) in particular may improve the lung function in CF patients (Donaldson et al 2006; Elkins et al 2006). HS has also been shown to increase mucociliary clearance in healthy subjects and in subjects with asthma or chronic obstructive lung disease (Pavia et al 1978; Daviskas et al 1996). Donaldson et al (2006) concluded that HS produces sustained elevation in airway surface liquid (ASL) volume, thereby improving the mucociliary clearance in the airways. Indeed, this thin layer of fluid acts as a low viscosity medium that allows cilia to beat effectively and thus ensure mucus clearance.

Because the airways epithelium is relatively permeable to water, the ASL volume is dictated by osmotic driving forces mainly established by the absorption of Na^+ through epithelial sodium channel (ENaC) and secretion of Cl^- through transmembrane conductance regulator chloride channel (CFTR) which, when mutated causes the cystic fibrosis disease (Matsui et al., 1998, 2000; Tarran et al., 2001). Besides having an important role in the regulation of ionic and fluid transepithelial transport, ENaC channels are also implicated in the regulation of urinary Na^+ reabsorption, extracellular homeostasis, and control of blood pressure. They are composed of three structurally related subunits (α,β,γ) and their activity is regulated by two distinct mechanisms : (i) changes in single channel gating (that is

open probability) or (ii) changes in the number of Na^+ channels expressed in the apical membrane in order to ensure the fine regulation of the osmotic equilibrium through the epithelium.

By disturbing this equilibrium, HS may increase the volume of ASL but its beneficial action is of short duration. Blockage of epithelial sodium channels (ENaC) previous to HS administration with the consequent prevention of ASL absorption is pursued as a strategy to improve the results obtained with saline (Tarran et al., 2006). However, a paradoxical effect was found by Donaldson et al. (2006) when the ENaC blocker, amiloride, was administered together with HS. Rather than improving lung function, amiloride negated the beneficial effect of HS on the measured mucus clearance.

Therefore our aim was to examine, using magnetic resonance imaging (MRI), the effects of different drugs affecting directly or indirectly the ENaC function before administration of HS or of physiological saline, on the fluid status of the whole lung. Measurements were performed in intact and spontaneously breathing Brown Norway (BN) rats. The choice for MRI was based on the fact that the technique has been demonstrated to be well suited to quantify fluid signals in the rat lung, in several models of inflammation (Beckmann et al., 2001, 2002, 2003; Karmouty Quintana et al., 2006).

MATERIALS AND METHODS

Experiments were carried out with the approval of the Veterinary Authority of the City of Basel (license number 1989).

Animals

Male Brown Norway (BN) rats, weighing 270-300 g, were supplied by IFFA CREDO (L'Arbresle, France). Upon arrival animals were kept at an ambient temperature of 22 ± 2°C under a 12 h normal phase light-dark cycle and fed with pellets (Nahr- und Futtermittel AG, Gossau, Switzerland) for at least one week before starting the experiments. Drinking water was freely available.

Intra-tracheal administration of substances

For substance administration, rats were anaesthetized (2% isoflurane; Abbott, Cham, Switzerland) and placed on dorsal position at a 45° angle. A laryngoscope was used to lift the lower jaw and keep the mouth open and the tongue displaced, allowing a clear view of the tracheal opening. A curved cannula with a diameter of 1.6 mm attached to a 1 ml syringe was then inserted into the trachea at the level above the carina (the ridge separating the openings of the left and right main bronchi at their junction with the trachea). Immediately after insertion of the cannula, 0.2 ml of fluid was sprayed into the trachea.

Experimental protocols

In a first series of experiments, the effects following i.t. administration of HS presenting different tonicities were examined: (i) 1.5 % NaCl (n=4); (ii) 3 % NaCl (n=4); and (iii) 6 % NaCl (n=4). MRI measurements were carried out before and at 30 min, 1 h and 4 h following HS.

In a second series of experiments, following conditions were examined to test the abilities of MRI to detect ENaC-mediated changes on HS-induced signals : (iv) amiloride administered at doses of 0.03, 0.3 or 3 mg/kg 20 min before HS (1.5 % NaCl); (v) amiloride (3 mg/kg) 20 min before physiological saline (0.9 % NaCl); (vi) amiloride (3 mg/kg) before HS (1.5% NaCl); (vii) vehicle (dextrose 5%) before HS (1.5% NaCl). MRI was performed at baseline (at least 3 h before substance application) and at time points 30 min, 1 h and 4 h.

In a third set of assays, following compounds were examined: (viii) the ENaC blocker, compound A, which had been demonstrated earlier to be 100 times more potent than amiloride (based on in vitro ENaC assay in cultured human bronchial cells), administered at doses of 0.1, 1, 10 and 100 µg/kg 20 min before 1.5% NaCl; (ix) the Kunitz-type serine protease inhibitor, aprotinin, administered at a dose of 1 µg/kg 2 h before 1.5% NaCl; (v) alpha-1-antitrypsin, a negative control for aprotinin (Bridges, 2001) administered at a dose of 15 nmol/kg, 2 h before 1.5% NaCl; (x) the amiloride analogue ethyl-isopropylamiloride (EIPA), which does not act in vitro on bronchial but on alveolar ENaC in cultured human bronchial epithelial cells (Yue & Matalon, 1997), administered at a dose of 3 mg/kg 20 min before 1.5 % NaCl. MRI

measurements were carried out at baseline (at least 3 h before substance application) and at 30 min, 1 h, 4 h and 6 h following HS.

MRI

During MRI signal acquisitions, rats were placed in supine position in a cradle made of Plexiglas. Body temperature was maintained at 37±1°C using warm air. Anesthesia was maintained with 2% isoflurane, in a mixture of O_2/N_2O (2:1), administered via a nose cone. All measurements were performed on spontaneously breathing animals; neither cardiac nor respiratory triggering was applied. As demonstrated earlier (Beckmann et al 2001, 2002), averaging over several respiratory cycles suppressed artifacts caused by movements of the chest and the heart without the necessity of triggering the data acquisition. Measurements were carried out with a Biospec 47/40 spectrometer (Bruker Medical Systems, Ettlingen, Germany) operating at 4.7 T and equipped with an actively shielded gradient system capable of generating a gradient of 200 mT/m. The operational software of the scanner was Paravision (Bruker).

For detection of fluid signals a gradient-echo sequence with the following parameters was applied (Beckmann et al. 2001): repetition time, 5.6 ms; echo time, 2.7 ms; flip angle of the excitation pulse, approximately 15°; field-of-view, 6x6 cm2; matrix size, 256x128; and slice thickness, 1.5 mm. A single slice image was obtained by computing the 2DFT of the averaged signal from 45 individual image acquisitions and interpolating the data set to 256 x 256 pixels. There was an interval of 530 ms between individual image acquisitions, resulting in a total acquisition time of 59 s for a single slice. The entire lung was covered by 18 consecutive transverse slices.

The volume of fluid signals was quantified using a semiautomatic segmentation procedure implemented in the IDL (Interactive Data Language Research Systems, Boulder, Colorado, USA) environment (version 5.1) on a Linux system. The procedure was extensively described in Beckmann et al (2001). Segmentation parameters were the same for all analyzed images, chosen to segment regions corresponding to high intensity signals. Because the fluid and vessel signals were of comparable intensities, the volume corresponding to the vessels was assessed on

baseline images and then subtracted from the volumes determined on post-treatment images.

Statistics

Anova (with the Bonferroni method) and Student's t-test comparisons were performed for the volume of fluid signals determined by MRI using the SigmaStat 3.1 (©2003 Systat Software, Inc., Point Richmond, CA) software.

RESULTS

Figure 1 shows axial sections through the chest of BN rats, acquired at various time points with respect to i.t. instillation (0.2 ml by spray) of saline solution of different tonicities. The volumes of fluid signals detected following HS, summarized in figure 2, were significantly larger than the volume of fluid administered (0.2 ml), and the response depended on the tonicity. Four hours after HS instillation fluid signals had vanished. The tonicity of 1.5% NaCl was then selected for the following experiments to provide a sufficient window to observe a possible increase of signal volume in the presence of ENaC blocker.

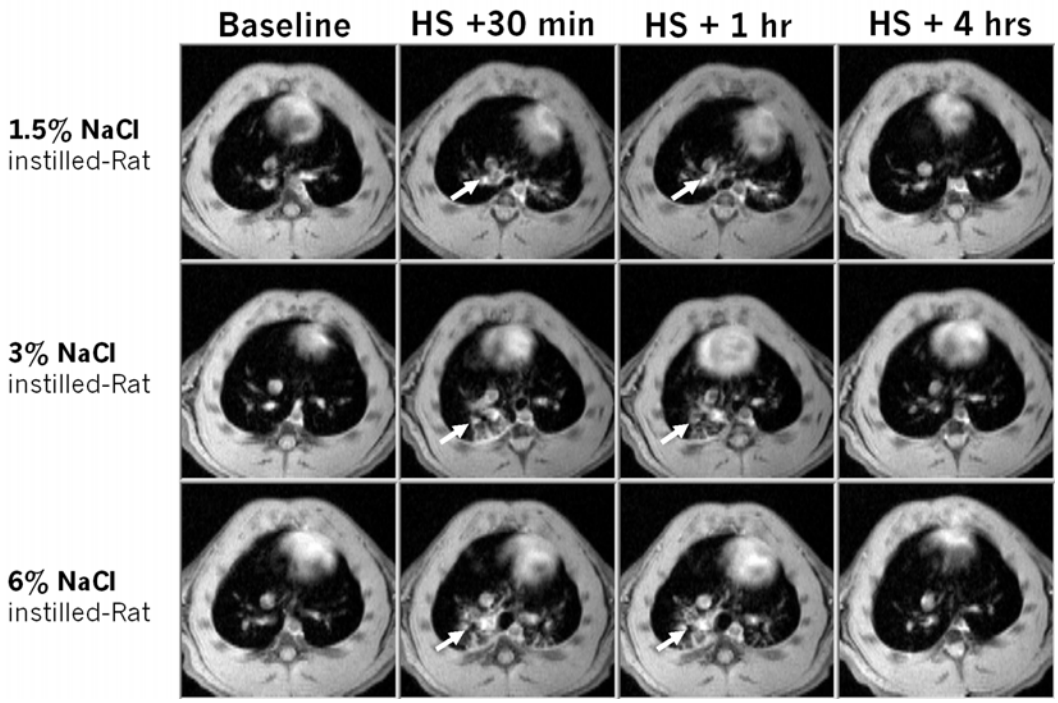

Figure 1 *– Representative transverse MR images of rat lung acquired before, and at 30 min, 1 h and 4 h after i.t. instillation of HS at tonicities of 1.5, 3 and 6 % NaCl (n=4 per group). The arrows indicate the fluid signals detected by MRI at the different time points.*

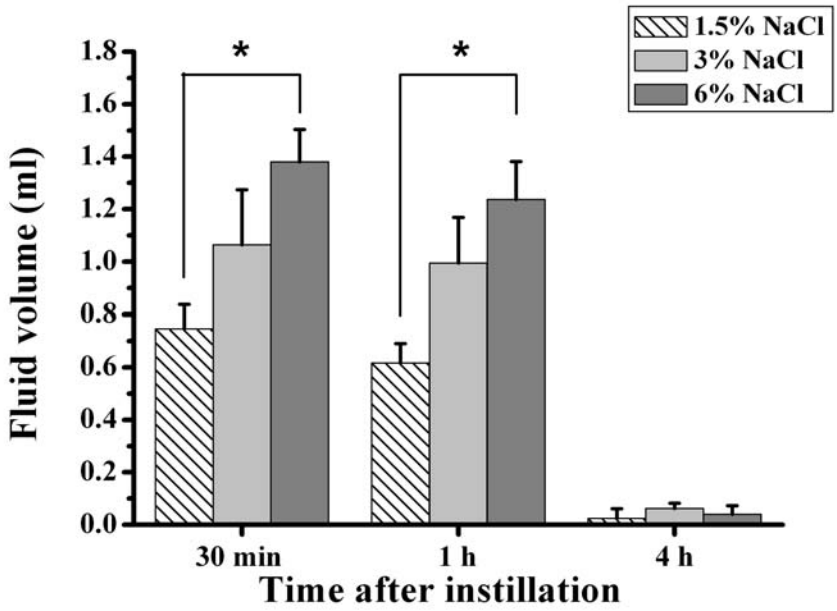

Figure 2 - *Volume (mean±sem, n=4 animals per group) of fluid signals detected by MRI in the lungs of BN rats, at 30 min, 1 h and 4 h following i.t. administration of NaCl 1.5%, 3% or 6%. The levels of significance * 0.01<p<0.05 correspond to Anova comparisons between the three groups, at each time point.*

Amiloride

Discontinuous fluid signals were detected by MRI, in the lungs of animals pre-treated with amiloride and located in the central regions of the lung corresponding to the main airways area. Signals were more prominent and of longer duration than those elicited in the lungs of rats pre-treated with the vehicle (figure 3). The volumes of signals detected by MRI were dependent on the dose of amiloride (figure 4). Also, the signal volumes were larger than the theoretical 0.4 ml one could expect from the volume of administered fluid.

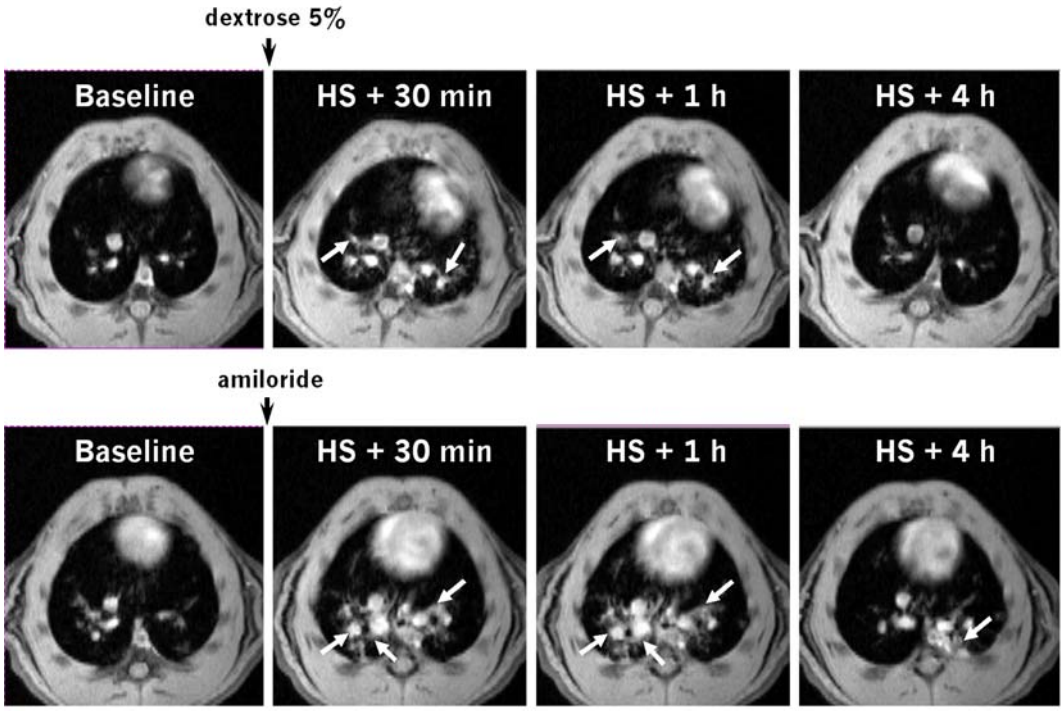

Figure 3 – *Representative transverse MR images of BN rats acquired 24hours before (baseline) and at 30 min, 1 h and 4 h after i.t. instillation of HS (1.5% NaCl, 0.2 ml) as a spray. Animals (n=6 per group and per time point) had been pre-treated with amiloride 3 mg/kg i.t (lower row) or its vehicle (dextrose 5%, 0.2 ml i.t.; upper row) 20 min before HS administration. Fluid signals (arrows) following HS were more prominent for the animal pre-treated with amiloride.*

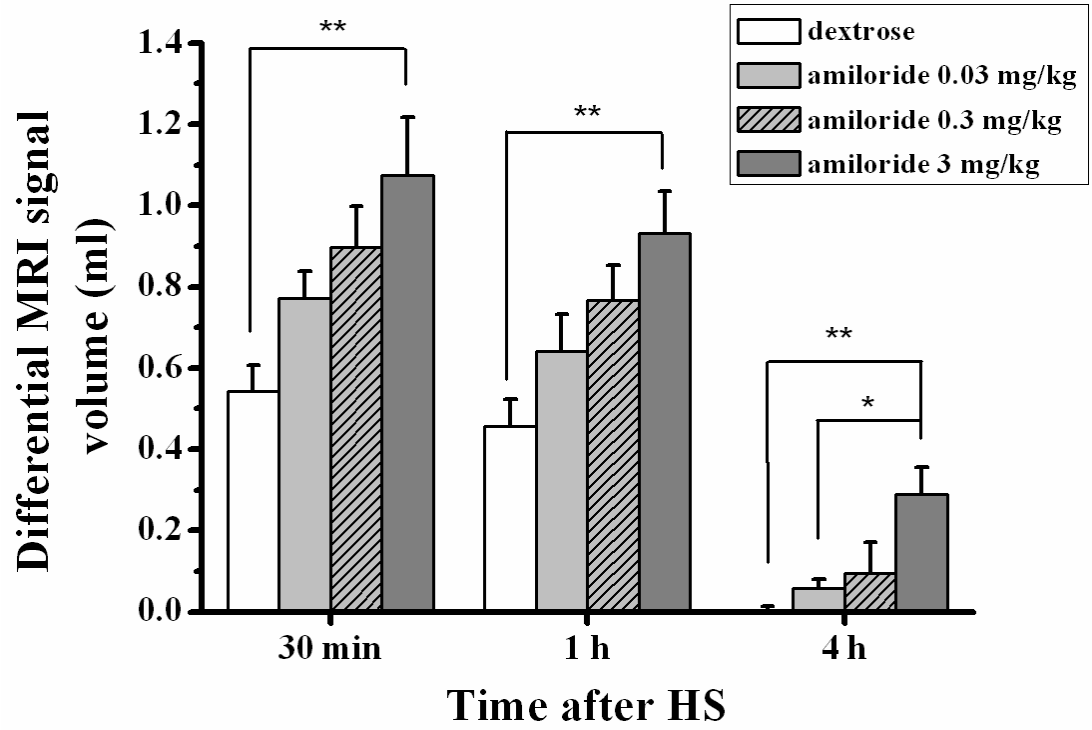

Figure 4 - *Volume (means±sem, n=6 per group) of fluid signals detected by MRI in the lungs of BN rats, at 30 min, 1 h and 4 h following i.t. administration of 1.5% NaCl. Animals were pre-treated (-20 min) with either amiloride at the specified doses, or by its vehicle (dextrose 5%). Levels of significance * 0.01<p<0.05 and ** 0.001<p<0.01 correspond to Anova comparisons between the four groups, at each time point.*

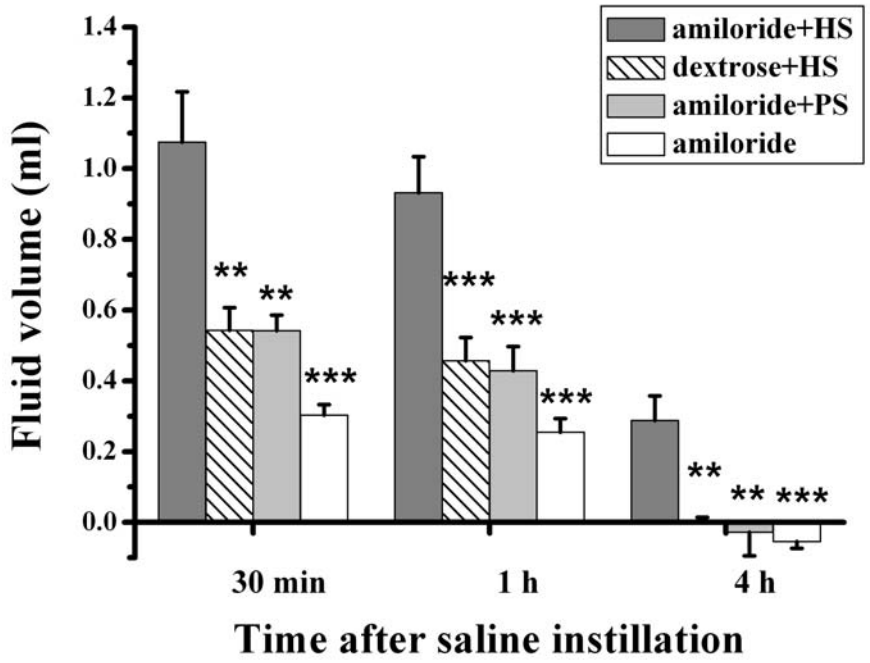

Figure 5 - *Volume (mean±sem, n=6 animals per group) of fluid signals detected by MRI in the lungs of BN rats, at 30 min, 1 h and 4 h following i.t. administration of HS (1.5% NaCl, 0.2 ml) or physiological saline (PS). Rats had received either amiloride (3 mg/kg i.t., 0.2 ml) or vehicle (dextrose 5% i.t., 0.2 ml) 20 min before saline. For amiloride administered alone, the first MRI acquisition took place at 50 min following the compound. The levels of significance ***p<0.001 and **0.001<p<0.01 correspond to Anova comparisons of the 4 groups, and tested 2 by 2 at each time point.*

Figure 5 compares the responses in the lungs of rats treated with amiloride followed by HS (1.5% NaCl) or physiological saline (0.9% NaCl), with dextrose followed by HS, or by amiloride alone. These data suggest that amiloride itself did not cause any significant effect in the lung (e.g., toxicity or mucus release) that could interfere with the fluid dynamics elicited by the salt addition.

Once established that the reference ENaC blocker, amiloride, dose-dependently increased osmotically-driven fluid volumes in the airways as detected by MRI, further compounds have been tested to validate the model based on other ENaC-mediated means to increase the hydration of airways. Althought significance was reached for 3mg/kg

Compound A

Figure 6 summarizes the MRI signal volumes obtained after pre-treatment with compound A, administered 20 min before HS instillation. The data show that compound A at a dose of 100 μg/kg had similar effects to amiloride at a dose of 3 mg/kg (figure 5).

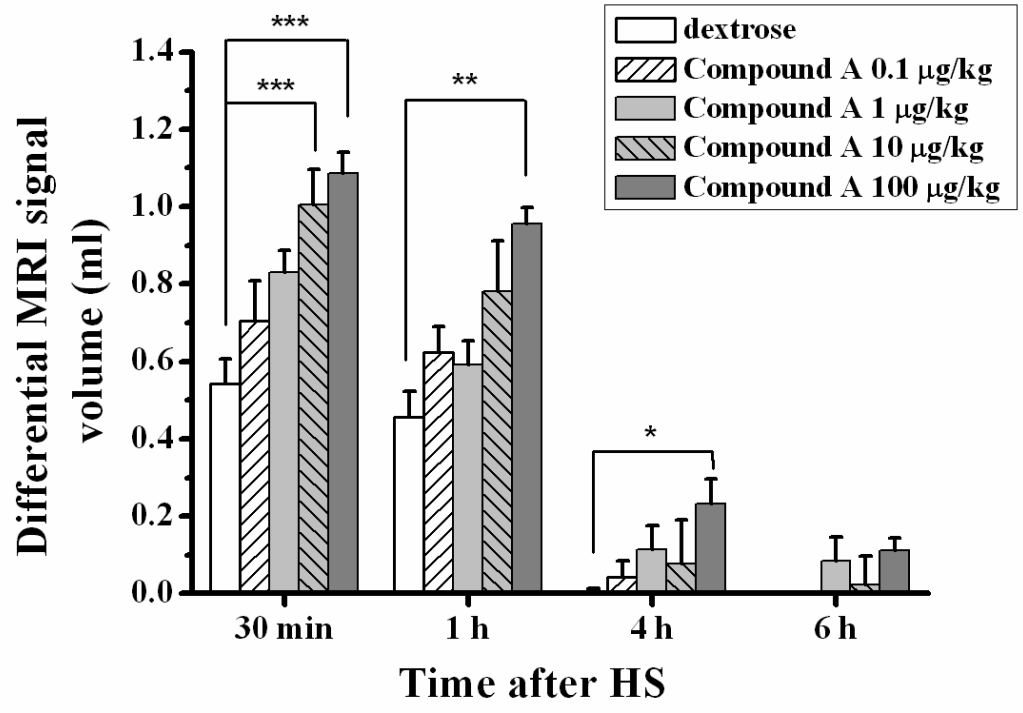

Figure 6 - *Volume (means±sem, n=6 animals per group) of fluid signals detected by MRI in the lungs of BN rats, at 30 min, 1 h and 4 h following i.t. administration of 1.5% NaCl. Animals were pre-treated (-20 min) with either compound A at the specified doses, or by its vehicle (dextrose 5%). Levels of significance * 0.01<p<0.05, ** 0.001<p<0.01 and *** p<0.001 correspond to Anova comparisons between the four groups, at each time point.*

Aprotinin and alpha-1-antitrypsin

Administration of aprotinin (1 μg/kg) 2 h prior to HS led to similar fluid signal volumes as those observed by MRI following pre-treatment with amiloride (3 mg/kg) or compound A (100 μg/kg), in the first hour after HS administration (figure 7). However, the signals observed in the lungs of rats pre-treated with aprotinin were of longer duration, detectable even 6 h after HS, suggesting that aprotinin had a longer duration of action than amiloride or compound A. Application of alpha-1-antitrypsin, 2 h before HS resulted in much smaller fluid responses following the osmotic shock, comparable to pretreatment with the vehicle (figure 7).

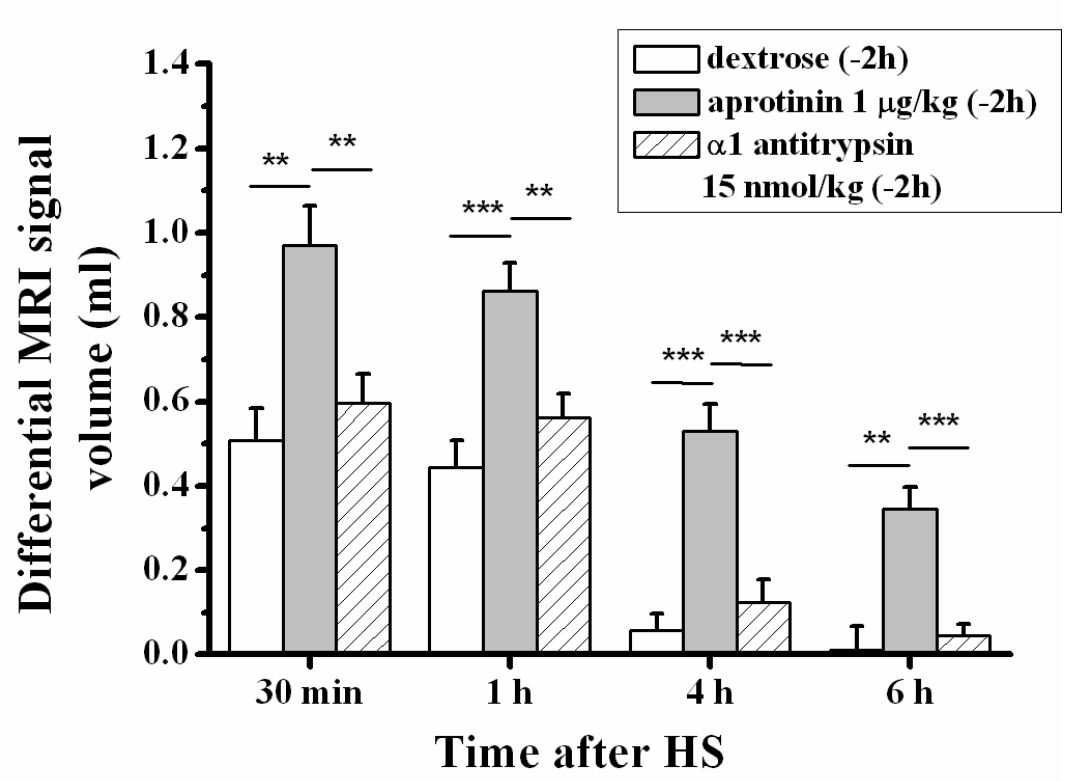

Figure 7 - *Volume (means±sem, n=6 animals per group) of fluid signals detected by MRI in the lungs of BN rats, at 30 min, 1 h, 4 h and 6 h following i.t. administration of 1.5% NaCl. Animals were pre-treated (-2 h) with vehicle (dextrose 5%), aprotinin (1 μg/kg) or alpha-1-antitrypsin (15 nmol/kg). Levels of significance ** 0.001<p<0.01 and *** p<0.001 correspond to Anova comparisons between the three groups of animals, at each time point.*

Ethyl-isopropyl amiloride (EIPA)

Challenge with HS 20 min after administration of EIPA (3 mg/kg) led to extensive formation of signals (figure 8), whose appearance was quite different from that of signals detected by MRI in the lungs of rats pre-treated with amiloride, compound A or aprotinin (figure 9). Whereas the signals in the lungs of rats that had received amiloride or compound A appeared to be more irregular and of weaker intensity, the signals following pre-treatment with EIPA were continuous, of higher intensity, and more widespread, covering the central as well as the peripheral regions of the lung (figure 9).

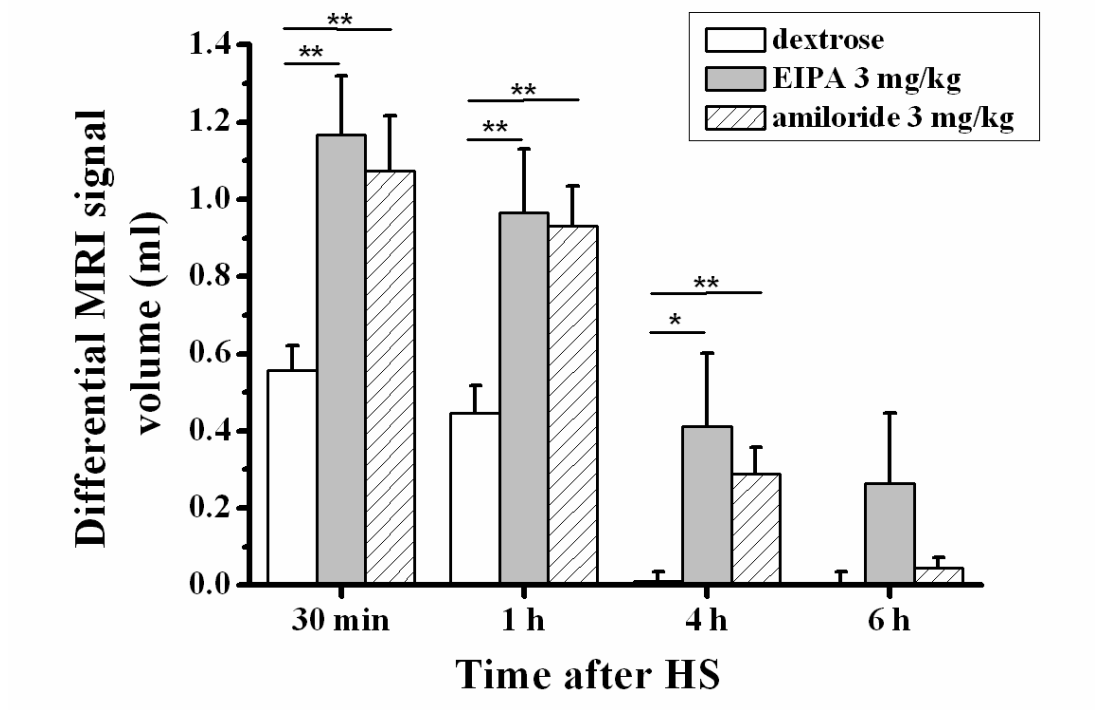

Figure 8 *- Volume (means±sem, n=6 animals per group) of fluid signals detected by MRI in the lungs of BN rats, at 30 min, 1 h, 4 h and 6 h following i.t. administration of HS (1.5% NaCl, 0.2 ml) as a spray. Rats had received vehicle (dextrose 5% i.t., 0.2 ml), EIPA or amiloride at the specified doses 20 min before HS. The levels of significance *0.01<p<0.05, **0.001<p<0.01 and ***p<0.001 correspond to t-test comparisons between the compound groups and the vehicle, at each time point following HS.*

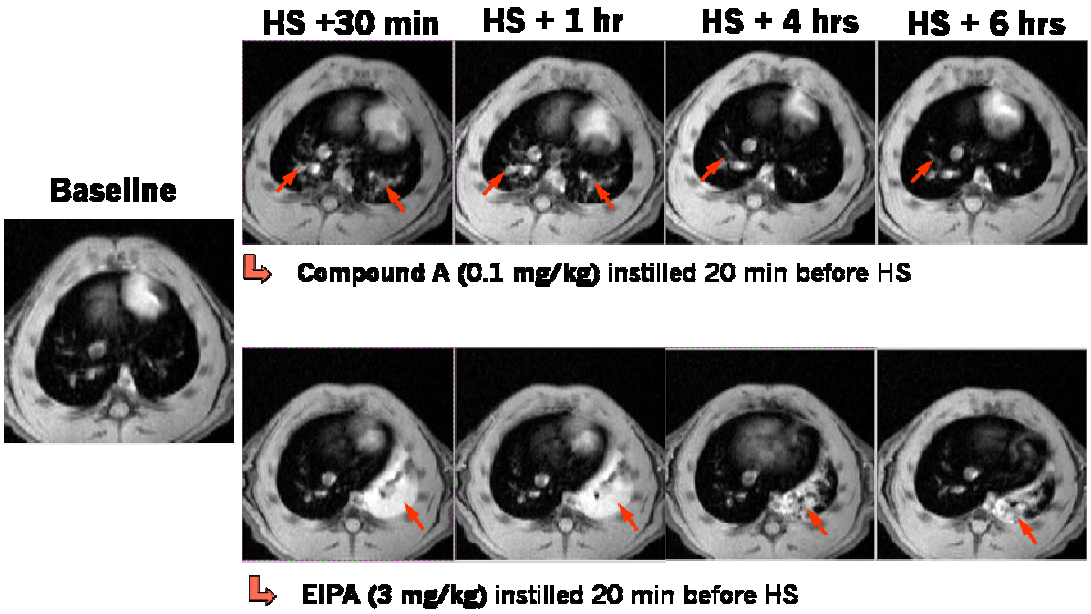

Figure 9 *- Representative transverse MR images of BN rats (n=6 per group) acquired 24hours before (baseline) and at 30 min, 1 h and 4 h after i.t. instillation of HS (1.5% NaCl, 0.2 ml) as a spray. Animals (n=6 per group and per time point) had been pre-treated with compound A 0.1 mg/kg i.t (upper row) or EIPA 3 mg/kg (lower row) 20 min before HS administration. Fluid signals (red arrows) following HS were more prominent and widespread to the peripheral lung region of the animal pre-treated with EIPA.*

DISCUSSION

Mucus clearance defends the lung against inhaled particles and bacteria. The efficiency of this process depends on an adequate volume of airway surface liquid (ASL), i.e., on hydration (Tarran et al., 2001a). It has been hypothesized for the pathogenesis of lung disease in CF patients that a lack of regulation of sodium absorption and chloride secretion causes depletion of the ASL, thus slowing mucus clearance and promoting the formation of adherent mucus plaques on airway surfaces. Mucus plaques and plugs obstruct airways and provide the nidus for infection (Mall et al., 2004; Matsui et al., 1998).

On the basis of this hypothesis, therapies that increase the ASL volume and therefore enhance the mucus clearance, should improve the lung function in CF patients. Inhaled HS has been shown to produce short-term stimulation of mucus clearance (Robinson et al., 1996, 1997) and to improve lung function (Ballmann and von der Hardt, 2002; Eng et al., 1996). HS has also been shown to increase mucociliary clearance in healthy subjects and in individuals with asthma or chronic obstructive lung disease (Pavia et al., 1978; Daviskas et al., 1996). In vitro studies on normal human airway epithelia demonstrated that HS increases the volume of ASL, but the effects were transient and, therefore, predicted to be of limited therapeutic benefit (Tarran et al., 2001b). These in vitro studies, however, demonstrated that slowing the absorption of sodium through epithelium with amiloride, an epithelial sodium-channel blocker, significantly extended the duration of the increase in the ASL volume. The amiloride-sensitive sodium channel ENaC is known for its role in body electrolyte and water regulation (Rossier et al., 2002). Altered sodium absorption was observed in lung diseases such as respiratory distress syndrome (Barker et al., 1997) and pulmonary edema (Scherrer et al., 1999). ENaC regulates the liquid balance at birth during the transition from the liquid-filled fetal lung to the air-filled organ (Barker et al., 1998), whereby all ENaC subunits are regulated at the transcriptional level (Talbot et al., 1999). Stanke et al. (2006) identified the amiloride sensitive sodium channel ENaC and the TNFα receptor TNFR1 as modifiers in CF.

The data obtained here in vivo for the whole rat lung demonstrate substantial fluid accumulation in the lungs of amiloride-pretreated animals that received also

HS. For the same tonicity of HS, the fluid content detected in amiloride-pretreated rats was significantly larger than in vehicle- (dextrose-) pretreated animals. Our observations are in agreement with those of Levin et al (2006), which indicated no blockage of water movement induced by amiloride. Such a blockage would have been the case if amiloride had inhibited aquaporins, as proposed by Donaldson et al (2006). However, it cannot be completely excluded that another component of the fluid signal (e.g. mucin release, interstitial edema) contributed as well to the increase observed in early time points following amiloride and HS, even if the data summarized in figure 5 suggest that the ENaC blocker alone or in the presence of physiological saline did not induce significant increase of the fluid volumes.

Of note, for amiloride-pretreated rats, significant fluid was still present in the lungs at 4 h after HS administration. In contrast, for animals that received no amiloride but were treated with HS, there was no remaining fluid at this time point. The remaining fluid in amiloride-treated rats would result in a transient impairment of lung function, since the fluid secreted in the lumen reduced the airway space. This could be the explanation for the lack of improvement in lung function observed by Donaldson et al (2006) in amiloride- and HS-treated patients in comparison to HS-only-treated individuals, and for the fact that Burrows et al (2006) found no evidence that the topical administration of a short-acting sodium channel blocker improves respiratory condition in people with CF. Our data suggest that, for assessing potential beneficial effects of amiloride in combination with HS on lung function, it would be important to perform the analysis at later time points than in the case HS is administered alone. Delayed evaluation would let enough time for the lung to properly absorb the high fluid content elicited by amiloride in the presence of a large hyperosmotic load.

With the aim of better understanding the fluid dynamics involved in our model, compounds with ENaC-related activity were also examined. As observed with amiloride, pre-treatment with the ENaC blocker, compound A, administered 20 min prior to HS, led to a dose-dependent formation of fluid signals in the lung, that were detectable up to 4 h after HS. Amiloride and compound A at doses of 3 mg/kg and 100 µg/kg, respectively, led to similar responses, suggesting that, under these conditions, compound A was approximately 30 times more potent than amiloride.

Despite a slight loose of potency in our in vivo model, these results are consistent with the fact that in vitro the effects of compound A on ENaC were 100 times more potent than amiloride (Data not shown).

Besides, the broad spectrum protease inhibitor, aprotinin, led to similar effects as the ENaC blockers, amiloride or compound A, in the first hour following HS. However, the signals detected by MRI in the lungs of aprotinin-treated rats persisted over a longer time interval: at 6 h after HS, the volume of signals was approximately 40% of that detected at 30 min post-HS administration. In addition, when compared to vehicle, pre-treatment with alpha-1-antitrypsin, a protease inhibitor which does not affect the Na+ transport in cultured human bronchial epithelial cell (Bridges et al., 2001), had no effect on the fluid volume following the osmotic shock. These findings are consistent with the view that an in-active ENaC population can be activated at the cell surface through cleavage by channel-activating proteases such as prostasin, which is inhibited by aprotinin, a Kunitz-type serine protease inhibitor (Adebamiro et al., 2005; Kleyman et al., 2006; Myerburg et al., 2006).

Extensive fluid signals were detected in the lungs of rats treated with EIPA, a compound that is structurally-related to amiloride, and with suggested low to inexistent affinity for the bronchial ENaC but high affinity for the alveolar channels (Yue & Matalon, 1997). Of note, the MRI signals observed in EIPA-pretreated rats were much more intense, had a continuous nature and appeared to be widespread (figure 9), having an appearance that resembled the edematous signals detected in the lungs of actively sensitized, allergen-challenged rats (Beckmann et al., 2001), while the signals observed for the other ENaC blockers appeared to be more irregular and to have a more central localization. These observations raise the hypothesis that the other ENaC blockers might act predominantly in the main conducting airways, while EIPA could be acting in distal airways and/or at the alveolar level. Based on their ion selectivity and unit conductance (Palmer, 1992), epithelial ion channels can be classified as high (H-type)- or low (L-type)-affinity channels, depending on their binding affinities for amiloride and its structural analogs benzamil, phenamil, and EIPA. H-type channels, the so-called classic Na^+ channels present in the apical membranes of bronchial epithelia with high transepithelial electrical resistance, have a high affinity for amiloride (K_i <0.5 μM). Furthermore, they display the following

structure/inhibitory pattern relationship: phenamil, benzamil > amiloride > EIPA (Smith and Benos, 1991). In contrast, L-type channels have somewhat lower affinity for amiloride, and exhibit a structure/inhibitory pattern distinct from that of H-type Na^+ channels, particularly in that EIPA, a compound with little or no inhibitory activity toward the classic Na^+ channels, can exhibit Na^+ transport across them equally, or even more effectively than amiloride. The presence of L-type channels in alveolar type II cells has been demonstrated in vitro (Matalon et al., 1992; Yue et al., 1995) and in vivo (Yue and Matalon, 1997). The existence of EIPA-inhibitable Na^+ channels in alveolar epithelial cells indicate that an increase in Na^+ transport plays an important role in limiting the amount of alveolar edema in O_2-damaged lungs (Yue and Matalon, 1997). Our observations suggest that the distribution of these H- and L-type channels in the lungs might explain the differences in the appearance of MRI signals in the lungs of rats pre-treated with EIPA or with the other ENaC blockers. Although the alveolar mechanism might not be directly related to mucociliary clearance efficacy, this information brought with our in vivo model may be relevant for further investigations in ENaC-related pharmacology.

In summary, proton MRI has the potential to non-invasively provide information on fluid dynamics in the lungs of spontaneously breathing rats. The technique is straightforward and gives quantitative and spatial information on the water content, thus having the potential to provide important information in the context of ENaC blocker research and its impact on the investigation of mucus clearance. The results obtained so far indicate that the MRI signals detected after treatment with amiloride, compound A, or aprotinin followed by HS administration are related to blockage of ENaC channels. However, more data, including histological ones, need to be gathered in order to understand better the mechanisms involved in the present model. Moreover, testing this protocol in pathological conditions could be of interest in the perspective of a translational application of this model.

ACKNOWLEDGEMENTS

The support from Dr Nelly Frossard, Dr Alexandre Trifilieff and Daniel Wyss is gratefully acknowledged.

REFERENCES

Ballmann M, von der Hardt H (2002). Hypertonic saline and recombinant human DNase: a randomised cross-over pilot study in patients with cystic fibrosis. J Cyst Fibros; 1:35-37.

Barker PM, Gowen CW, Lawson EE, Knowles MR (1997). Decreased sodium ion absorption across nasal epithelium of very premature infants with respiratory distress syndrome. J Pediatr; 130:373–377.

Barker PM, Nguyen MS, Gatzy JT, Grubb B, Norman H, Hummler E, Rossier B, Boucher RC, Koller B (1998). Role of gammaENaC subunit in lung liquid clearance and electrolyte balance in newborn mice Insights into perinatal adaptation and pseudohypoaldosteronism. J Clin Invest; 102:1634–1640.

Beckmann N, Tigani B, Ekatodramis D, Borer R, Mazzoni L, Fozard JR (2001). Pulmonary edema induced by allergen challenge in the rat: noninvasive assessment by magnetic resonance imaging. Magn Reson Med; 45:88-95.

Beckmann N, Tigani B, Sugar R, Jackson AD, Jones G, Mazzoni L, Fozard JR (2002). Noninvasive detection of endotoxin-induced mucus hypersecretion in rat lung by MRI. Am J Physiol Lung Cell Mol Physiol; 283:L22-L30.

Beckmann N, Tigani B, Mazzoni L, Fozard JR (2003). Magnetic resonance imaging of the lung provides potential for non-invasive preclinical evaluation of drugs. Trends Pharmacol Sci; 24:550-554.

Bridges RJ, Newton BB, Pilewski JM, Devor DC, Poll CT, Hall RL (2001). Na+ transport in normal and CF human bronchial epithelial cells is inhibited by BAY 39-9437. Am J Physiol Lung Cell Mol Physiol.;281(1):L16-23

Burrows E, Southern K, Noone P (2006). Sodium channel blockers for cystic fibrosis. Cochrane Database Syst Rev; 3:CD005087.

Daviskas E, Anderson SD, Gonda I, Eberl S, Meikle S, Seale JP, Bautovich G (1996). Inhalation of hypertonic saline aerosol enhances mucociliary clearance in asthmatic and healthy subjects. Eur Respir; 9:725–732.

Deeley RG, Westlake C, Cole SP (2006). Transmembrane transport of endo- and xenobiotics by mammalian ATP-binding cassette multidrug resistance proteins. Physiol Rev; 86:849-899.

Donaldson SH, Bennett WD, Zeman KL, Knowles MR, Tarran R, Boucher RC (2006). Mucus clearance and lung function in cystic fibrosis with hypertonic saline. N Engl J Med; 354:241–250.

Elkins MR, Robinson M, Rose BR, Harbour C, Moriarty CP, Marks GB, Belousova EG, Xuan W, Bye PT and the National Hypertonic Saline in Cystic Fibrosis (NHSCF) Study Group (2006). A controlled trial of long-term inhaled hypertonic saline in patients with cystic fibrosis. N Engl J Med; 354:229–240.

Eng PA, Morton J, Douglass JA, Riedler J, Wilson J, Robertson CF (1996). Short-term efficacy of ultrasonically nebulized hypertonic saline in cystic fibrosis. Pediatr Pulmonol; 21:77–83.

Karmouty Quintana H, Cannet C, Schaeublin E, Zurbruegg S, Sugar R, Mazzoni L, Page CP, Fozard JR, Beckmann N (2006). Identification with MRI of the pleura as a major site of the acute inflammatory effects induced by ovalbumin and endotoxin challenge in the airways of the rat. Am J Physiol Lung Cell Mol Physiol; in press.

Kleyman TR, Myerburg MM, Hughey RP (2006). Regulation of ENaCs by proteases: An increasingly complex story. Kidney Int; 70:1391-1392.

Levin MH, Sullivan S, Nielson D, Yang B, Finkbeiner WE, Verkman AS (2006). Hypertonic saline therapy in cystic fibrosis: Evidence against the proposed mechanism involving aquaporins. J Biol Chem; in press.

Machen TE (2006). Innate immune response in CF airway epithelia: hyperinflammatory? Am J Physiol Cell Physiol; 291:C218-C230.

Mall M, Grubb BR, Harkema JR, O'Neal WK, Boucher RC (2004). Increased airway epithelial Na+ absorption produces cystic fibrosis-like lung disease in mice. Nat Med; 10:487-493.

Marcet B, Boeynaems JM (2006). Relationships between cystic fibrosis transmembrane conductance regulator, extracellular nucleotides and cystic fibrosis. Pharmacol Ther; in press.

Matalon S, Kirk KL, Bubien JK, Oh Y, Hu P, Yue G, Shoemaker R, Cragoe EJ Jr, Benos DJ (1992). Immunocytochemical and functional characterization of Na+ conductance in adult alveolar pneumocytes. Am J Physiol (Cell Physiol 31); 262:C1228-C1238.

Matsui H, Grubb BR, Tarran R, Randell SH, Gatzy JT, Davis CW, Boucher RC (1998). Evidence for periciliary liquid layer depletion, not abnormal ion composition, in the pathogenesis of cystic fibrosis airways disease. Cell; 95:1005-1015.

Myerburg MM, Butterworth MB, McKenna EE, Peters KW, Frizzell RA, Kleyman TR, Pilewski JM (2006). Airway surface liquid volume regulates ENaC by altering the serine protease-protease inhibitor balance: a mechanism for sodium hyperabsorption in cystic fibrosis. J Biol Chem 281(38):27942-9.

Palmer G (1992). Epithelial Na channels: function and diversity. Ann Rev Physiol; 54:51-66.

Pavia D, Thomson ML, Clarke SW (1978). Enhanced clearance of secretions from the human lung after the administration of hypertonic saline aerosol. Am Rev Respir Dis; 117:199–203.

Robinson M, Regnis JA, Bailey DL, King M, Bautovich GJ, Bye PT (1996). Effect of hypertonic saline, amiloride, and cough on mucociliary clearance in patients with cystic fibrosis. Am J Respir Crit Care Med; 153:1503–1509.

Robinson M, Hemming AL, Regnis JA, Wong AG, Bailey DL, Bautovich GJ, King M, Bye PT (1997). Effect of increasing doses of hypertonic saline on mucociliary clearance in patients with cystic fibrosis. Thorax; 52:900-903.

Robinson M, Daviskas E, Eberl S, Baker J, Chan HK, Anderson SD, Bye PT (1999). The effect of inhaled mannitol on bronchial mucus clearance in cystic fibrosis patients: a pilot study. Eur Respir J; 14:678–685.

Rossier BC, Pradervand S, Schild L, Hummler E (2002). Epithelial sodium channel and the control of sodium balance: interaction between genetic and environmental factors. Annu Rev Physiol; 64:877–897.

Scherrer U, Sartori C, Lepori M, Allemann Y, Duplain H, Trueb L, Nicod P (1999). High-altitude pulmonary edema: from exaggerated pulmonary hypertension to a defect in transepithelial sodium transport. Adv Exp Med Biol; 474:93–107.

Smith PR, Benos DJ (1991). Epithelial Na+ channels. Ann Rev Physiol; 53:509-530.

Stanke F, Becker T, Cuppens H, Kumar V, Cassiman JJ, Jansen S, Radojkovic D, Siebert B, Yarden J, Ussery DW, Wienker TF, Tummler B (2006). The TNFalpha receptor TNFRSF1A and genes encoding the amiloride-sensitive sodium channel ENaC as modulators in cystic fibrosis. Hum Genet; 119:331-343.

Talbot CL, Bosworth DG, Briley EL, Fenstermacher DA, Boucher RC, Gabriel SE, Barker PM (1999). Quantitation and localization of ENaC subunit expression in fetal, newborn, and adult mouse lung. Am J Respir Cell Mol Biol; 20:398–406.

Tarran R, Grubb BR, Gatzy JT, Davis CW, Boucher RC (2001a). The relative roles of passive surface forces and active ion transport in the modulation of airway surface liquid volume and composition. J Gen Physiol; 118:223-236.

Tarran R, Grubb BR, Parsons D, et al (2001b). The CF salt controversy: in vivo observations and therapeutic approaches. Mol Cell; 8:149-158.

Yue G, Russell WJ, Benos DJ, Jackson RM, Olman MA, Matalon S (1995). Increased expression and activity of sodium channels in alveolar type II cells of hyperoxic rats. Proc Natl Acad Sci USA; 92:8418-8422.

Yue G, Matalon S (1997). Mechanisms and sequelae of increased alveolar fluid clearance in hyperoxic rats. Am J Physiol (Lung Cell Mol Physiol 16); 272:L407-L412.

PRELIMINARY REPORT

Bleomycin-induced lung injury assessed non-invasively and in spontaneously breathing mice by proton MRI

Blé FX, Cannet C, Gerard C, Zurbruegg S,
Karmouty Quintana H and Beckmann N.

The following section deals with preliminary data generated by monitoring lung MRI signal changes in a murine model of bleomycin-induced fibrosis. These data were compared to histological demonstration of the inflammatory status of the lung as well as the fibrotic changes. Herein, we point out the promising perspective of using MRI to non-invasively detect and follow signal changes that are related to plasma leakage, mucus secretion and tissue densification, all features of the bleomycin-induced murine model which is commonly used in experimental fibrosis investigation.

Being aware that the low number of animals followed during this study is not sufficient for statistically relevant interpretation, it would be necessary to complete this report with additional experiments before submitting the results, although our findings are disserted here as a manuscript.

Bleomycin-induced lung injury assessed non-invasively and in spontaneously breathing mice by proton MRI

François-Xavier Blé, MSc; Catherine Cannet, MSc; Gerard Christelle, BSc; Stefan Zurbruegg, BSc; Harry Karmouty-Quintana, PhD; and Nicolau Beckmann, PhD.

ABSTRACT

Proton magnetic resonance imaging (MRI) techniques were applied to assess non-invasively and in spontaneously breathing mice, structural changes in the lung following a single intranasal administration of bleomycin (BLM). Mice were scanned by MRI prior to BLM or vehicle administration and at 1, 7, 14, 21 and 28 days after treatment. Histological analyses to demonstrate lung inflammatory status and fibrotic changes were performed at days 7, 14 and 28.

Prominent localized MRI signals were detected in the lungs of BLM-treated mice 7 days after instillation of the fibrogenic agent. At this time point, a marked

perivascular and peribronchial infiltration of inflammatory cells but no fibrosis was observed on histological sections. At day 14 and later the MRI signals were less intense but more widespread, expanding to the peripheral parenchymal regions. These observations were in line with histology demonstrating peribronchial and alveolar collagen deposition as well as release of mucus, all hallmarks of fibrosis, from day 14 to 28.

These preliminary data demonstrate the ability of proton MRI to detect in the murine lung the acute inflammatory response and long duration fibrotic changes induced by BLM. The images obtained in the small rodents revealed strikingly similar features to those generated from idiopathic fibrosis patients, indicating the potential value of the model to represent human lung fibrosis.

INTRODUCTION

Pulmonary fibrosis is a progressive and lethal lung disease that results as a consequence of an overexuberant repair process, characterized by an excessive fibroblast proliferation, an absolute increase in lung collagen content, and abnormalities in the ultrastructural appearance and spatial distribution of collagen types (Brewster et al., 1990; Roche et al., 1989).

Bleomycin (BLM) is an antibiotic with activity against gram-negative bacteria (Ueda et al., 1983), that is useful as chemotherapy in the treatment of cancer. The use of BLM as an antineoplastic drug is, however, limited because it produces a dose-dependent pneumonitis, which often progresses to interstitial pulmonary fibrosis in humans (Gong et al., 2005). Local instillation of BLM in rodents is often used to model interstitial pulmonary fibrosis (Hay et al., 1991) as it occurs in humans. The general events that lead to fibrosis include the initial damage, development of alveolitis and inflammation, and, subsequently, excessive accumulation of collagen in the lung. Due to the rapid induction of severe lung injury following BLM treatment that leads to pulmonary fibrosis, this model has been regarded by some to mimic more closely the forms of human pulmonary fibrosis which follow adult respiratory distress syndrome in patients who have survived into the second week of disease (Coalson, 1982). Although cautious interpretation is crucial when data from

acute models are extrapolated to progressive installation of human pulmonary fibrosis, the murine model has proven the capability to replicate the major structural and biochemical abnormalities of the disease.

Early studies demonstrated that C57BL/6 mice were consistently prone to bleomycin-induced pulmonary fibrosis, whereas Balb/c mice were inherently resistant (Harrison & Lazo, 1988). The availability of this animal model of pulmonary fibrosis provides the opportunity to investigate, using transgenic technology, novel pharmacological approaches that can be used to treat and prevent this disease (Chua et al., 2005).

The goal of the present study was to evaluate the potential of proton MRI in assessing non-invasively structural changes following a single intranasal instillation of BLM in C57BL/6 mice. In this longitudinal study, MRI measurements were performed in spontaneously breathing mice, and neither cardiac nor respiratory gating was used. Histological analysis was also carried out at different time points after BLM to help the characterization of signals detected by MRI at the same time points. .

MATERIAL AND METHODS

Experiments were carried out with the approval of the Veterinary Authority of the City of Basel (license number 1989).

Animals

Twelve 8-week-old C57BL6 male mice were purchased from Janvier (Le Genest-St-Isle, France). Animals were maintained in a temperature- and humidity-controlled environment, with free access to standard mouse chow and tap water.

Intranasal instillation of bleomycin/saline

Animals were anaesthetised (3% isoflurane; Abbott, Cham, Switzerland) in a chamber and then instilled intranasally by passive aspiration with bleomycin hydrochloride (Euro Nippon Kayaku GmbH, Frankfurt am Main, Germany; 300µg per mouse dissolved in 25µl saline; n=10) or vehicle (25µl saline; n=2).

MRI acquisitions

Mice were examined by MRI prior to BLM (or saline) administration (baseline), and at days 1, 7, 14, 21 and 28 after treatment. Due to severe toxic effects of BLM characterized by considerable signs of distress (loss of weight of more than 10% and lack of grooming), some of the animals instilled with the antibiotic (4 out of 10) were terminated without having been submitted to MRI.

MRI measurements were carried out in vivo with a Biospec 47/40 spectrometer (Bruker Medical Systems, Karlsruhe, Germany) operating at 4.7 T, equipped with an actively shielded gradient system capable of generating a gradient of 200 mT/m. A birdcage resonator of 32 mm diameter was used for excitation and detection. Gradient-echo images were acquired with the following parameters: repetition time 5.6 ms, echo time 3.5 ms, band width 100 kHz, flip angle of the excitation pulse approximately 10°, matrix size 256 x 128, slice thickness 0.75 mm and field of view 3 x 3 cm^2. A single slice image (acquisition time of 74 s) was obtained by computing the two-dimensional Fourier transform of the averaged signal from 60 individual acquisitions and interpolating the data set to 256 x 256 pixels. The entire lung was covered by 16 consecutive transverse slices.

During measurements, mice were anaesthetized with 1.5% isoflurane in a mixture of O2/N2O (1:2), administred via a face cone. Animals were allowed to breathe spontaneously, and neither respiratory nor cardiac gating was applied. Body temperature was maintained at 37±1°C by a flow of warm air.

MR Image Analysis

The volume of MRI signals was quantified using a semi-automatic segmentation procedure implemented in the IDL (Interactive Data Language Research Systems, Boulder, Colorado, USA) environment on a Linux system. Images were first weakly lowpass filtered with a Gaussian profile filter and then transformed into a set of four grey level classes using adaptive Lloyd-Max histogram quantitation (Jain, 1989). The highest grey level class in the transformed images could be extracted interactively by use of a region grower. Contour serving as a growing border was drawn to control

region growing manually. To eliminate high intensity signals of the lung vessels from the stimulus-induced signals, the volume corresponding to the vessels was assessed on baseline images and then could be subtracted from the volumes determined on post-stimulus images.

Histology

Immediately after MRI acquisitions on days 7, 14 and 28, two BLM-instilled mice were sacrificed. The two control mice (treated with saline) were sacrificed on day 28. Animals were killed by intraperitoneal injection of 0.2 ml of pentobarbitone (250 mg/kg). The trachea was immediately ligated to avoid collapse and the entire lung was harvested and immersed in 10% neutral buffered formalin for 72 h. The lungs were then cut longitudinally in order to include all lobes. After dehydration of tissues through increasing graded series of ethylic alcohol and processing to paraffin wax, sections were embedded in blocks. Slices of 3 μm thickness were cut so as to observe the main bronchi of each lobe. Slices were stained with hematoxylin and eosin to assess the general morphology, with Verhoeff/Van Gieson‘s method for the demonstration of elastic fibers in arteries and to determine perivascular edema, as well as with Alcian Blue/Periodic Acid Schiff’s (AB/PAS) for demonstrating secreted mucus and mucus-containing goblet cells. Masson trichrome staining was used for the demonstration of fibrosis.

RESULTS

Figure 1a shows MRI transverse sections acquired from the same mouse at different time points after intranasal BLM. Similarly to the baseline condition, no MRI signals were detected in the lung 24 h after BLM (figure 1a). However, 7 days following BLM treatment, MRI signals of high intensity were observed in localized and central (bronchic) regions of the lung (figure 1a). Images acquired from day 14 onwards revealed the presence of less intense but more widespread signals throughout the lung. Figure 1b presents the volumes of signals as a function of time for each animal participating into the study. It can be appreciated that until day 14, the responses were quite variable. Mice labeled as T in figure 1b were terminated

because of considerable distress; for these animals in particular, large signal volumes of at least 150 µl were detected by MRI.

Four out of five mice which survived the first two weeks following the profibrotic agent, demonstrated increased volumes of MRI signals (figure 1b) as illustrated in figure 1a by a widespread distribution of discrete signals in the parenchymal peripheral regions. For one of the mouse that reached the study endpoint, prominent MRI signals of moderate intensity were still present on day 28. Volumetric evaluation of the MRI signals from day 14 to 28 revealed a sustained volume of signals (figure 1b) representing approximately 50% of the total lung volume. Of note, from baseline to the endpoint of the study, no MRI signals were observed in both saline-instilled mice (data not shown).

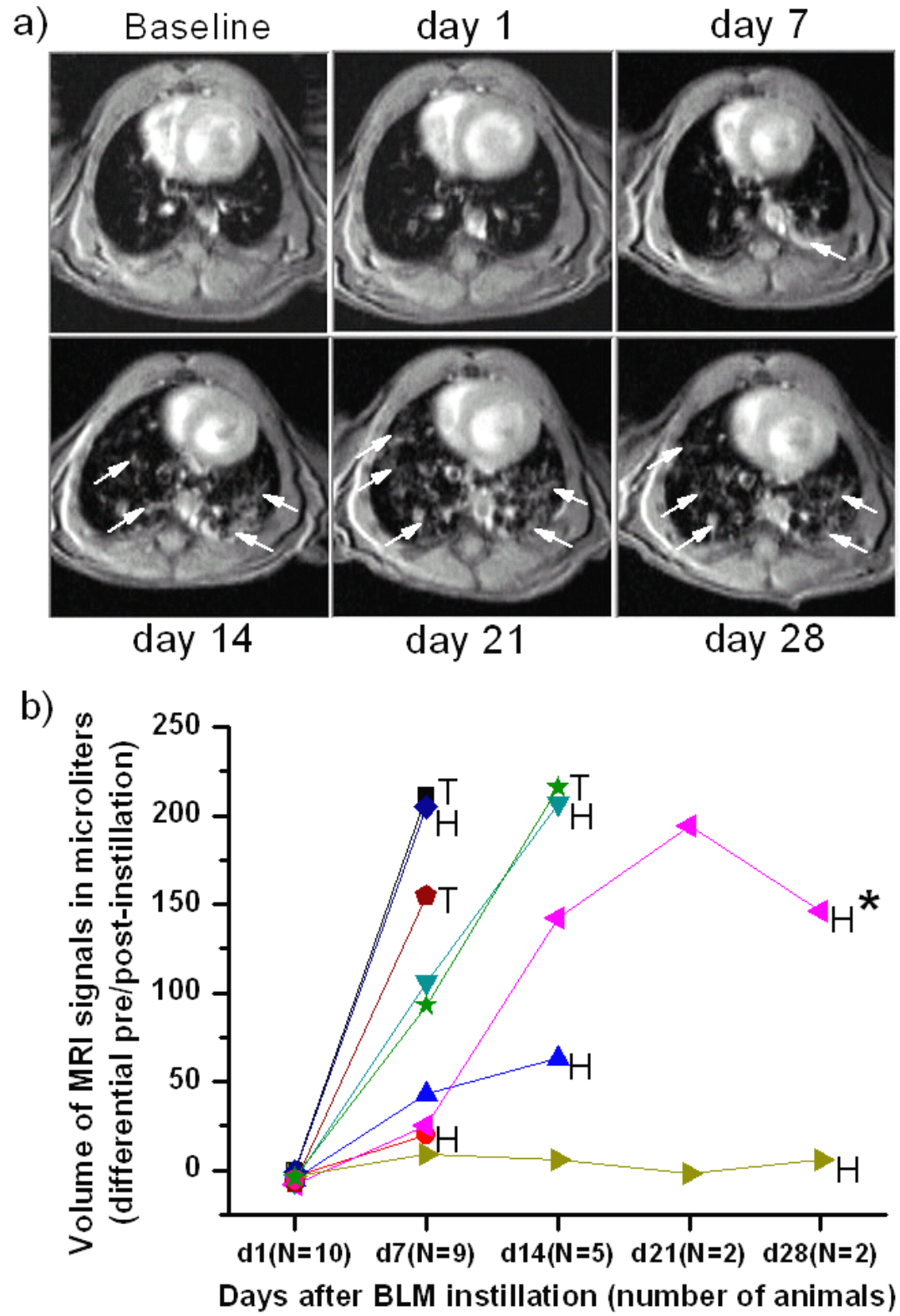

Figure 1 – a) *Transverse MR images of the same mouse acquired prior to (baseline), and at 1, 14, 21 , and 28 days after intranasal administration of BLM (15mg/ kg). White arrows indicate high intensity signals.* ***b)*** *Individual courses of volume of high intensity signal detected in bleomycin – instilled mice. T: terminated distressed mice, H: mice sacrificed for histology, *: mouse whose images are presented in fig. 1a.*

In figure 2, a transverse MRI section from a BLM-instilled mouse acquired on day 14 is compared to MR images corresponding to a similar rat model (Karmouty-Quintana et al, 2007) and to a patient suffering from idiopathic fibrosis (Puderbach et al., 2007). The three examples display striking similarities in the texture and appearance of the MRI signals. Widespread and diffuse signals of moderate intensity were detected in the fibrotic lungs in all three species. Moreover, ring-shaped signals of higher intensity and located in the central bronchial regions of the lung were observed in BLM-instilled mice as well as in the fibrotic patient, in which this particular mark was diagnosed as bronchiectasis.

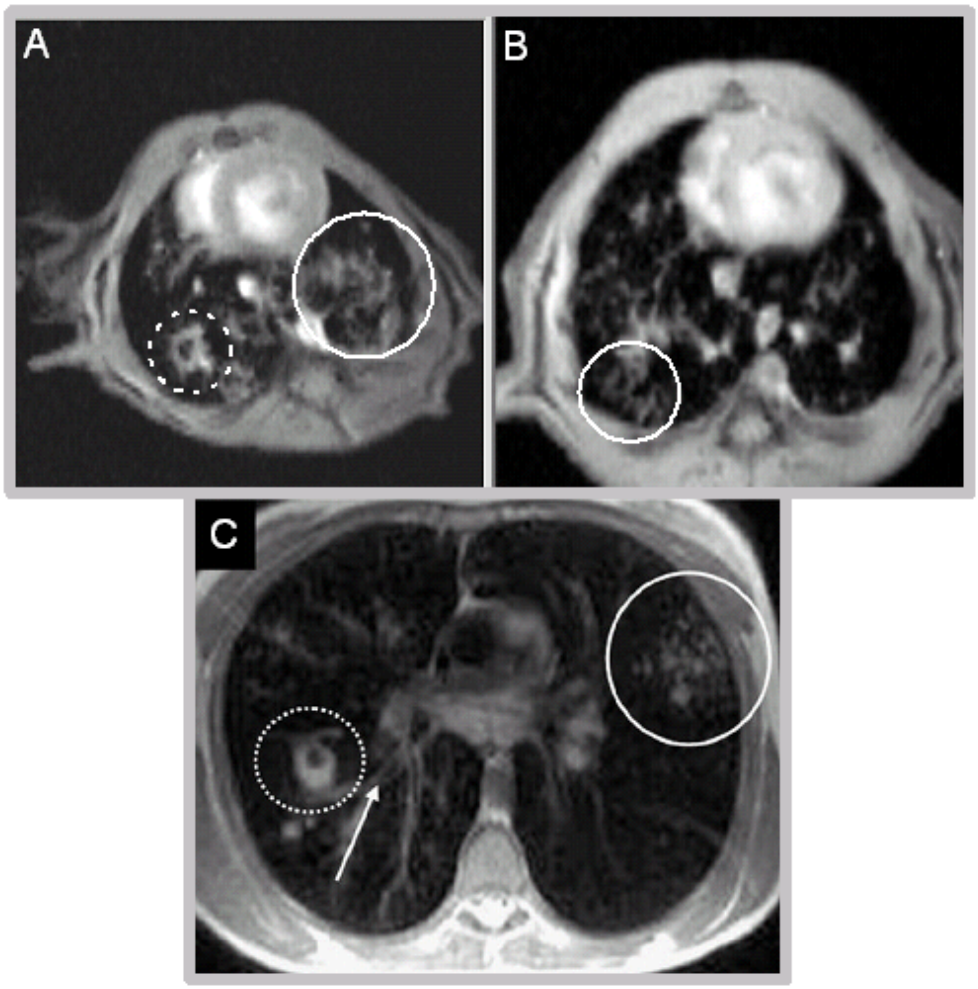

Figure 2 *– Transverse MRI section from bleomycin-instilled mouse (A), rat (B; image courtesy of Karmouty-Quintana et al., 2007) and from fibrotic patient (C; image courtesy of Puderbach et al., 2007) Solid circles indicate widespread and patchy signal from the parenchyma, dot circles : bronchiectasis-like signals and arrow: mucus obstructed airways.*

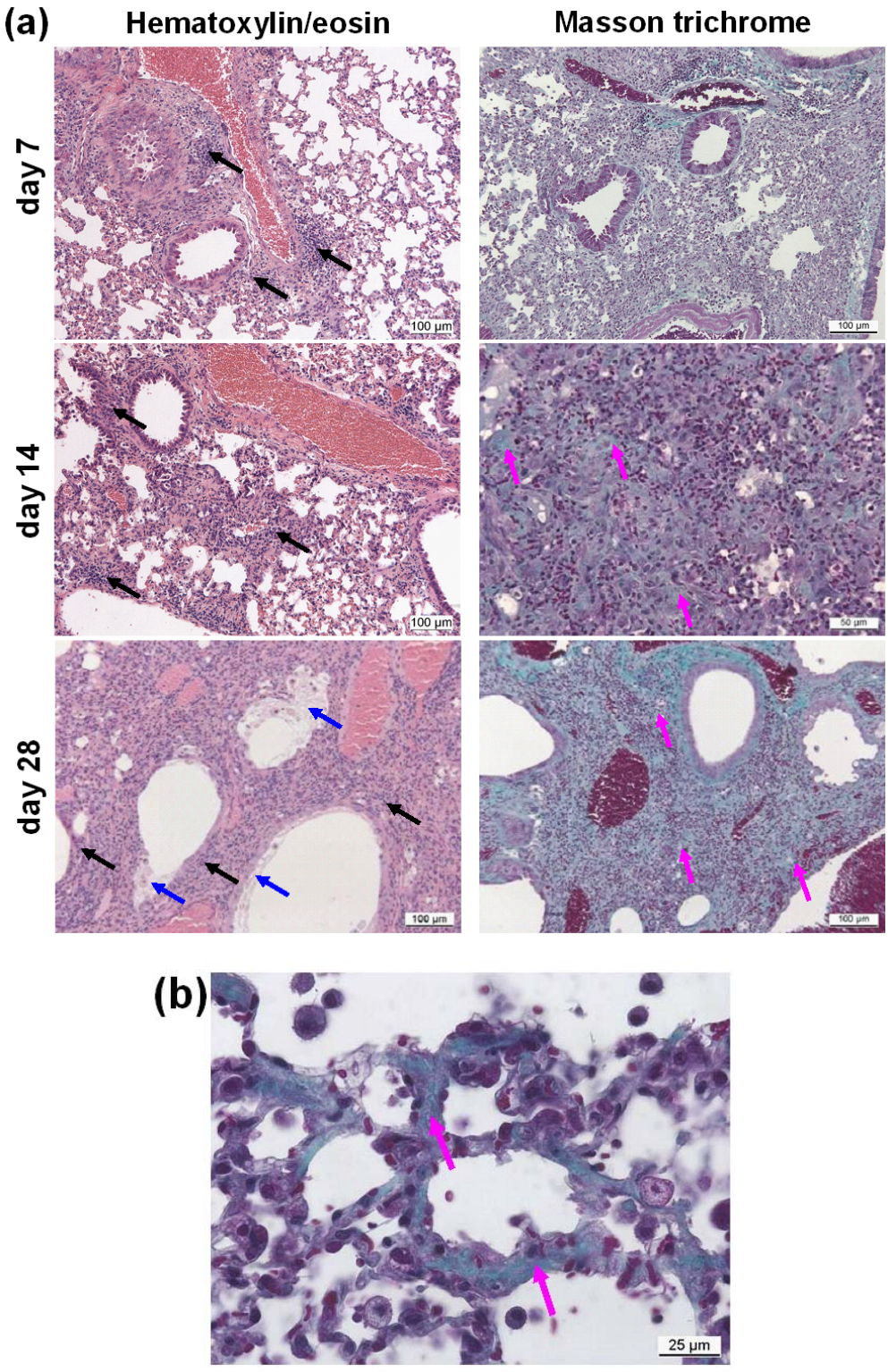

Figure 3 (a) *– Lung histological sections from mice sacrificed 7, 14 and 28 days after intranasal instillation of bleomycin (15 mg/kg). The left column illustrates hematoxylin and eosin-stained sections where cell infiltration (black arrows) and mucus load (blue arrows) are observed. The right column shows Masson trichrome-stained sections demonstrating fibrotic collagen deposition (pink arrows).* ***(b)*** *– Magnification of a Masson trichrome-stained lung section from a mouse sacrificed 14 days after bleomycin instillation. Pink arrows show thickening of the alveolar wall by collagen deposition.*

Histological assessment at day 7, demonstrating marked perivascular, peribronchial and parenchymal infiltration of mono- and polymorphonuclear cells but no incidence of fibrosis at this time point (figure 3a), in agreement with the appearance of MRI signals. Histology of lung sections collected 2 weeks after BLM confirmed the persistence of infiltrated inflammatory cells, as well as the installation of a diffuse fibrosis with a thickening of the alveolar wall (figure 3b). At this time point, the lungs of BLM-challenged mice were severely damaged with disruption of the fine elastica network of the parenchyma (data not shown). Histology of BLM-treated lungs 4 weeks after the treatment revealed maintained severe diffuse infiltration of pro-inflammatory cells, and severe pulmonary fibrosis as demonstrated by Masson trichrome staining, as well as a large load of mucus in the bronchial lumen (Figure 3a). Histological analysis demonstrated neither inflammatory reaction nor fibrosis in saline-instilled mice sacrificed on day 28 (data not shown).

DISCUSSION

Although there is no satisfactory animal model of human pulmonary fibrosis, the BLM murine model is relatively well characterized and does exhibit certain features found in the human pathophysiology (Chua et al., 2005). It has been extensively used to analyze the mechanism of the disease. The main objective of the present work was to validate proton MRI as a longitudinal readout in this largely used murine model of lung fibrosis.

As the validated MRI readout is intended to be used as surrogate for pharmacological studies in experimental fibrosis, we aimed at having a minimal interference between the imaging procedure and the pathophysiology of the model. Thus, measurements were performed in spontaneously breathing animals, since artificial mechanical ventilation, especially if applied repeatedly, may cause lung damage (Walder et al., 2005) that can potentially interfere with the disease model. The novelty of the current study is the demonstration that conventional proton MRI applied under conditions of spontaneous breathing can detect lung injury following BLM treatment.

Local administration of BLM resulted in pronounced inflammation leading to severe fibrosis in the whole lung, processes that were accompanied by signal changes detected here by proton MRI. Despite a variable amplitude and kinetics of the response to bleomycin (as shown on Figure 1b), the individual MRI monitoring of the same mice throughout the study and the direct comparison with histology at the end time point provided enough information to present, at least, a descriptive report.

The initial response to BLM instillation is the induction of an acute inflammatory response characterized by gross perivascular infiltration at 1 week following treatment, as has been found in the present study. In experiments performed by Izbicki et al (2002), mono-nuclear cells were present around large airways and vessels and no evidence of fibrotic development was observed before day 6 after BLM-treatment. This is consistent with our histological evaluation performed at one week demonstrating severe perivascular and parenchymal infiltration of mono- and poly-nuclear cells but no evidence of fibrosis. These results are also in line with the MRI evaluation, where no changes in signal volumes were observed until the 7th day following BLM administration.

Although the initial acute inflammatory reaction and the installation of fibrosis typically coexist between 7 and 14 days after administration of BLM (Chaudhary et al., 2006; Izbicki et al. 2002), in the present study the severity of the induced initial response, illustrated by considerable signs of distress (loss of weight of more than 10% and lack of grooming) in 4 of 10 BLM- instilled mice, was probably responsible for the persistence of a severe cellular infiltration after 2 weeks in survivors.

Evidence from the literature suggests that the major fibro-proliferative phase induced by BLM in mice occurs from day 10 to 14 following its administration and that this process co-exists with inflammation (Aono et al., 2005). These observations are in line with our MRI and postmortem findings from the second week after BLM instillation. Localized MRI signals detected at day 7 progressed to a more discrete but also more diffuse appearance after the second week following bleomycin. Consistently, the first evidence of fibrotic development was not observed in histological slides of lungs harvested prior to 14 days after bleomycin instillation. Separately from plasma leakage- or mucus-related signals consideration, the fibrogenic processes result in a higher density of tissue present in the lung that

subsequently induces a reduction of the tissue/air inhomogeneities normally present in the lung, thus leading to an MRI signal increase.

Fourteen days after the BLM exposure, the diffuse MRI signals reached the peripheral regions of the lung, thus fitting to the alveolar extent of the damage demonstrated by histology. Consistently with these observations, increased fibroblast proliferation and fibronectin-rich fibrillar matrix deposition has been observed in the alveolar epithelium of BLM-treated mice (Aono et al., 2005). Collagen deposition has also been reported 14 days after BLM administration (Koslowski et al.,2003; Lucey et al. 1996). It is assumed that following injury, inflammatory cells enter the lung and together with local cells release mediators that stimulate fibroblast proliferation and collagen deposition within the lung interstitium (McAnulty & Laurent, 1995).

At later time points, the reduced number of monitored animals precluded a meaningful interpretation of the subsequent pathologic changes. Nevertheless, MRI signals detected in the animal that remained alive 28 days after bleomycin fitted with histological demonstration of thickened alveolar wall, severe diffuse infiltration maintenance and mucus loading in the airways, features that are also observed in human fibrosis. Interestingly, comparative MRI sections from mouse, rat and human fibrotic lung showed clear similitude in the appearance of the signal, as diffuse and patchy signals were detected in the peripheral regions of the lung as well as bronchiectasis-like marks in both mouse and human images (figure 2). This resemblance in the signal texture first point to the fact that the animal models of bleomycin-induced fibrosis are relevant support to reproduce global anatomical and physiological changes observed in the human fibrosis; and secondly highlight direct translational values of MRI techniques through the different species.

However, one of the main concern with the use of proton MRI to follow up bleomycin-induced lung injury comes from the fact that both inflammatory (and accompanied plasma leakage) and fibrotic phases coexist and are hardly dissociable by a conventional gradient-echo sequence, in spite of distinctions in signal texture. This issue could be adressed in future investigations of the model by e.g. the implementation of the magnetization transfer technique that might potentially differentiate fluid-originated from tissue densification-induced signal changes.

Finally, a significant fraction of the mice treated with BLM presented important signs of distress and were, therefore, sacrificed in the first two weeks following exposure of the antibiotic, despite using previously published doses for which no fatalities had been reported (Chaudhary et al., 2006). Extensive edema as detected 1 week after exposure by MRI (highest signal volumes at day 7 on figure 1b) was the most probable cause of distress in these animals. In future longitudinal studies, reducing the dose of BLM is certainly advisable to ensure the survival of a large number of animals.

In summary, the data presented here show that proton MRI can detect, in spontaneously breathing mice, responses that reflect inflammatory and morphological changes in the mouse lung induced by intranasal instillation of BLM. Localized signals related to plasma leakage accompanying cell infiltration, detected at day 7 after BLM, progressed later to more diffuse and patchy fibrosis-related signals that correlated with peripheral alveolar expansion of the damage demonstrated by histology. These observations point out the opportunity of exploring proton MRI as a tool to evaluate effects of therapeutic regimens in this experimental murine model of lung fibrosis.

ACKNOWLEDGEMENTS

The support from Dr Nelly Frossard, Dr Alexandre Trifilieff and Daniel Wyss is gratefully acknowledged.

REFERENCES

Aono Y, Nishioka Y, Inayama M, Ugai M, Kishi J, Uehara H, Izumi K, Sone S. Imatinib as a novel antifibrotic agent in bleomycin-induced pulmonary fibrosis in mice. Am J Respir Crit Care Med. 2005; 171(11):1279-85.

Brewster CE, Howarth PH, Djukanovic R, Wilson J, Holgate ST, Roche WR. Myofibroblasts and subepithelial fibrosis in bronchial asthma. Am J Respir Cell Mol Biol 1990;3:507–511

Chaudhary NI, Schnapp A, Park JE. Pharmacologic Differentiation of Inflammation and Fibrosis in the Rat Bleomycin Model. Am J Respir Crit Care Med. 2006;173:769-776.

Chua F, Gauldie J, Laurent GJ. Pulmonary fibrosis: searching for model answers. Am J Respir Cell Mol Biol. 2005; 33(1):9-13.

Coalson JJ The ultrastructure of human fibrosing alveolitis Virchows Arch [Pathol Anat] 1982; 395:181-199

Gong LK, Li XH, Wang H, Zhang L, Chen FP, Cai Y, Qi XM, Liu LL, Liu YZ, Wu XF, Huang CG, Ren J. Effect of Feitai on bleomycin-induced pulmonary fibrosis in rats. J Ethnopharmacol. 2005;96:537-544.

Harrison JH Jr, Lazo JS. High dose continuous infusion of bleomycin in mice: a new model for drug-induced pulmonary fibrosis. J Pharmacol Exp Ther. 1987; 243(3):1185-94.

Hay J, Shahzeidi S and Laurent G, Mechanisms of bleomycin-induced lung damage, Archives of Toxicology 1991; 65:81–94

Izbicki G, Segel MJ, Christensen TG, Conner MW and Breuer R, Time course of bleomycin-induced lung fibrosis, International Journal of Experimental Pathology 2002; 83**:**111–11

Jain AK. Fundamentals of digital image processing. Englewood Cliffs: Prentice Hall; 1989.

Karmouty-Quintana H, Cannet C, Zurbruegg S, Blé FX, Fozard JR, Page CP, Beckmann N. Bleomycin-induced lung injury assessed noninvasively and in spontaneously breathing rats by proton MRI. J Magn Reson Imaging. 2007 Oct;26(4):941-9.

Koslowski R, Knoch K, Kuhlisch E, Seidel D, Kasper M. Cathepsins in bleomycin-induced lung injury in rat. Eur Respir J. 2003;22:427-435

Lucey EC, Ngo HQ, Agarwal A, Smith BD, Snider GL, Goldstein RH. Differential expression of elastin and alpha 1(I) collagen mRNA in mice with bleomycin-induced pulmonary fibrosis. Lab Invest. 1996; 74(1):12-20.

McAnulty RJ, Laurent GJ. Pathogenesis of lung fibrosis and potential new therapeutic strategies. Exp Nephrol. 1995;3:96-107.

Puderbach M, Eichinger M, Gahr J, Ley S, Tuengerthal S, Schmahl A, Fink C, Plathow C, Wiebel M, Muller FM, Kauczor HU. Proton MRI appearance of cystic fibrosis: comparison to CT. Eur Radiol. 2007; 17(3):716-24.

Roche WR, Beasley R, Williams JH, Holgate ST. Subepithelial fibrosis in the bronchi of asthmatics. Lancet 1989;1:520–524

Ueda Y, Saito A, Fukuoka Y, Yamashiro Y, Ikeda Y, Taki H, Yasuda T, and Saikawa I. Interactions of beta-lactam antibiotics and antineoplastic agents. Antimicrob Agents Chemother. 1983; 23:374–378

Walder B, Fontao E, Totsch M, Morel DR. Time and tidal volume-dependent ventilator-induced lung injury in healthy rats. Eur J Anaesthesiol 2005; 10:785-794

GENERAL DISCUSSION

There is an obvious demand for new therapies in the area of respiratory diseases that are among the most prevalent and the most rapidly expanding in prevalence world wide. Animal models used in pulmonary disease research have proven and are still extensively providing enormous potential for elucidating biological processes implicated in lung disorders, and subsequently for testing new treatments. In small rodents, analyses of broncho alveolar lavage fluid and histology are used to derive information on e.g. pulmonary inflammation or assessments of airway resistance and whole body plethysmography are used to obtain functional information on the lung. The main limitation of these techniques is that they are invasive and/or they provide global assessment of lung function. The determination of the water content in the lung, indicating the presence of fluid in the interstitial and/or in the luminal area of the lung and/or tissue density changes, can be a meaningful indicator of lung disease features such as plasma exudation, mucus production, hydration of airway secretion and tissue densification that participate to lung functional impairment. Magnetic resonance imaging may answer this demand since it allows to non-invasively and directly quantify the water content of biological tissues and thus provides a potential alternative method for investigations in the domain of experimental pulmonary disease research. This had not been achieved in the case of murine models of pulmonary disease. The objective of the present thesis was therefore we to the use of MRI as a relevant method to depict in the lung of small rodents features related to the modelled disease. This has been successfully met as illustrated by the findings described in this thesis.

1) Succesful assessement of lung MR images in a murine model of airway inflammation

First, we developed and set up a murine model of asthma in which MRI was applied as a non-invasive tool to detect fluid signal changes induced by multiple allergen challenge. Although spatial resolution constitutes an evident challenge when performing studies in mice, some characteristics specifically related to the anatomy and physiology of the murine species such as the high respiratory and cardiac rates, the large volume occupied by the large vasculature and the heart in the thoracic

cavity, have rendered this detection even more challenging. However, we have been able to report for the first time the feasibility of detecting inflammation-related changes in the lungs of spontaneously breathing mice applying proton MRI without cardiac and respiratory gating (manuscript 1). As previously described by Beckmann et al. (2001) in the rat, potential artifacts caused by movements were suppressed by averaging the echo signals from a number of individual image acquisitions. The gradient-echo sequence produced sharp images from the mouse chest without any triggering. No intubation or mechanical ventilation was necessary and the animals breathed spontaneously. Thus, this procedure easily enables repetitive measurements and circumvents lung damage that might be caused by mechanical ventilation (Abdulnour et al., 2006). Moreover, thanks to the acquisition of sharp images, an accurate quantification of the induced response was feasible and reproducible. Providing information on a regional basis MRI enabled detection fluid signal in the anterior, apical region. The location of the inflammatory response was confirmed by histology at the hilar region, which is consistent with the fact that inflammatory processes take place in the main airways.

As illustrated by these observations, one of the main asset of MRI use over the non-invasive technique of functional assessment by plethysmography is the spatial information. Imaging of the entire lung providing information on a regional basis may help to improve the understanding of the pathophysiology of respiratory diseases and to detect small local effects that might be masked by the global assessment of the lung function, as the non-diseased lung may compensate for the functional impairment of the diseased lung.

Besides, since the validation of the method was the main objective of the thesis, parallel evaluation using histological and bronchoalveolar lavage analyses were required to identify the MRI signal components. We demonstrated in manuscript 1 that fluid signals detected in the lungs by MRI were related to airway plasma leakage and mucus production, both important features of airway inflammation (Bousquet et al., 2000; Kay, 2001a; 2001b). Additionally, texture-related information provided on the MR images, and repeated measurements, taking advantage of the non-invasive property of the imaging method, emphasized two different phases in the course of MRI signals in response to multiple allergen

challenge. The early phase reflected primarily plasma leakage, while the second one was related to secreted mucus.

2) Validation of MRI use for pharmacological purpose: the example of S1P pharmacology

Once the murine model of airway inflammation characterized, the relevance of MRI use in experimental drug research was successfully illustrated by its application on selective pharmacological tools and genetically modified animals. In these studies, the effect of anti-inflammatory drug was detected by MRI and confirmed by histology and BAL fluid analyses (manuscript 2). By studying sphingosine-1-phosphate (S1P) pharmacology, the incidence of plasma leakage on fluid signal detection was highlighted in our murine model of airway inflammation. FTY720, which is a S1P agonist for 4 of the 5 S1P receptors [see Zhang and Schluesener (2007) for a recent review], and the selective agonist for $S1P_1$ subtype AUY954 (Pan et al., 2006), were able to significantly prevent the formation of fluid signal induced by allergen challenge, whereas $S1P_3$ receptor deletion in mice had no influence (manuscript 2). This was consolidated by histology showing (i) a slight reduction of infiltration, (ii) no modification of mucus load in the absence and presence of the drugs pretreatment. The decrease of signal was therefore mainly attributed to the plasma leakage component. The S1P1 receptors expressed on the endothelium has been previously demonstrated to be protective against vascular leakage in vivo (Sanna et al., 2006). Thus, our results suggest that the drug acted on endothelial receptor present on airway vasculature, enhancing barrier permeability. Similarly, we have used JTE013, a selective antagonist of $S1P_2$ receptor which signaling pathway is opposed to $S1P_1$ (Sanchez et al., 2007; Sugimoto at al., 2003). JTE013 was responsible for a reduction of allergen-induced MRI signals, without inducing any other detectable changes neither in the differential cell count from BAL fluid nor on histology (manuscript 3). Besides demonstrating that the fluid MRI signal measurements are of relevance for the evaluation of anti-inflammatory drug effects, these results point out the fact that MRI might be in some instance more

sensitive than classical routine techniques to detect drug-related changes in the lung of allergic mice.

3) Selective detection of mucus secretion by MRI

In case of both edema and mucus inflammatory features are simultaneously present in the lung or not affected by the examined drug effects, one concern is the difficulty to dissociate the components of MRI fluid signals. For that reason, efforts have been concentrated on the development of a specific probe that was able to enhance MRI sensitivity to detect mucus. Keeping in perspective to apply this probe to the murine model of lung inflammation, we first developed the protocol in a well described (Beckmann et al., 2002) and simpler model of mucus hypersecretion in the rat. The objective of specifically enhancing the mucus-related detection by MRI has been successfully met thanks to the use of the contrast agent NVP-BCR249/250 that bound specifically to mucus (as demonstrated by histology). Additionally, in comparison to other methods of assessment of mucociliary clearance that are most commonly performed using inhaled radiolabeled aerosols and scintigraphy (Foster and Wagner 2001; Morgan et al 2004) or measuring fluorescent polystyrene microspheres using serial bronchoalveolar lavage fluid (BAL) analyses (Coote et al 2004), the method developed here allows for the non-invasive measurement of the resultant effect of mucus release/clearance balance, at high spatial resolution in small rodents, and do not imply the use of any radioactive probe. This study highlights the potential of using exogenous contrast agent/probe in lung MRI and points out the perspective that molecular imaging approaches using targeted contrast agent in this context can become a relevant tool for *in vivo* pharmacological studies in the future.

4) Detection of secretion hydration in the airways by MRI: example of ENaC-mediated effects

Further validations of the MRI capabilities to non-invasively detect fluid secretion in the lung of small rodents were motivated by the fact that only *in vitro* and *ex vivo* methods are currently supporting the assessement of the hydration of the

airway surface liquid. This outcome measure is of special interest for investigations targeting the ion transport defect that results in underhydrated airway secretions in cystic fibrosis. We demonstrated in this thesis the usefulness of MRI to non-invasively follow in spontaneously breathing rats the level and the duration of airway hydration induced by hypertonic saline and modulated by different compounds that interact directly or indirectly with epithelial Na^+ channels. In response to the reference ENaC blocker amiloride, prominent fluid signals were detected in the central regions of the lung and this response was dose dependent. Fluid signals of longer duration were also assessed by MRI in the main airways region after aprotinin treatment, suggesting that the compound inhibited the ENaC activation by endogenous protease activity (Bridges et al., 2001). Additionally, EIPA which has a low affinity to bronchial ENac but inhibits Na^+ transport through the alveolar epithelium (Yue & Matalon, 1997) induced the formation of widespread fluid signals detected in the peripheral region of the lung.

The fact that the elicited response consists in transient water movement is rendering the direct histological validation of the level of hydration extremely complicated. Therefore, to date, additional activities will need to be pursued to better characterize this model. However, based upon pharmacological profiles consistent with an ENaC-mediated effect, we demonstrated the potential utility of MRI to provide with a non-invasive readout of the whole lung (indicating the site of therapeutic action) to assess in a rat model the duration of action of ENaC-based therapeutics for treatment of airway disease such as cystic fibrosis. Furthermore, the perspective of transferring this model to the mouse can be envisaged since transgenic model of cystic fibrosis are available for this species.

5) Assessment of lung fibrosis by MRI in a murine model

Promising preliminary results have been generated monitoring a murine model of bleomycin-induced fibrosis, showing that detection of early inflammatory-related response and long lasting morphological changes in the lung is also feasible using MRI in spontaneously breathing mice. Localized signals related to plasma leakage accompanying cell infiltration, detected at day 7 after BLM, progressed later

to more diffuse and patchy fibrosis-related signals that correlated with peripheral alveolar expansion of the damage demonstrated by histology.

The main advantage of the MRI technique over morphological histological analysis is the non-invasiveness of the method that allows repeated measurements of the same animal followed on a long period. Furthermore, in contrast to micro-computed tomography technique that is also currently in development for non-invasive assessement of fibrotic changes in mice (Cavanaugh et al., 2006), MRI do not deliver radiation doses which could interfere, if repetitive, with the pathological fibrotic process implicated in this model. Despite the fact that multiple mechanisms (infiltration, tissue densification, mucus production) may be responsible for the behaviour of the MRI signals in this model, after proper characterization based on the use of standard (usually invasive) and functional comparative procedures, the readouts can be used as surrogate markers for further investigations using transgenic mouse and testing compounds.

6) What validation is missing

It is established that the presence of fluid in the interstitial and luminal airway spaces is characteristic of inflamed lung and participates significantly to the functional impairment by obstructing the luminal airway space and thus reducing the airflow (Yager et al., 1995). Similarly, thickening of the tissue in case of pulmonary fibrosis impairs gas exchange and lung elasticity, leading to a loss of function. Nevertheless, the detection of fluids and tissue densification in the lung by proton MRI *per se* does not consist in a direct estimation of the function. Therefore a combination of technique would be of interest to further investigate the relationship between lung fluid detection and loss of function by combining proton MRI measurements with parallel functional assessment.

Besides addressing inflammation-related fluid signals, MRI is also able to provide important information on the functional status of the lung. Recently developed techniques using hyperpolarized gas MRI are extremely attractive in this context. Regional information on ventilation and gas diffusion are the primary readouts (Chen et al., 2000; Chen at al.,2003; Dupuich et al., 2003). But the

application of hyperpolarized gas MRI for routine acquisition is not trivial since a complex and not commercially available instrumentation is required for the generation of hyperpolarized gas, and its controlled delivery to the animal. Therefore, the non-invasiveness, the simplicity and the availability of the plethysmography (Hamelmann et al., 1997) would make it a more convenient method for routine functional assessment to combine with proton MRI fluid detection.

In addition to functional consideration, multimodality imaging could be another perspective to further validate the MRI use in . Indeed, there is no "all-in-one" imaging modality providing optimal sensitivity, specificity and temporospatial resolution. Owing to its relatively low sensitivity, MRI is of limited value for detecting molecular processes in vivo; nevertheless, its high spatial resolution provides a good anatomical reference for molecular data obtained with high-sensitivity, low resolution imaging modalities. This might be achieved by post-processing of data obtained in different imaging sessions from optical imaging, micro-CT, MRI etc, or by simultaneous multimodality small-animal imaging such as PET–MRI (Benveniste et al., 2005; Slates et al., 1999), PET–CT and SPECT–CT (Del Guerra & Belcari, 2002; Fahey, 2003). Combining imaging data requires compatibility of data formats for the various modalities as well as sophisticated software tools for image coregistration (fusion), data visualization, and integration across modalities. The integration of multimodal imaging information into bioinformatics platforms comprising non-imaging data (gene/protein expression data, pharmacodynamic, pharmacokinetic, and pharmacogenetic databases, histological data, atlases) will be mandatory in the future for handling the ever increasing complexity of biomedical information.

Overall, proton MRI allows the assessment of diverse hallmarks of lung disease in spontaneously breathing animals, providing accurate, sensitive and biologically relevant information that can be used to study disease progression and ultimately to explore new alternatives that could have a decisive impact in treating respiratory diseases in pre-clinical and clinical stages of drug development.

CONCLUSION

Through the publications and additional data disserted in this thesis, detection of hallmarks of diverse pulmonary pathologies or defence mechanisms ranging from mucus production, plasma leakage and hydration of airway secretions as well as changes in lung morphology as a result of experimentally induced pulmonary fibrosis have been successfully validated non-invasively and in spontaneously breathing rodents by proton MRI.

The main asset of proton MRI is its ability to detect this variety of changes in the lung in a non-invasive manner and under conditions of spontaneous respiration. This characteristic gives MRI a clear advantage in pulmonary research as the same animal can be used as its own control for baseline measurements and can be monitored repeatedly over time without affecting its physiology, the only restriction being its exposure to the anaesthetic. Moreover, the ability of MRI to provide information from the entire lung and on a regional basis is also a great advantage as drugs and disease process can have a greater effect on different regions of the lung. This was highlighted in this thesis, when in the murine model of allergen-induced lung inflammation, the plasma leakage and mucus-related signals detected in the early phase were clearly located in the proximal part of the lung, corresponding to the bronchial area. Moreover, in the rat model of hypertonic saline-induced hydration of airway secretion, ENaC-mediated effects were observed in the central bronchial regions under amiloride pre-treatment versus in the peripheral alveolar region under EIPA pre-treatment. These examples demonstrate the potential of MRI to visualize localized pathological changes that cannot be observed by BAL, or lung function measurements using Penh approaches or in artificially ventilated animals. However, it is important to mention that validation experiments are still necessary to fully define the nature of the signals observed by MRI.

Due to the world wide increase of MRI equipped lab and its non-invasive properties, versatility and sensitivity, the use of MRI could be envisaged more routinely to complete and/or replace the methods used nowadays to evaluate experimental pulmonary diseases models in small rodents.

The models validated in this thesis have been or will be used to screen compounds developed by Novartis for their potential beneficial properties to modulate mucus release, hydration of airway secretion, edema, or development of pulmonary fibrosis. They may also be used for research purpose to follow up the development of a disease in murine model.

In addition to the models of respiratory disease validated in this thesis, there are other possibilities in pulmonary research that can be explored further by MRI. Such examples include:

- Exploring other models of chronic disease such as smoke exposure model to investigate the long-term changes like airways remodelling
- Investigating changes in lung perfusion in models of pulmonary hypertension
- Phenotyping of transgenic murine models of airway disease

Extensively, the further challenge of proton MRI will be its transition to the clinic where the main aim of MRI would be to diagnose the early onset of pulmonary pathologies such as fibrosis and COPD and to assess the effect of a drug in modulating the disease progression in chronic diseases such as severe asthma, COPD, or cystic fibrosis. The main hurdle of MRI in the clinic will be to distinguish the different aspects of pulmonary disease that co-exist in the same patient such as oedema and mucus plugging, and to establish gold standards allowing it to be utilised in different centres.

REFERENCES

Abdulnour RE, Peng X, Finigan JH, et al. (2006). Mechanical stress activates xanthine oxidoreductase through MAP kinase-dependent pathways. *Am J Physiol Lung Cell Mol Physiol* **291**:L345-L353.

Aso Y, Toneda Y & Kikkawa Y (1976). Morphologic and biochemical study of pulmonary changes induced by bleomycin in mice. *Laboratory Investigation* **35**: 558–568.

Ballmann M, von der Hardt H (2002). Hypertonic saline and recombinant human DNase: a randomised cross-over pilot study in patients with cystic fibrosis. *J Cyst Fibros* **1(1)**:35-7.

Barnes PJ (1996). Pathophysiology of asthma. *Br J Clin Pharmacol* **42**: 3-10.

Beckmann N, Mueggler T, Allegrini PR, Laurent D & Rudin M (2001 a). From anatomy to the target: contributions of magnetic resonance imaging to preclinical pharmaceutical research. *Anat Rec* **265**: 85-100.

Beckmann N, Tigani B, Ekatodramis D, Borer R, Mazzoni L & Fozard JR (2001 b). Pulmonary edema induced by allergen challenge in the rat: noninvasive assessment by magnetic resonance imaging. *Magn Reson Med* **45**: 88-95.

Beckmann, N, Tigani, B, Mazzoni, L & Fozard, J.R (2001 c). MRI of lung parenchyma in rats and mice using a gradient-echo sequence. *NMR Biomed* **14**: 297-306.

Beckmann N, Tigani B, Sugar R, Jackson AD, Jones G, Mazzoni L, & Fozard JR (2002). Noninvasive detection of endotoxin-induced mucus hypersecretion in rat lung by MRI. *Am J Physiol Lung Cell Mol Physiol* **283**: L22-L30.

Beckmann N, Cannet C, Zurbruegg S, Rudin M & Tigani B (2004). Proton MRI of lung parenchyma reflects allergen-induced airway remodelling and endotoxin-aroused hyperresponsiveness: A step toward ventilation studies in spontaneously breathing rats. *Magn Reson Med* **52**: 258-268.

Benveniste H, Fowler JS, Rooney W, Ding YS, Baumann AL, Moller DH, Du C, Backus W, Logan J, Carter P, Coplan JD, Biegon A, Rosenblum L, Scharf B, Gatley JS, Volkow ND (2005). Maternal and fetal 11C-cocaine uptake and kinetics measured in vivo by combined PET and MRI in pregnant nonhuman primates. *J Nucl Med* **46**:312-320.

Boesch C (1999). Molecular aspects of magnetic resonance imaging and spectroscopy. *Mol Aspects Med* **20**: 185-318.

Boucher RC (1994). The genetics of cystic fibrosis: a paradigm for uncovering new drug targets. *Curr Opin Biotechnol* **5(6)**:639-42.

Bousquet J, Jeffery PK, Busse WW, Johnson M, Vignola AM (2000). Asthma. From bronchoconstriction to airways inflammation and remodeling.*Am J Respir Crit Care Med* **161(5)**:1720-45.

Brewster CE, Howarth PH, Djukanovic R, Wilson J, Holgate ST, Roche WR (1990). Myofibroblasts and subepithelial fibrosis in bronchial asthma. *Am J Respir Cell Mol Biol* **3(5)**:507-11.

Busse WW, Gern JE (1997).Viruses in asthma. *J Allergy Clin Immunol* **100(2)**:147-50.

Calhoun WJ, Reed HE, Moest DR, Stevens CA (1992). Enhanced superoxide production by alveolar macrophages and air-space cells, airway inflammation, and alveolar macrophage density changes after segmental antigen bronchoprovocation in allergic subjects. *Am Rev Respir Dis* **145(2 Pt 1)**:317-25.

Canning BJ (2003). Modeling asthma and COPD in animals: a pointless exercise? *Curr Opin Pharmacol* **3**: 244-250.

Cavanaugh D, Travis EL, Price RE, Gladish G, White RA, Wang M, Cody DD (2006). Quantification of bleomycin-induced murine lung damage in vivo with micro-computed tomography. *Acad Radiol* **13(12)**:1505-12.

Chen XJ, Hedlund LW, Moeller HE, Chawla MS, Maronpot RR & Johnson GA (2000). Detection of emphysema in rat lungs by using magnetic resonance measurements of 3He diffusion. *Proc Natl Acad Sci* **97**: 11478-11481.

Chen BT, Brau AC & Johnson GA (2003). Measurement of regional lung function in rats using hyperpolarized 3helium dynamic MRI. *Magn Reson Med* **49**: 78-88.

Chen Q, Rabach L, Noble P, et al (2005). IL-11 receptor alpha in the pathogenesis of IL-13-induced inflammation and remodeling. *J Immunol* **174**:2305-2313.

Coalson JJ (1982). The ultrastructure of human fibrosing alveolitis. *Virchows Arch [Pathol Anat]* **395**: 181-199. BOOK

Coote K, Nicholls A, Atherton HC, Sugar R, Danahay H (2004). Mucociliary clearance is enhanced in rat models of cigarette smoke and lipopolysaccharide-induced lung disease.
Exp Lung Res **30(1)**:59-71.

Corteling R, Trifilieff A (2004). Gender comparison in a murine model of allergen-driven airway inflammation and the response to budesonide treatment. *BMC Pharmacol* **15**: 4-4.

Cortijo J, Cerda-Nicolas M, Serrano A, Bioque G, Estrela JM, Santangelo F, Esteras A, Llombart-Bosch A, Morcillo EJ (2001). Attenuation by oral N-acetylcysteine of bleomycin-induced lung injury in rats. *Eur Respir J* **17(6)**:1228-35.

Crouch E (1990). Pathobiology of pulmonary fibrosis. *Am J Physiol* **259(4 Pt 1)**:L159-84.

Daviskas E, Anderson SD, Gonda I, Eberl S, Meikle S, Seale JP, Bautovich G (1996). Inhalation of hypertonic saline aerosol enhances mucociliary clearance in asthmatic and healthy subjects. *Eur Respir J* **9(4)**:725-32.

Deeley RG, Westlake C, Cole SP (2006). Transmembrane transport of endo- and xenobiotics by mammalian ATP-binding cassette multidrug resistance proteins. *Physiol Rev* **86(3)**:849-99.

Del Guerra A, Belcari N (2002). Advances in animal PET scanners. *Q J Nucl Med* **46**:35-47.

De Monchy JG, Kauffman HF, Venge P, Koeter GH, Jansen HM, Sluiter HJ, De Vries K (1985). Bronchoalveolar eosinophilia during allergen-induced late asthmatic reactions. *Am Rev Respir Dis* **131(3)**:373-6.

Donaldson SH, Bennett WD, Zeman KL, Knowles MR, Tarran R, Boucher RC (2006). Mucus clearance and lung function in cystic fibrosis with hypertonic saline. *N Engl J Med* **354**:241–250.

Dupuich D, Berthezene Y, Clouet PL, Stupar V, Canet E, Cremillieux Y (2003). Dynamic 3He imaging for quantification of regional lung ventilation parameters. *Magn Reson Med* **50(4)**:777-83.

Fahey FH (2003). Instrumentation in positron emission tomography. Neuroimaging *Clin N Am* **13**: 659-669.

Fine A, Goldstein RH & Snider GL (1991). Animal models of pulmonary fibrosis. In The Lung Scientific Foundation. Ed. Crystal RG & West JB et al. Raven Press Ltd, New York, USA, pp 2047-2057. BOOK

Foster WM, Wagner EM (2001). Bronchial edema alters (99m)Tc-DTPA clearance from the airway surface in sheep. *J Appl Physiol* **91(6)**:2567-73.

Gewalt SL, Glover GH, Hedlund LW, Cofer GP, MacFall JR & Johnson GA (1993). MR microscopy of the rat lung using projection reconstruction. *Magn Reson Med* **29**: 99-106.

Gong H, Sinz MW, Feng Y, Chen T, Venkataramanan R, Xie W (2005). Animal models of xenobiotic receptors in drug metabolism and diseases. *Methods Enzymol* **400**:598-618.

Gounni AS, Lamkhioued B, Ochiai K, Tanaka Y, Delaporte E, Capron A, Kinet JP, Capron M (1994). High-affinity IgE receptor on eosinophils is involved in defence

against parasites.
Nature **13;367(6459)**:183-6.

Greiff L, Erjefalt I, Svensson C, Wollmer P, Alkner U, Andersson M, Persson CG (1993). Plasma exudation and solute absorption across the airway mucosa. *Clin Physiol* **13(3)**:219-33.

Gross TJ, Hunninghake GW (2001). Idiopathic pulmonary fibrosis. *N Engl J Med* **16;345(7)**:517-25.

Guggino WB (2001). Cystic fibrosis salt/fluid controversy: in the thick of it. *Nat Med* **7(8)**:888-9.

Haile S, Lefort J, Joseph D, Gounon P, Huerre M, Vargaftig BB (1999). Mucous-cell metaplasia and inflammatory-cell recruitment are dissociated in allergic mice after antibody- and drug-dependent cell depletion in a murine model of asthma. *Am J Respir Cell Mol Biol* **20(5):**891-902.

Hamman L & Rich AR (1935). Fulminating diffuse interstitial fibrosis of the lungs. *Trans Am Clin Climatol Assoc* **51**: 154-163.

Hamelmann E, Schwarze J, Takeda K, Oshiba A, Larsen GL, Irvin CG, Gelfand EW (1997). Noninvasive measurement of airway responsiveness in allergic mice using barometric plethysmography.*Am J Respir Crit Care Med* **156(3 Pt 1)**:766-75.

Harrison JH Jr, Lazo JS (1988). Plasma and pulmonary pharmacokinetics of bleomycin in murine strains that are sensitive and resistant to bleomycin-induced pulmonary fibrosis. *J Pharmacol Exp Ther* **247(3)**:1052-8.

Hay DW, Muccitelli RM, Vickery-Clark LM, Novak LS, Osborn RR, Gleason JG, Yodis LA, Saverino CM, Eckardt RD, Sarau HM, et al (1991). Pharmacologic and pharmacokinetic profile of SK&F S-106203, a potent, orally active eptidoleukotriene receptor antagonist, in guinea-pig. *Pulm Pharmacol* **4(3)**:177-89.

Hedlund LW, Cofer GP, Owen SJ & Johnson GA (2000). MR-compatible ventilator for small animals: computer-controlled ventilation for proton and noble gas imaging. *Magn Reson Imaging* **18**: 753-759.

Holgate ST, Lackie P, Wilson S, Roche W, Davies D (2000). Bronchial epithelium as a key regulator of airway allergen sensitization and remodeling in asthma. *Am J Respir Crit Care Med* **162(3 Pt 2)**:S113-7.

Hoymann HG (2006) Invasive and noninvasive lung function measurements in rodents. *J Pharmacol Toxicol Methods* **291(3)**:L466-72.

Hunninghake GW, Kalica AR (1995). Approaches to the treatment of pulmonary fibrosis.
Am J Respir Crit Care Med **151(3 Pt 1)**:915-8.

Inman MD, Ellis R, Wattie J, Denburg JA, O'Byrne PM (1999). Allergen-induced increase in airway responsiveness, airway eosinophilia, and bone-marrow eosinophil progenitors in mice.
Am J Respir Cell Mol Biol **21(4)**:473-9.

International consensus statement (2000) Idiopathic pulmonary fibrosis: diagnosis and treatment. *Am J Respir Crit Care Med* **161**: 646–664.

Izbicki G, Segel MJ, Christensen TG, Conner MW, Breuer R (2002). Time course of bleomycin-induced lung fibrosis. *Int J Exp Pathol* **83(3)**:111-9.

Jarjour NN, Calhoun WJ, Kelly EA, Gleich GJ, Schwartz LB, Busse WW (1997). The immediate and late allergic response to segmental bronchopulmonary provocation in asthma. *Am J Respir Crit Care Med* **155(5)**:1515-21.

Jayaraman S, Joo NS, Reitz B, Wine JJ, Verkman AS (2001). Submucosal gland secretions in airways from cystic fibrosis patients have normal [Na(+)] and pH but elevated viscosity. *Proc Natl Acad Sci U S A* **3;98(14)**:8119-23.

Jeffery PK (2001). Remodeling in asthma and chronic obstructive lung disease. Am *J Respir Crit Care Med* **164**: S28–S38.

Karol MH (1994). Animal models of occupational asthma. *Eur Respir J* **7**: 555-568.

Katzenstein AL, Myers JL (1998). Idiopathic pulmonary fibrosis: clinical relevance of pathologic classification. *Am J Respir Crit Care Med* **157(4 Pt 1)**:1301-15.

Kay AB (2001). Allergy and allergic diseases. First of two parts. *N Engl J Med* **344**:30–37.

Kay AB (2001). Allergy and allergic diseases. Second of two parts. *N Engl J Med* **344**:109-113.

Knowles MR, Boucher RC (2002). Mucus clearance as a primary innate defense mechanism for mammalian airways. *J Clin Invest* **109(5)**:571-7.

Kilburn KH (1968). A hypothesis for pulmonary clearance and its implications.*Am Rev Respir Dis* **98(3)**:449-63.

Kumar RK, Foster PS (2002). Modeling allergic asthma in mice: pitfalls and opportunities. *Am J Respir Cell Mol Biol* **27(3)**:267-72.

Kroegel C, Luttmann W, Zeck-Kapp G, Matthys H, Kapp A, Virchow JC (1994). Cell biology and function of eosinophilic granulocytes in immunologic inflammation. *Immun Infekt* **22(3)**:104-13.

Krouse ME (2001). Is cystic fibrosis lung disease caused by abnormal ion composition or abnormal volume? *J Gen Physiol* **118(2)**:219-22.

Lasky JA, Ortiz LA (2001). Antifibrotic therapy for the treatment of pulmonary fibrosis. *Am J Med Sci* **322(4)**:213-21.

Lazenby AJ, Crouch EC, McDonald JA, Kuhn C 3rd (1990). Remodeling of the lung in bleomycin-induced pulmonary fibrosis in the rat. An immunohistochemical study of laminin, type IV collagen, and fibronectin. *Am Rev Respir Dis* **142(1)**:206-14.

Lazo JS, Hoyt DG, Sebti SM, Pitt BR (1990). Bleomycin: a pharmacologic tool in the study of the pathogenesis of interstitial pulmonary fibrosis. *Pharmacol Ther* **47(3)**:347-58.

Liu WL, Boulos PB, Lau HY, Pearce FL (1991). Mast cells from human gastric mucosa: a comparative study with lung and colonic mast cells. *Agents Actions* **33(1-2)**:13-5.

Levin MH, Sullivan S, Nielson D, Yang B, Finkbeiner WE, Verkman AS (2006). Hypertonic saline therapy in cystic fibrosis: Evidence against the proposed mechanism involving aquaporins. *J Biol Chem* **1;281(35)**:25803-12.

Machen TE (2006). Innate immune response in CF airway epithelia: hyperinflammatory? *Am J Physiol Cell Physiol* **291(2)**:C218-30.

Marcet B, Boeynaems JM (2006). Relationships between cystic fibrosis transmembrane conductance regulator, extracellular nucleotides and cystic fibrosis. *Pharmacol Ther* **112(3)**:719-32.

McAnulty RJ, Moores SR, Talbot RJ, Bishop JE, Mays PK, Laurent GJ (1991). Long-term changes in mouse lung following inhalation of a fibrosis-inducing dose of 239PuO2: changes in collagen synthesis and degradation rates. *Int J Radiat Biol* **59(1)**:229-38.

McCusker C, Chicoine M, Hamid Q, Mazer B (2002). Site-specific sensitization in a murine model of allergic rhinitis: role of the upper airway in lower airways disease. *J Allergy Clin Immunol* **110(6)**:891-8.

Möller HE, Chen XJ, Saam B, Hagspiel KD, Johnson GA, Altes TA, De Lange EE & Kauczor HU (2002). MRI of the lungs using hyperpolarized noble gases. *Magn Reson Med* **47**: 1029-1051.

Moqbel R (1996). Eosinophil-derived cytokines in allergic inflammation and asthma. *Ann NY Acad Sci* **796**: 209-217.

Morgan L, Pearson M, de Iongh R, Mackey D, van der Wall H, Peters M, Rutland J (2004). Scintigraphic measurement of tracheal mucus velocity in vivo. *Eur Respir J* **23(4)**:518-22.

Murray AB, Ferguson AC, Morrison BJ (1985). Non-allergic bronchial hyperreactivity in asthmatic children decreases with age and increases with mite immunotherapy. *Ann Allergy* **54(6)**:541-4.

Pan S, Mi Y, Pally C, Beerli C, Chen A, Guerini D, Hinterding K, Nuesslein-Hildesheim B, Tuntland T, Lefebvre S, Liu Y, Gao W, Chu A, Brinkmann V, Bruns C, Streiff M, Cannet C, Cooke N, Gray N (2006). A monoselective sphingosine-1-phosphate receptor-1 agonist prevents allograft rejection in a stringent rat heart transplantation model.*Chem Biol* **13**(11):1227-34.

Pavia D, Thomson ML, Clarke SW (1978). Enhanced clearance of secretions from the human lung after the administration of hypertonic saline aerosol. *Am Rev Respir Dis* **117(2)**:199-203.

Platts-Mills TA, Wheatley LM (1996). The role of allergy and atopy in asthma. *Curr Opin Pulm Med* **2(1)**:29-34.

Persson MG, Friberg SG, Gustafsson LE, Hedqvist P (1995). The promotion of patent airways and inhibition of antigen-induced bronchial obstruction by endogenous nitric oxide. *Br J Pharmacol* **116(7)**:2957-62.

Puchelle E, de Bentzmann S, Zahm JM (1995). Physical and functional properties of airway secretions in cystic fibrosis--therapeutic approaches. *Respiration* Suppl 1:2-12.

Rahmoune H, Shephard KL (1995). State of airway surface liquid on guinea pig trachea.*J Appl Physiol* **78(6)**:2020-4.

Robinson D, Hamid Q, Bentley A, Ying S, Kay AB, Durham SR (1993). Activation of CD4+ T cells, increased TH2-type cytokine mRNA expression, and eosinophil recruitment in bronchoalveolar lavage after allergen inhalation challenge in patients with atopic asthma. *J Allergy Clin Immunol* **92(2)**:313-24.

Robinson PJ, Hegele RG & Schellenberg RR (1997). Allergic sensitization increases airway reactivity in guinea pigs with respiratory syncytial virus bronchiolitis. *J Allergy Clin Immunol* **100**: 492-498.

Roche WR, Beasley R, Williams JH, Holgate ST (1989). Subepithelial fibrosis in the bronchi of asthmatics. *Lancet* **11;1(8637)**:520-4.

Rogers DF (2004). Airway mucus hypersecretion in asthma: an undervalued pathology? *Curr Opin Pharmacol* **4**: 241-250.

Rogers DF (2005). Mucociliary dysfunction in COPD: effect of current pharmacotherapeutic options. *Pulm Pharmacol Ther* **18**: 1-8.

Rudin M, Beckmann N, Porszasz R, Reese T, Bochelen D & Sauter A (1999). In vivo magnetic resonance methods in pharmaceutical research: current status and perspectives. *NMR Biomed* **12**: 69-97.

Rudin M & Weissleder R (2003). Molecular imaging in drug discovery and development. *Nat Rev Drug Discov* **2**: 123-131.

Sanchez T, Skoura A, Wu MT, Casserly B, Harrington EO and Hla T (2007). Induction of vascular permeability by the sphingosine-1-phosphate receptor–2 (S1P2R) and its downstream effectors ROCK and PTEN. *Arterioscler Thromb Vasc Biol* **27**;1312-1318.

Sakai K, Yokoyama A, Kohno N, Hiwada K (1999). Effect of different sensitizing doses of antigen in a murine model of atopic asthma. *Clin Exp Immunol* **118(1)**:9-15.

Schuster C, Wuthrich B (2003). Anaphylactic drug reaction to celecoxib and sulfamethoxazole: cross reactivity or coincidence? *Allergy* **58(10)**:1072.

Schuster DP, Kovacs A, Garbow J & Piwnica-Worms D (2004). Recent advances in imaging the lungs of intact small animals. *Am J Respir Cell Mol Biol* **30**: 129-138

Shapiro SD (2000). Animal models for COPD. *Chest* **117**: 223S-227S.

Sims DE, Horne MM (1997). Heterogeneity of the composition and thickness of tracheal mucus in rats. *Am J Physiol* **273(5 Pt 1)**:L1036-41.

Slates RB, Farahani K, Shao Y, Marsden PK, Taylor J, Summers PE, Williams S, Beech J, Cherry SR (1999). A study of artefacts in simultaneous PET and MR imaging using a prototype MR compatible PET scanner. *Phys Med Biol* **44**: 2015-2027.

Smith HR, Larsen GL, Cherniack RM, Wenzel SE, Voelkel NF, Westcott JY, Bethel RA (1992). Inflammatory cells and eicosanoid mediators in subjects with late asthmatic responses and increases in airway responsiveness. *J Allergy Clin Immunol* **89(6)**:1076-84.

Snider GL, Hayes JA, Korthy AL (1978). Chronic interstitial pulmonary fibrosis produced in hamsters by endotracheal bleomycin: pathology and stereology. *Am Rev Respir Dis* **117(6)**:1099-108.

Stupar V, Canet-Soulas E, Gaillard S, Alsaid H, Beckmann N, Cremillieux Y (2007). Retrospective cine 3He ventilation imaging under spontaneous breathing conditions: a non-invasive protocol for small-animal lung function imaging. *NMR Biomed* **20(2)**:104-12.

Sugimoto N, Takuwa N, Okamoto H, Sakurada S, Takuwa Y (2003). Inhibitory and stimulatory regulation of Rac and cell motility by the G12/13-Rho and Gi pathways

integrated downstream of a single G protein-coupled sphingosine-1-phosphate receptor isoform. *Mol Cell Biol* **23(5)**:1534-45.

Tarran R (2004). Regulation of airway surface liquid volume and mucus transport by active ion transport. *Proc Am Thorac Soc* **1(1)**:42-6.

Tarran R, Grubb BR, Gatzy JT, Davis CW, Boucher RC (2001 a). The relative roles of passive surface forces and active ion transport in the modulation of airway surface liquid volume and composition**.** *J Gen Physiol* **118(2)**:223-36.

Tarran R, Grubb BR, Parsons D, Picher M, Hirsh AJ, Davis CW, Boucher RC (2001 b).The CF salt controversy: in vivo observations and therapeutic approaches. *Mol Cell* **8(1)**:149-58.

Thrall RS, McCormick JR, Jack RM, McReynolds RA, Ward PA (1979). Bleomycin-induced pulmonary fibrosis in the rat: inhibition by indomethacin. *Am J Pathol* **95(1)**:117-30.

Thrall RS, Swendsen CL, Shannon TH, Kennedy CA, Frederick DS, Grunze MF, Sulavik SB (1987). Correlation of changes in pulmonary surfactant phospholipids with compliance in bleomycin-induced pulmonary fibrosis in the rat. *Am Rev Respir Dis* **136(1)**:113-8.

Tigani B, Schaeublin E, Sugar R, Jackson AD, Fozard JR & Beckmann N (2002). Pulmonary inflammation monitored noninvasively by MRI in freely breathing rats**.** *Biochem Biophys Res Commun* **292**: 216-221.

Tigani B, Cannet C, Zurbrugg S, Schaeublin E, Mazzoni L, Fozard JR & Beckmann N (2003). Resolution of the oedema associated with allergic pulmonary inflammation in rats assessed noninvasively by magnetic resonance imaging. *Br J Pharmacol* **140**: 239-246.

Tonnel AB, Joseph M, Gosset P, Fournier E, Capron A (1983). Stimulation of alveolar macrophages in asthmatic patients after local provocation test. *Lancet* **25;1(8339)**:1406-8.

Trifilieff A, El-Hashim A, Bertrand C (2000). Time course of inflammatory and remodeling events in a murine model of asthma: effect of steroid treatment. Am *J Physiol Lung Cell Mol Physiol* **279(6)**:L1120-8.

Ueda Y, Saito A, Fukuoka Y, Yamashiro Y, Ikeda Y, Taki H, Yasuda T, & Saikawa I (1983). Interactions of beta-lactam antibiotics and antineoplastic agents. *Antimicrob Agents Chemother* **23**: 374–378.

Usuki J, Fukuda Y (1995). Evolution of three patterns of intra-alveolar fibrosis produced by bleomycin in rats. *Pathol Int* **45(8)**:552-64.

Van Vyve T, Chanez P, Bernard A, Bousquet J, Godard P, Lauwerijs R, Sibille Y (1995). Protein content in bronchoalveolar lavage fluid of patients with asthma and control subjects.*J Allergy Clin Immunol* **95(1 Pt 1)**:60-8.

Vasquez YR, Spina D (2000). What have transgenic and knockout animals taught us about respiratory disease? *Respir Res* **1(2)**:82-6.

Wanner A, Salathe M, O'Riordan TG (1996). Mucociliary clearance in the airways. *Am J Respir Crit Care Med* **154(6 Pt 1)**:1868-902.

Wardlaw AJ (1993). The role of air pollution in asthma.*Clin Exp Allergy* **23(2)**:81-96.

Widdicombe JH, Bastacky SJ, Wu DX, Lee CY (1997). Regulation of depth and composition of airway surface liquid. *Eur Respir J* **10(12)**:2892-7.

Wine JJ (1999). The genesis of cystic fibrosis lung disease. *J Clin Invest* **103(3)**:309-12.

Winters SL, Yeates DB (1997). Roles of hydration, sodium, and chloride in regulation of canine mucociliary transport system. J *Appl Physiol* **83(4)**:1360-9.

Yager D, Kamm RD, Drazen JM (1995). Airway Wall Liquid Sources and Role as an amplifier of bronchoconstriction. *Chest* **107**:105-110

Yue G, Matalon S (1997). Mechanisms and sequelae of increased alveolar fluid clearance in hyperoxic rats. *Am J Physiol* (*Lung Cell Mol Physiol 16*) **272**:L407-L412.

Zhang Z, Schluesener HJ (2007). FTY720: a most promising immunosuppressant modulating immune cell functions. *Mini Rev Med Chem* **7**:845-850.

LIST OF PUBLICATIONS AND PRESENTATIONS

PUBLICATIONS

Blé FX, Cannet C, Zurbruegg S, Karmouty-Quintana H, Bergmann R, Frossard N, Trifilieff A, Beckmann N. Allergen-induced lung inflammation in actively sensitized mice assessed by MRI. *Radiology*. Accepted.

Blé FX, Cannet C, Zurbruegg S, Frossard N, Trifilieff A, Beckmann N. Time course of lung fluid signals assessed by MRI in a murine model of allergen-induced inflammation: A comparison of two strains. *Am J Physiol Lung Cell Physiol*. In preparation

Blé FX, Cannet C, Zurbruegg S, Gérard C, Frossard N, Beckmann N, and Trifilieff A. A S1P2 antagonist inhibits allergen-induced increase in MRI fluid signals in mouse via a non mast cell-dependent mechanism. *J Immunol*. In preparation

Blé FX, Cannet C, Zurbruegg S, Frossard N, Trifilieff A, Beckmann N. Local instillation of FTY720 to the lung reduces MRI fluid signals in a murine model of allergen-induced inflammation: example of a S1P1 agonism. *J Pharmacol Exp Ther*. In preparation

Blé FX, Cannet C, Zurbruegg S, Danahay H, Collingwood S, Beckmann N. ENaC-mediated effects assessed by proton MRI in a rat model of hypertonic-induced hydration of airways secretions.*Am J Physiol Lung Cell Physiol*. In preparation

Blé FX, Schmitd P, Kneuer R, Cannet C, Quintana HK, Zurbruegg S, Gremlich HU, Beckmann N. In-vivo assessments of mucus dynamics in the lungs using a Gd-Cy5.5-bilabeled contrast agent. *Radiology*. In preparation

Quintana HK, Cannet C, Zurbruegg S, Blé FX, Fozard JR, Page CP, Beckmann N. Bleomycin-induced lung injury assessed non-invasively in spontaneously breathing rats by proton MRI. J. *Magn. Reson. Imaging* 2007; in press.

Beckmann N, Quintana HK, Blé FX, Cannet C, Zurbruegg S, Tigani B, Fozard JR. Magnetic Resonance Imaging (MRI) of the Lung as a Tool for the Non-Invasive Evaluation of Drugs in Rat Models of Airways Diseases
ALTEX (Alternatives to Animal Experimentation), 23, 420-428 (2006).

Beckmann N, Crémillieux Y, Tigani B, Quintana HK, Blé FX, Fozard JR. Lung MRI in Small Rodents as a Tool for the Evaluation of Drugs in Models of Airways Diseases. In: „In Vivo MR Techniques in Drug Discovery and Development" (Editor: N. Beckmann), pp. 351 - 372. Taylor & Francis, New York (2006).

Quintana HK, Cannet C, Zurbruegg S, Blé FX, Fozard JR, Page CP, Beckmann N. Proton MRI as a noninvasive tool to assess elastase-induced lung damage in spontaneously breathing rats. *Magn Reson Med*. 2006 Dec;56(6):1242-50.

Tigani B, Cannet C, Karmouty-Quintana H, Blé FX, Zurbruegg S, Schaeublin E, Fozard JR, Beckmann N. Lung inflammation and vascular remodeling after repeated allergen challenge detected noninvasively by MRI. *Am J Physiol Lung Cell Mol Physiol*. 2007 Mar;292(3):L644-53

Beckmann N, Kneuer R, Gremlich HU, Karmouty-Quintana H, Blé FX, Muller M. In Vivo mouse imaging and spectroscopy in drug discovery. *NMR Biomed*. 2007 May;20(3):154-85.

Beckmann N, Cannet C, Karmouty-Quintana H, Tigani B, Zurbruegg S, Blé FX, Crémillieux Y, Trifilieff A. Lung MRI for experimental drug research. *Eur J Radiol* 2007; in press.

PRESENTATIONS

Blé FX, Cannet C, Frossard N, Trifilieff A, Beckmann N. Proton MRI as a non-invasive tool to characterize a murine model of allergic pulmonary inflammation. ISMRM in Berlin (Germany). 2007 May (Poster)

Blé FX, Cannet C, Frossard N, Trifilieff A, Beckmann N. MRI as a non-invasive tool to characterize a murine model of allergic pulmonary inflammation. 3rd International Workshop of Pulmonary Functional Imaging in Heidelberg (Germany) 2006 Oct. (Oral Presentation)

Quintana HK, Blé FX, Cannet C, Zurbruegg S, Schaeublin E, Sugar RM, Beckmann N. Experimental pulmonary disease assessed by proton MRI. 3rd International Workshop of Pulmonary Functional Imaging in Heidelberg (Germany) 2006 Oct. (Poster)

ACKNOWLEDGEMENTS

First, I would like to thank my supervisor, Dr Nicolau Beckmann, for having given me the opportunity to perform my PhD in his laboratory and for having supported and trusted me throughout my doctoral project. Thanks to his confidence and precious advices, I have been able to take in charge my PhD research project at all stages in a relative freedom. In particular, I would like to thank him for having communicated me his enthusiasm for science, scientific challenges and innovative ideas. In addition, I would like to thank my university advisor, Dr Nelly Frossard, for her academical support and for the careful reading of my thesis dissertation.

I would like also to thank everybody that has worked with me during the last 3 years. I am very grateful to the Respiratory Disease Area of Novartis Pharma for the generous funding that has made this research possible. I would also like to recognize the unprecedented interest and enthusiasm shown towards the project by the senior management of Novartis Pharma of both Respiratory Disease Area and Discovery Technologies.

I also have many words of praise for Dr Alexandre Trifilieff, Dr. John Fozard and Dr. Lazzaro Mazzoni for their extensive advices and understanding of lung physiology and pharmacology. I would like to pay tribute to Catherine Cannet and Christelle Gérard for their expert essential assistance with histology and to Stephan Zurbrügg, Daniel Wyss and Dr. Harry Karmouty Quintana for their all round assistance with the experiments. Many thanks to Elisabeth Schäublin for her great support in BAL fluid lavage, from cell counting to assays, and Alexandra Suter for her help in ordering of all I desperately needed! I also acknowledge Dr. Hans-Ulrich Gremlich and Dr. Bruno Tigani for their constructive scientific comments. In addition I would like to thank Dr Rainer Kneuer and Dr Phillip Schmitd for their fantastic support in chemistry. Of note, I have also a special thought for the rodent community: sorry for the mice and rats that were involved in the experiments of this thesis.

I also have words of appreciation for the “coffee machine team” composed of Bruno Tigani, Bobby Gremlich, Yann Sénéchal, Cédric Berger, Harry Karmouty Quintana,

Stephan Zurbrügg and Nicolau Beckmann for the great discussions about science and life in general during those many numerous coffee breaks.
I am grateful to my friends from Saint Louis and Colmar for the endless pokers, the numerous meals and bloc parties that contributed to my enjoying life time in Alsace. In this regard, I also gratefully acknowledge all the Pontajou family members for their support, friendship and the generously shared apero and meals.
I have also a special thought for my childhood friends from Vendée who did not forget to send me support and encouragement messages all along my PhD, as well as for my Uni' friends for the "refreshing" and enjoyable week-ends spend in Paris.

I would like to address special thanks to my parents who believed in me and encouraged me all along my studies until the end of my PhD. In addition, many thanks go also to my sisters Aurélie and Marjorie and their family for their encouragements and continuous support throughout my thesis.

I would like to finish by unlimited thanks to you, my sweet Léa, for all your love, efforts, patience, care and support all along the enjoyable as well as difficult times we shared together during my PhD.

Résumé

L'imagerie par résonance magnétique est capable de détecter le contenu en eau des tissus biologiques et ainsi d'estimer localement et de manière non invasive l'infiltration d'eau et/ou la sécrétion de fluides et/ou la densification tissulaire. Dans les maladies pulmonaires comme l'asthme, les bronchopathies chroniques obstructives ou la fibrose, la fuite plasmatique, la sécrétion de mucus et l'épaississement des tissus du poumon composent parmi les signes pathologiques majeurs qui contribuent directement à l'amoindrissement de la fonction pulmonaire.

Ces caractéristiques sont, en outre, bien conservées dans les modèles expérimentaux de maladies pulmonaires chez le petit rongeur. Un intérêt particulier est porté vers le développement et l'utilisation de modèles chez la souris qui a fourni, en parallèle des avancées en matière de génie génétique et de biologie molécuaire, un pertinent support *in vivo* pour l'investigation et la compréhension des maladies pulmonaires. De nos jours, les méthodes de routine employées pour l'évaluation de l'état pathologique des poumons dans ces modèles sont terminales, ou ne fournissent qu'une estimation globale de la fonction des voies respiratoires sans information d'ordre spatial.

Ainsi, nous avons mis au point une méthode utilisant l'IRM afin détecter différents signes pathologiques induits dans un modèle d'asthme chez la souris. Lors de cette thèse, nous avons démontré et validé la pertinence de l'IRM dans la détection et le suivi de signaux associés à la fuite plasmatique et aux sécrétions de mucus dans les voies aériennes, qui sont deux caractéristiques majeures de la réponse inflammatoire suite à la provocation allergénique. Afin de valider de façon plus approffondie nos observations, nous avons démontré l'utilité de la méthode dans une étude pharmacologique. Nous avons choisi d'étudier la pharmacologie du sphingosine-1-phosphate (S1P) car de récentes publications indiquaient l'implication de ce médiateur endogène dans les mécanismes inflammatoires et dans le maintien de la perméabilité des tissus. Dans deux études examinant les effets (i) de l'agoniste général du S1P, le FTY720 et (ii) de l'antagoniste sélectif du $S1P_2$, le JTE013, l'incidence de la fuite plasmatique dans la détection des signaux IRM a été mise en évidence dans notre modèle d'inflammation pulmonaire chez la souris et a été confirmée par histologie et par analyse du lavage broncho-alvéolaire.

De plus, la technique ayant été précédemment mise au point chez le rat, durant les travaux de thèse nous avons progressé dans les investigations concernant l'utilisation de l'IRM du poumon pour cette espèce. Ainsi, nous sommes parvenus à détecter de façon sélective et à suivre la progression des sécrétions de mucus par IRM en utilisant un agent de contraste spécifique dans un modèle d'hypersécrétion de mucus induite par endotoxine chez le rat. En outre, nous avons également démontré les capacités de l'IRM dans l'estimation et le suivi de l'hydratation des sécrétions des voies aériennes. En effet, dans un modèle non-inflammatoire chez le rat, la formation de signaux IRM liés à la présence de fluide a été induite par l'instillation d'une solution hypertonique et accrue de manière dose dépendente par l'administration de différents composés agissant directement ou indirectement sur les canaux sodiques épithéliaux, responsables de la régulation du niveau d'hydratation du liquide de surface des voies aériennes. Ces études ont été menées avec succés chez le rat dans la perspective d'un futur transfert chez la souris permettant d'utiliser des animaux transgéniques.

Enfin, nous avons en partie validé l'utilisation de l'IRM dans un modèle moins aigü de fibrose induite par bléomycine chez la souris. Ce modèle a été choisi pour sa capacité à reproduire les caractéristiques globales de la fibrose pulmonaire humaine ainsi que pour sa facilité à être mis en place. Dans cette étude, nous avons été capable de localiser et de suivre par IRM la course des signaux liés aux composantes inflammatoire et fibrotique incluant la fuite plasmatique, la sécrétion de mucus et l'épaissisement des tissus qui ont été confirmées par analyse histologique des poumons.

En résumé, ce travail a permis d'apporter la preuve que l'IRM peut contribuer de façon significative à la recherche dans le domaine des maladies pulmonaires chez le petit rongeur. Les résultats obtenus soutiennent que l'utilisation de l'IRM, comme un outil non-invasive et fournissant des informations d'ordre spatial et temporel, peut être envisagée en complément et/ou en remplacement des méthodes pratiquées aujourd'hui pour l'évaluation de modèles expérimentaux chez le petit rongeur.

Abstract

Magnetic resonance imaging (MRI) is able to detect water content in the biological tissue and thus to non-invasively assess on a regional basis infiltrated water and/or secreted fluids and/or tissue densification. In pulmonary diseases such as asthma, chronic obstructive pulmonary diseases or fibrosis, plasma exudation, mucus secretion and thickening of the lung tissue constitute hallmarks of the pathological status that directly contribute to functional impairment. These features are well conserved in experimental pulmonary disease models in the small rodents. A particular interest is given to murine models that have provided, in parallel to the technological progress in genetic engineering and molecular biology, a reliable *in vivo* support for lung disease understanding and investigation. Nowadays, routine methods used to evaluate disease state of the lung in these models are either terminal or gives functional estimation of the global airways.

Therefore, we have set up a method using MRI technique to non-invasively depict different hallmarks occurring in a murine model of asthma. In this thesis, we have demonstrated that proton MRI provides a relevant mean to assess and follow signals associated with the plasma leakage and mucus secretions in the lung, which are both important features of the inflammatory response following allergenic provocation. To further confirm these findings, we have also validated in this model the effect of pharmacological tools. We chose to study sphingosine-1-phosphate (S1P) pharmacology on the basis of recent publications indicating a possible implication of this endogenous mediator in inflammation and lung barrier integrity in models of asthma. In two studies examining the effects of the general S1P agonist FTY720 and of the $S1P_2$ antagonist JTE013, the incidence of plasma leakage on fluid signal detection was highlighted in our murine model of airway inflammation and confirmed by histology and BAL fluid analyses.

Additionally, since the technique had been previously set up in the rat, we extended the knowledge in this species. In this regard, we achieved the selective detection and monitoring of mucus dynamics by MRI with the use of a specific contrast agent in a model of endotoxin-induced mucus hypersecretion. Besides, we also demonstrated the capabilities of MRI to follow the hydration of airway secretions. In this non-inflammatory model, the formation of MRI fluid signals were induced by hypertonic saline instillation and dose-dependently enhanced by different compounds that interact directly or indirectly with epithelial Na^+ channel (ENaC), a major regulator of airway surface liquid hydration. These studies have been successfully performed in the rat with the perspective of future translation to murine models for transgenic application.

Finally, we have partially validated the application of this technique to a less acute model, the murine bleomycin-induced fibrosis. This model has been chosen regarding its admitted relevance to mimic global characteristics of human pulmonary fibrosis in addition to its simplicity to be set up. In this study, we have been able to follow by MRI the course of edematous, mucous and/or fibrotic features in correlation with histological findings.

In summary, the present work is bringing evidence of possible contributions of MRI in pulmonary disease investigations in mouse and rat, and postulates for its use to complete and/or replace the methods used nowadays to evaluate experimental murine models.